BOUNDARY LUBRICATION OF STAINLESS STEEL AND CoCrMo IN AQUEOUS SYSTEMS

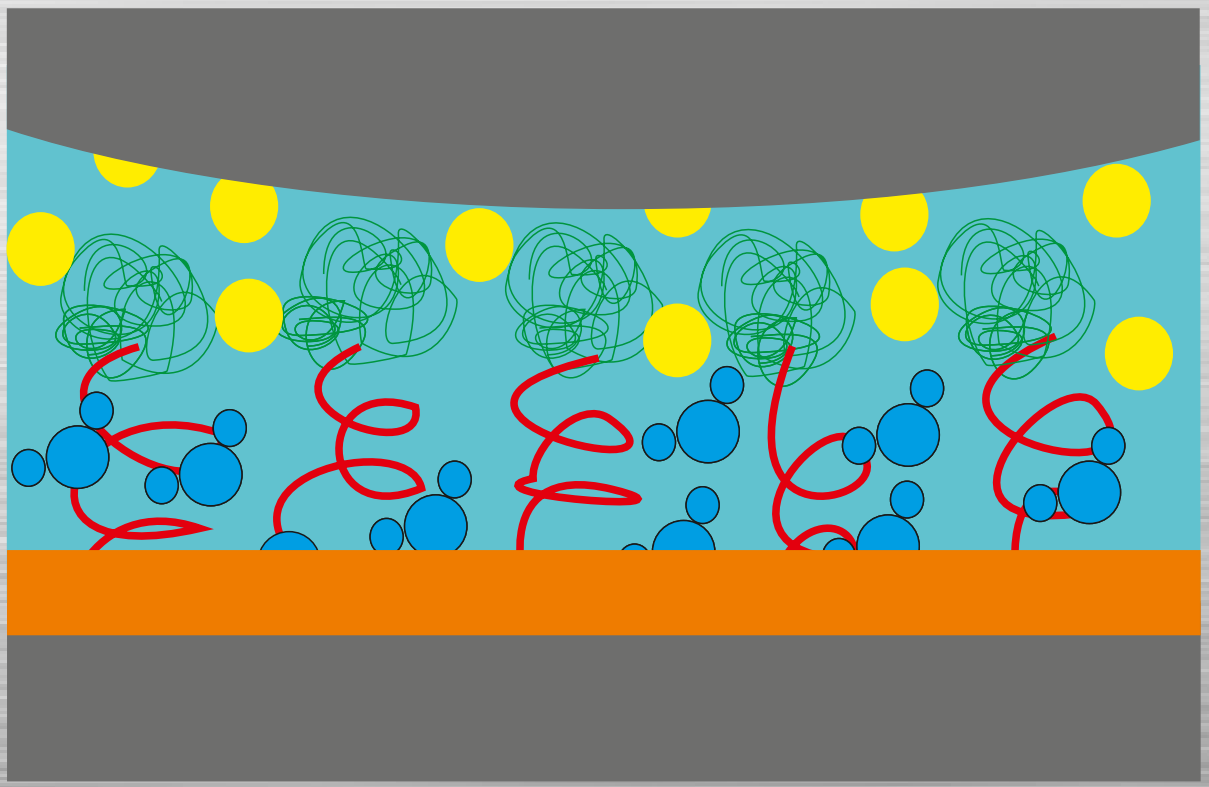

Jincan Yan

Boundary lubrication of stainless steel and CoCrMo in aqueous systems

Jincan Yan

De promotiecommissie is als volgt samengesteld:

prof. dr. G.P.M.R. Dewulf, Universiteit Twente, voorzitter en secretaris
prof. dr. ir. E. van der Heide, Universiteit Twente, promotor
prof. dr. T. Ren, Shanghai Jiao Tong University, promotor
dr. X. Zeng, Universiteit Twente, copromotor
prof. dr. G.J. Vancso, Universiteit Twente
prof. dr. ir. G.J. Verkerke, Universiteit Twente
prof. dr. Z. Jin, University of Leeds and Xian Jiao Tong University
prof. dr. rer. nat. A. Pich, RWTH Aachen University

This research was carried out under EU Marie Curie CIG, grant no. PCIG10-GA-2011-303922.

Jincan Yan
Boundary lubrication of stainless steel and CoCrMo alloy in aqueous system
Ph.D. Thesis, University of Twente, Enschede, The Netherlands,
October 2014
ISBN 978-90-365-3758-2

Keywords: tribology, boundary lubrication, hydration lubrication, stainless steel, CoCrMo alloy, O/W emulsion, graphene oxide, surface-active polymers.

BOUNDARY LUBRICATION OF STAINLESS STEEL AND CoCrMo IN AQUEOUS SYSTEMS

PROEFSCHRIFT

ter verkrijging van
de graad van doctor aan de Universiteit Twente,
op gezag van de rector magnificus,
prof. dr. H. Brinksma,
volgens besluit van het College voor Promoties
in het openbaar te verdedigen
op woensdag 8 oktober 2014 om 12:45 uur

door

Jincan Yan

geboren op 13 maart 1981
te Anhui, China

Dit proefschrift is goedgekeurd door:

de promotoren: prof. dr. ir. E. van der Heide
prof. dr. T. Ren
de copromotor: dr. X. Zeng

Summary

Oil-based lubricants are widely used in many mechanical applications, but they cannot be used for applications with a high risk of polluting the environment or for applications that involve a bio-medical environment. Water-based lubricants are of high interest to use as alternative because they can potentially overcome these problems while maintaining the required high level of tribological performance. Also water is a natural medium for lubrication in the human body, such as synovial fluid in human joints. A water based environment requires interacting surfaces that combine hardness, wear resistance and corrosion resistance. Typically, stainless steel and CoCrMo alloys are used for such tribological applications including food processing equipment as well implants.

In this thesis, a new concept of aqueous lubrication, i.e. lubrication by hydration of surface active polymers combined with graphene oxide from water or an oil-in-water (O/W) emulsion, is presented.

Based on the literature review and the lubrication concept, this work started with the interaction of bearing steel, stainless steel and CoCrMo with several newly developed additives. Tribological study showed boron-nitrogen containing additive had superior friction-reducing and anti-wear properties than the additive only containing boron during the interacting with bearing steel, due to the formation of both BN and B_2O_3 according to XPS and XANES analysis. Further study indicated boron-nitrogen containing additives (DOB and ODOC) and phosphorous-nitrogen containing additive (DBOP) were not only functional for bearing steel and stainless steel, but also functional for CoCrMo, especially for the friction-reducing property of ODOC and anti-wear property of DOB.

Firstly, the aqueous lubrication by using O/W emulsions incorporating the aforementioned additives was examined. The friction profile of the O/W emulsion was quite different to that of the oil lubricant. It exhibited three stage frictional behaviour, including running-in, water dominated status and oil dominated status, because of the plate-out behaviour of O/W emulsion during friction process. The tribological performance of the O/W emulsions was similar to that of the oil lubricants with the same additives, especially for the anti-wear properties and the friction reducing property of ODOC. XPS results showed that

the lubricating films consisted of an adsorption layer and a reaction layer. The adsorption layer was formed by the coordination of nitrogen-containing additives on the metal surface. The reaction layer originated from the tribochemical reaction of the active elements in the additives with the metal surface. The main chemical compositions of the reaction films from O/W emulsions were similar to that of oil lubricants containing the same additives.

Secondly, the CoCrMo alloy was coated with surface-active polymers PAA and PEG and graphene oxide layers. Enhanced friction reducing capability was found in water based fluids for the polymeric coatings in combination with a graphene oxide. The synergy effect on friction reducing ability between graphene oxide and the surface-active polymer coatings was demonstrated at both macro scale by using a ball on disk configuration and at micro scale by preliminary AFM measurements.

Finally, an amphiphilic coating, PEG-lactide, was combined with graphene oxide and used with the O/W emulsions for CoCrMo. The tribological performance of PEG-lactide coating in O/W emulsion was enhanced further compared to the performance of the PEG coated surfaces: a clear indication of the advantage of using hydrophilic and lipophilic group containing surface-active polymers for emulsion lubrication.

The overall maximum reduction in friction that was achieved for a sliding contact of coated engineering surfaces from CoCrMo at low sliding velocity and moderate contact pressure was of about 63 % compared to uncoated CoCrMo sliding in water at the same operational conditions.

Samenvatting

Olie-gebaseerde smeermiddelen worden breed ingezet voor diverse mechanische toepassingen, maar ze kunnen niet gebruikt worden voor toepassingen waar het risico bestaat op milieuvervuiling of voor toepassingen in een biomedische omgeving. Water gebaseerde smeermiddelen zijn dan een zeer interessant alternatief omdat ze in potentie deze beperkingen niet hebben en tegelijkertijd het gewenste hoge niveau in tribologisch gedrag kunnen bieden. Daarbij komt dat water een natuurlijke basis is voor smering in het menselijk lichaam, zoals bijvoorbeeld in het synoviaal vocht in menselijke gewrichten. Een water-gebaseerde omgeving vraagt om contactvlakken die hardheid, slijtvastheid en corrosieweerstand combineren. Roestvaststaal en CoCrMo-legeringen worden veelal toegepast onder dit soort omstandigheden, waaronder toepassingen in voedselverwerkingsmachines en implantaten.

In dit proefschrift wordt een nieuw concept voor watersmering beschreven: smering door hydratatie van oppervlakte-actieve polymere deklagen gecombineerd met grafeenoxide vanuit water of een olie-in-water (O/W) emulsie.

Op basis van de literatuurstudie en het globale smeringsconcept, is het onderzoek gestart met het bestuderen van de interactie tussen verschillende nieuw ontwikkelde additieven en lagerstaal, roestvast staal en CoCrMo. De tribologische studie laat zien dat boor-stikstof houdende additieven een superieur wrijvings- en slijtagegedrag vertonen in combinatie met lagerstaal, ten opzichte van additieven die alleen boor bevatten. Dit vanwege de vorming van zowel BN als B_2O_3, aangetoond met XPS en XANES analyses. Vervolgonderzoek geeft aan dat boor-stikstof houdende additieven (DOB and ODOC) en fosfor – stikstof houdende additiven (DBOP) niet alleen in combinatie met lagerstaal en roestvaststaal functioneren, maar ook in combinatie met CoCrMo, met name ten aanzien van de wrijvingsverlagende eigenschappen van ODOC en de bescherming tegen slijtage door DOB.

Allereerst is watersmering met O/W emulsies op basis van de hierboven genoemde additieven onderzocht en beoordeeld. Het wrijvingsprofiel van de O/W emulsie verschilde sterk van die van de olie. Het wrijvingsgedrag bestaat uit

drie fases, met een inloopfase, een water-gedomineerde fase en een olie-gedomineerde fase. Dit vanwege het 'plate-out' gedrag van de O/W emulsie tijdens het wrijvingsproces. Het tribologisch gedrag van de O/W emulsies was vergelijkbaar met het gedrag van de olie met dezelfde additieven, met name voor de wrijvings- en slijtage verlagende eigenschappen van ODOC. XPS resultaten lieten zien dat de smeerfilm bestaat uit een adsorptielaag en een verbindingenlaag. De adsorptielaag aan het metallische loopvlak is gestuurd ontstaan door de stikstofhoudende additieven. De verbindingenlaag vindt zijn oorsprong in de tribo-chemische reactie van de actieve elementen met het metallische loopvlak. De chemische samenstelling van de verbindingenlaag door smering met de O/W emulsie is hoofdzakelijk gelijk aan de verbindingenlaag door smering met alleen de van additieven voorziene olie.

Daarna is CoCrMo bedekt met een oppervlakte-actieve polymere coating op basis van PAA en PEG en met een grafeenoxide deklaag. De wrijvingsverlagende eigenschappen van de polymere deklagen in water verbeterden door de combinatie met grafeenoxide. Het synergistisch effect op wrijvingsverlaging van grafeenoxide en de oppervlakte-actieve polymere coating is aangetoond op de macro-schaal door metingen met een kogel-op-schijf configuratie en op de micro-schaal door inleidende metingen met een AFM.

Tenslotte is een amfifiele coating, PEG-lactide, gecombineerd met grafeenoxide aangebracht op CoCrMo en toegepast met de O/W emulsies. Het tribologisch gedrag van de PEG lactide coating in de O/W emulsie is verder verbeterd ten opzichte van het gedrag van het PEG gecoate systeem in dezelfde emulsie: een duidelijke aanwijzing naar het voordeel van het gebruik van hydrofiele en lipofiele groepen in oppervlakte-actieve polymeren in combinatie met emulsiesmering.

De algemene wrijvingsverlaging die is bereikt voor een glijdend contact van technische oppervlakken uit CoCrMo met coating, met een lage glijsnelheid en een gematigde contactdruk, is maximaal ongeveer 63% ten opzichte CoCrMo zonder coating van het glijdende contact in water met dezelfde operationele condities.

Nomenclature

Abbreviations

BL	boundary lubrication
ML	mixed lubrication
HL	hydrodynamic lubrication
PEG	poly(ethylene glycol)
PAA	poly(acrylic acid)
O/W	oil in water
PBS	phosphate buffered saline
SBF	simulated body fluid
BS	bovine serum
HA	hyaluronic acid
Agg	aggrecan
PVA	poly(vinylalcohol)
DMAA	dimethylacrylamide
PU	polyurethane
pHEMA	poly(2-hydroxyethyl methacrylate)
ATRP	atom transfer radical polymerization
MPC	2(methacryloyloxy)ethyl phosphorylcholine
UHMWPE	ultra high molecular weight poly ethylene
HBSS	Hanks' balanced salt solution
BSA	bovine serum albumin
EDTA	2,2',2'',2'''-(Ethane-1,2-diyldinitrilo)tetraacetic acid
SZP	superficial zone protein
DLC	diamond-like carbon
FCVA	filtered cathodic vacuum arc technique
PIII	plasma immersion ion implantation
ECAD	electrochemically-assisted deposition
APTMS	aminopropyltrimethoxysilane
PLA	polylactide
GO	graphene oxide
COF	coefficient of friction

WSD	wear scar diameter
XANES	X-ray absorption near edge structure spectroscopy
XPS	X-Ray photoelectron spectroscopy
DCM	double-crystal monochromator
TEY	total electron yield
AW	anti wear
SXM	scanning XPS microprobe
ATR–FTIR	attenuated total reflectance Fourier transform infrared spectrum
AFM	atomic force microscopy

Symbols

symbol	**unit**	**definition**
f	[-]	coefficient of friction
η	Pa·s	viscosity of the lubricating oil
F_N	N	normal load
v	m/s	velocity
R_{a1}	nm	surface roughness based on the area of the surfaces 1 (ball)
R_{a2}	nm	surface roughness based on the area of the surfaces 2 (ring)
R_a	nm	composite roughness

Contents

Part I

Part II

Paper A: J. Yan, X. Zeng, T. Ren and E. van der Heide. Boundary lubrication of stainless steel and CoCrMo alloy materials based on three ester-based additives. Tribology International, 2014, 73, 88-94.

Paper B: J. Yan, X. Zeng, T. Ren and E. van der Heide. Boundary lubrication of stainless steel and CoCrMo alloys based on phosphorous and boron compounds in an oil-in-water emulsion. Applied Surface Science, 2014, 315, 415-424..

Paper C: J. Yan, X. Zeng, T. Ren and E. van der Heide. The synergy between graphene oxide and surface-active polymers in aqueous lubrication of CoCrMo alloys. Submitted to Scientific Reports, 06-2014.

Paper D: J. Yan, X. Zeng, E. van der Heide and T. Ren. The tribological performance and tribochemical analysis of novel borate esters as lubricant additives in rapeseed oil. Tribology International, 2014, 71, 149–157.

Publication (not included in the thesis)

Paper E: J. Yan, X. Zeng, E. van der Heide, T. Ren and Y. Zhao. The tribological behaviour and tribochemical study of B–N type borate esters in rapeseed oil—compound *versus* salt, RSC Advances, 2014, 4, 20940–20947.

Conference contributions

1. J. Yan, X. Zeng, T. Ren and E. van der Heide. The synergy effect between graphene oxide and poly(ethylene glycol) for the boundary lubrication of CoCrMo alloy in aqueous system. The 7th China International Symposium on Tribology (CIST7), April 27-30, 2014, Xuzhou, China, p336-338.

2. J. Yan, X. Zeng, E. van der Heide and T. Ren. The tribochemical study of novel phosphorous-nitrogen (P-N) type phosphoramidate additives in water. The 5th World Tribology Congress, September 8-13, 2013, Torino, Italy, p37.

3. J. Yan, X. Zeng, T. Ren and E. van der Heide. Boundary lubrication of stainless steel and CoCrMo materials based on phosphorous or boron containing additives. The 5th World Tribology Congress, September 8-13, 2013, Torino, Italy, p32.

4. J. Yan, X. Zeng, E. van der Heide and T. Ren. The tribological study of novel borate esters as lubricant additives in rapeseed oil, BP Castrol-RSC 2013 International Symposium on Tribology and Lubricants, November 19-21, 2013, Shanghai, China.

Chapter I Introduction

Lubrication plays an important role in manufacturing processes, in machine components but also in the human body, as it reduces friction and prevents excessive wear of interacting surfaces. A conventional lubricant consists of a base oil and additives, yet aqueous media-based lubrication is drawing more and more attention because of the advantages related to fire resistance, thermal conductivity, toxicity and biodegradability [1, 2]. The use of water-based lubrication in engineering can be traced back to about 2400 BC, when Egyptians most likely used water as a lubricant in transporting statues, of which an example is shown in Fig. 1.1 [3]. Currently, aqueous fluids are used extensively as lubricants in metal working processes and in food processing. Furthermore, examples of well performing aqueous lubricants can be found in biological systems [4-8]. Water-based liquids, for example, function excellently as lubricants in joints such as exist in knees or hips, with a coefficient of friction that could be less than 0.002 [9]. Until now this ultra-low level of friction has not been reached with engineering surfaces and man-made aqueous systems. Compared to oil, water has many unique properties, such as the polarity of the molecule, which makes that aqueous lubrication technology distinctively differs from oil-based lubrication. However, water-based lubricants also have specific disadvantages, such as corrosiveness, the risk of vaporization and low viscosity [10-12].

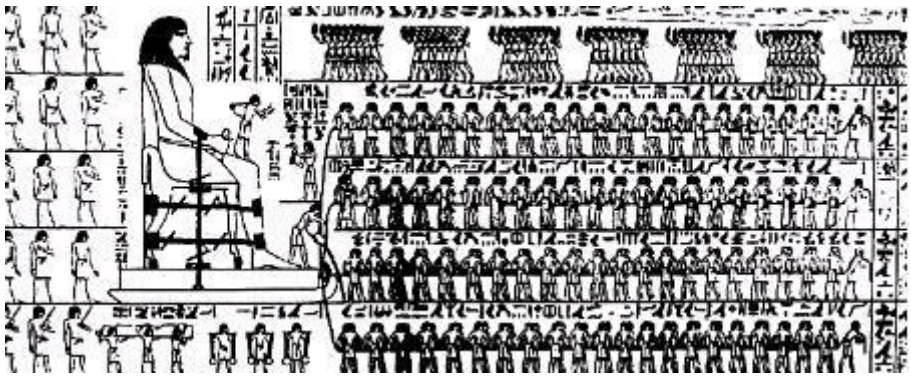

Fig. 1.1 Transporting an Egyptian statue by means of lubrication, extracted from [3]

Lubrication is the process, or technique, employed to reduce the friction and wear between two load-bearing surfaces by the application of a lubricant. Three distinct regimes can be observed with respect to the mode of lubrication, as the load increases on two contacting surfaces in relative motion, i.e. boundary lubrication (BL), mixed lubrication (ML) and hydrodynamic lubrication (HL), as shown in Fig. 1.2 [13]. This curve is named after Stribeck who expressed the relationship between the coefficient of friction f, viscosity of the lubricating oil η, normal load F_N, and velocity v, already in 1902 [14]. Boundary lubrication occurs when the bodies approach at the level of the asperities. The frictional heat developed by the local pressures and interfacial shear initiates chemically reactive constituents of the lubricant to react with the contacting surfaces, forming a highly protective layer. This boundary film is capable of maintaining surface separation and of preventing excessive wear. The velocity difference of the two surfaces is accommodated by shearing of the thin boundary layer. Boundary lubrication is defined as 'a condition of lubrication in which the friction and wear between two surfaces in relative motion are determined by the properties of the surfaces, and by the properties of the lubricant other than bulk viscosity' [15]. Typically f is in the range of $0.1 < f < 0.3$.

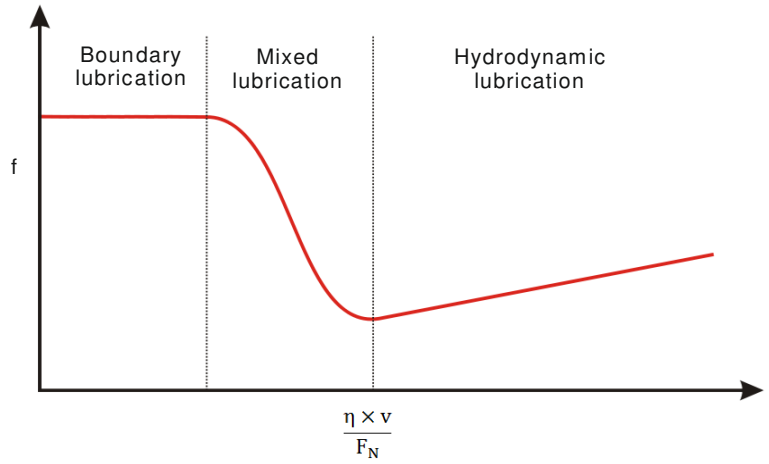

Fig. 1.2 The regimes of lubrication and Stribeck curve

Several studies focus on the mechanisms of aqueous lubrication, and major efforts are made to reduce the friction force in aqueous systems with sliding contacts. The latter are mainly directed to enhancing the film formation ability [16, 17]. Other researches are focused on minimizing wear and corrosion by materials technology and the application of alternative materials. Water-based

lubrication depends strongly on the performance of the lubricant in the boundary lubrication regime, as the viscosity of water is generally too low to generate the pressure that is needed to enter the mixed lubrication regime. Poor performance in the boundary lubrication regime directly causes high friction and high wear which, combined with the high risk of electrochemical corrosion, currently limits the use of water as a lubricant.

1.1 Tribological system

The tribological system approach is used in this thesis to study the tribology of boundary lubrication in aqueous systems. Basically this means that a tribological contact situation is separated from the applications studied, by using a hypothetical system envelope. The contact situation separated by this envelope is regarded as a system, i.e. a set of elements, interconnected by structure and function. Fig. 1.3 shows the tribosystem that is used in this thesis and which is assumed to be representative for the applications of interest. It includes three elements [18], which are the interacting surfaces in relative motion, the lubricating aqueous medium and the surrounding environment [19]. The connections between the system and the rest of the application are reduced to input: the operating variables, and output: friction and wear. An overview of possible operating variables is given by [20] for human joints and in [21] for metal forming operations. These references show that the set of variables, involved in tribological contact situations of interest and their relative importance, strongly depends on the actual application. In this thesis the sliding velocity and the load or contact pressure are taken as main operating variables. The loss-output of the tribosystems is described in this thesis by measuring and classifying the friction and wear characteristics, of critical aspects, of the tribological systems at a laboratory scale.

1.2 Objective of this research

The overall objective of this thesis is to explore new lubrication concepts for aqueous environments and, more specifically, to reveal the tribochemical mechanisms that determine the tribological response of poly(ethylene glycol)-*graft*-poly(acrylic acid) (PEG-*g*-PAA) coatings on engineering surfaces of

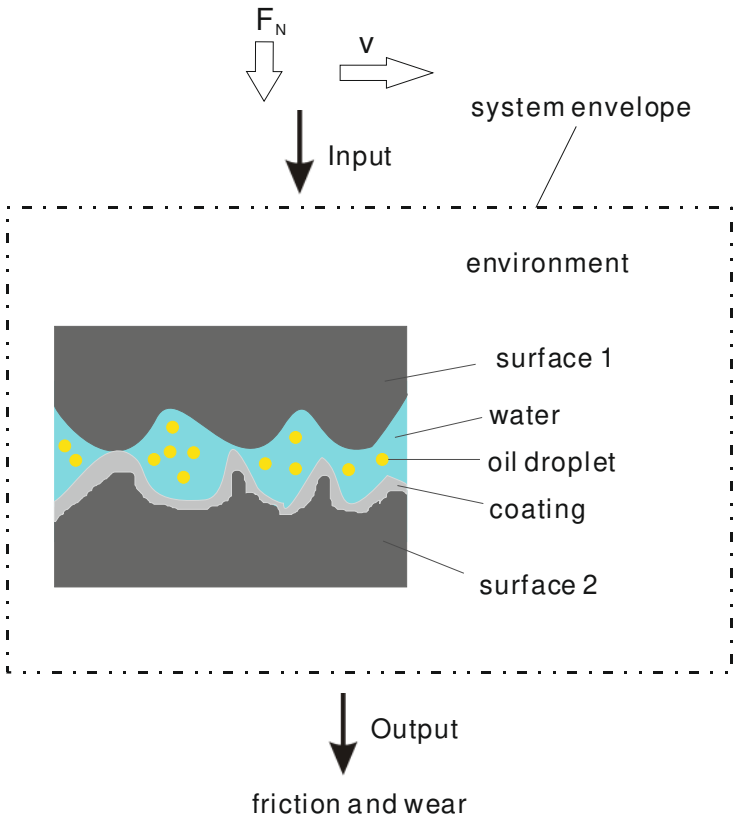

Fig. 1.3 Schematic tribological system

stainless steel and CoCrMo-alloys, hydrated with water only, and hydrated with 2.0 wt. % additives oil in water (O/W) emulsions. The latter includes exploring new additives that can be functional to stainless steel and CoCrMo.

1.3 Outline of this thesis

This thesis consists of two parts: Part I and Part II. Part I starts with an introduction. In Chapter II water lubrication is reviewed and the approaches for aqueous lubrication are summarized. The mechanism and chemistry of hydration lubrication, and brush coatings used in hydration lubrication has been reviewed as well. Sections of Chapter II show the current use of hydration lubrication for stainless and CoCrMo. Furthermore, inorganic and organic coatings are presented for the two metallic surfaces that, although developed for other applications, can be used potentially in biomedical applications.

Chapter III summarizes the assumptions that are made and gives an overview of the new concepts that are developed in this work, having in mind biomedical

applications. This chapter introduces the concept of a brush coating and it introduces graphene oxide. Lubrication with emulsion as well as the emulsion lubrication of amphiphilic coatings is utilized.

Chapter IV focuses on measuring friction in the boundary lubrication regime. The friction and wear behaviour in O/W emulsions as well as the interaction between metals and additives are examined. Next, the tribological properties of CoCrMo both at the micro scale (based on an AFM protocol) and at the macro scale (based on a pin-on-disk protocol) are studied.

Finally, Chapter V presents the conclusions of the thesis accompanied by recommendations for future research.

Part II presents detailed scientific achievements, which are discussed in research papers. Paper A and Paper B discusses the boundary lubrication of stainless steel and CoCrMo in oil, in water and in O/W emulsion systems. Paper C discusses the preparation, characterization and macro-scale tribological performance of hydrophilic coatings on CoCrMo alloy in different aqueous media. Paper D contains the reference measurements which serve as a start of this research. This paper is focused on the interaction between new additives and bearing steel.

The relationship of the chapters of Part I and the papers of Part II, as well as the schematic process, is outlined following Fig. 1.4.

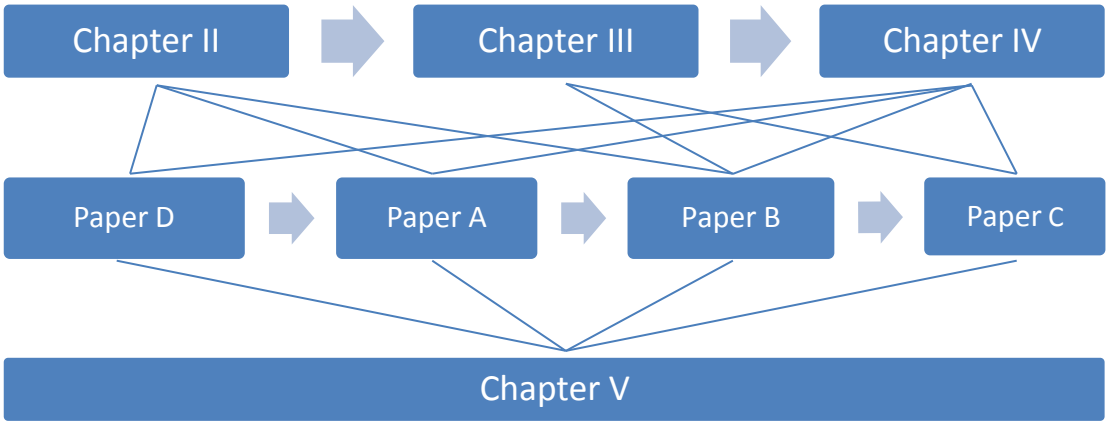

Fig 1.4 The schematic outline of the thesis and the relationship of the chapters and the papers

Chapter II Lubrication in an aqueous environment

2.1 Why aqueous lubrication?

Control over friction and wear during sliding is needed to ensure the proper functioning of the tribological system. One of the approaches is to use well selected and carefully formulated lubricants, as lubricants can provide a low shear strength layer separating the interacting surfaces. Thus, lubrication can reduce the mechanical damages that arise from accommodating the velocity difference in sliding contacts. The lubricant film can be a solid, e.g. graphite and MoS_2, a solid/liquid dispersion, a liquid, or, exceptionally, a gas. Most of the conventional lubricants are liquids. Many liquids have been used as lubricants to minimize the friction, heat, and wear between mechanical parts in contact with each other. Typically, lubricants are oil based or water based. Oil lubrication is traditionally used for mechanical applications, and lubrication theory and technology were developed based on using oil in these systems. The classical Reynolds Equation is used to describe the pressure distribution in oil films of bearings [22]. Most of the commercial additives are for oil-based lubrication [23]. However, oil-based lubricants have some major drawbacks such as poor biodegradability and high toxicity for humans. As such, oil-based lubricants cannot be used for applications with a high risk of polluting the environment or for applications that involve a bio-medical environment, respectively. Water-based lubricants, on the one hand, can potentially overcome these problems while maintaining the required high level of tribological performance. There are some examples of successful application in hydraulic fluids, cutting fluid for metal working and other fields as a substitute for the oil-based lubricants [24]. On the other hand, water is a natural medium for biological lubrication and can also be found in some biomedical devices [40, 41].

2.1.1 Oil lubrication

Oil lubrication is widely used for mechanical components. Typically, a lubricant consists of a mixture of a base oil and additives to improve the properties of the base stock. For the base oil, mineral oil is typically used, as it is thermally more stable than vegetable oil and cheaper than synthetic esters. Traditionally

formulated oil-based additives contain phosphorus, sulphur, chlorine and other metal elements e.g. zinc, to reduce friction and to minimize wear. Much of the current research on lubricant technology is directed towards replacing these metals by an alternative with less ash formation during use. Furthermore, environmental legislation has created a need for chlorine-free, odourless and low phosphorus additives. Phosphorus–nitrogen additives with lower phosphorus content have been successfully used for boundary lubrication of ball bearing steel AISI 52100 because they can be easily prepared and proved to be multifunctional [25-28]. The boundary film formed with phosphorus–nitrogen additives consists mainly of $FePO_4$ [29]. Other kinds of alternative additives, i.e. borate calcium and borate esters, have received extensive attention because of the expected high anti-wear potential and pleasant odour [30]. Borate calcium used to be difficult to dissolve in oil, while more and more application can be found now because it can be produced as nano scale particles which can enhance the dispersion into base media [31, 32]. Also borate calcium was found to form $CaCO_3$ which is proved to be a robust film [33, 34]. The problem for borate esters was the poor hydrolytic stability, while the hydrolytic stability can be enhanced by introducing nitrogen and some other elements [35, 36]. Furthermore, phosphorous, calcium and boron elements have a positive impact on the development of cells and tissues which can be studied as a start for being potentially used in a biomedical environment [37].

2.1.2 Water lubrication for mechanical systems and production processes

Current industrial applications involving water-based lubrication make use of the cooling capability, low toxicity and fire resistance properties of aqueous fluids [38]. Water obviously plays an important role in the lubrication, yet water has very poor lubricating properties related to the low viscosity [39]. Therefore, technology is developed to change the base stock from water to other fluids such as polyethylene glycol and other water-soluble compounds [40]. Secondly, work focused on lubricating additives is conducted to enhance the tribological properties of the lubricating fluid. These additives cannot be dissolved in water directly, but they can be dissolved in oil and mixed with water using emulsifiers. The resulting fluid is called an oil-in-water (O/W) emulsion and the lubrication with an O/W emulsion is referred to as emulsion lubrication. The beneficial lubricating and cooling properties of O/W emulsions have driven their

application in metal forming operations such as rolling, cutting, ironing or grinding [41-45]. O/W emulsions are also widely used as lubricants/coolants in the ironing of beverage and food containers [45]. They have the dual capability of providing good cooling and lubrication. Non-inflammability and low cost are additional features of O/W emulsions which make them attractive, for example, for cold rolling of steel [46, 47].

An O/W emulsion is generally regarded as a two-phase heterogeneous mixture of oil and water, where the oil component remains in the dispersed phase and water forms the continuous phase, see Fig. 2.1. The oil phase contains base oil, lubricating additives, and an emulsifier. The emulsifier keeps the droplets from combining together. The molecular structure of an emulsifier has, in general, hydrophilic and lipophilic ends. The hydrophilic end is made of polar bonds and is soluble in water, while the lipophilic end is soluble in oil. When the emulsion is formed, the oil droplets formed by the process are such that the hydrophilic ends orient towards the water phase and lipophilic hydrocarbon chains orient towards the oil phase [48-50].

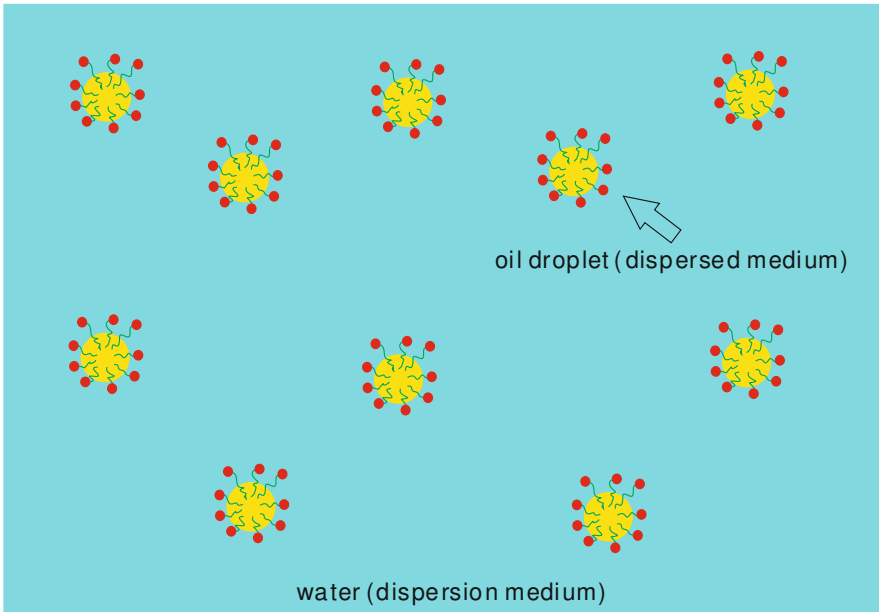

Fig. 2.1 Oil-in-water emulsion showing the oil droplets dispersed in water with the interaction with the emulsifier. An emulsifier is a surfactant with hydrophilic heads (red dots) and lipophilic tails (green chains).

Researchers have conventionally attributed emulsion effectiveness in lubricating contacts to the idea that droplets 'plate out' onto exposed metal surfaces, but the mechanisms related to oil droplet entrainment in the contact are not yet well understood especially with respect to the tribochemical interaction between the additives and the metals. The 'plate out' process is schematically drawn in Fig. 2.2 [51-53]. In stage a), the oil droplets suspend in water, then in stage b) the oil droplets adsorb onto the metal surface. Then, the oil droplets plate out on the surface as shown in stage c), finally the multiple plated droplets form an oil film. The film-forming ability of O/W emulsions as a function of emulsifier concentration was studied by Cambiella et al. [48]. The emulsifier content exerts a strong influence on all the emulsion properties, such as stability, droplet size distribution, surface and interfacial tension, wetting ability, as well as on the lubricating behaviour. Frequently used emulsifiers in the lubrication are nonionic surfactants [54, 55]. For instance, polysorbate 80 (commercial name Tween-80) is a nonionic surfactant and emulsifier derived from polyethoxylated sorbitan and oleic acid [56].

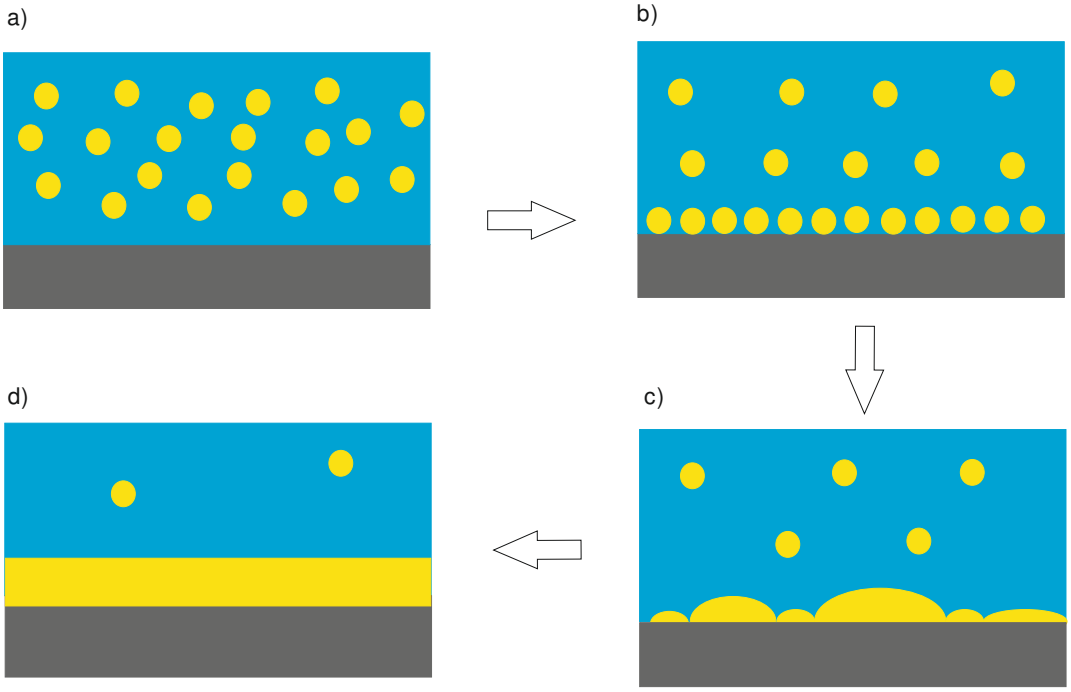

Fig. 2.2 Plate-out process of oil droplets in O/W emulsion, a) the oil droplets (yellow) dispersed in water (blue); b) the oil droplets adsorbed onto the metal (black) surface; c) the oil droplets spread on the metal surface and turn to completely plated droplets; d) multiple plated droplets form an oil film.

2.1.3 Synovial fluid – a natural water-based lubricant

Synovial fluid is a viscous fluid found in the cavities of synovial joints. Besides the function in the nutrition of articular cartilage, synovial fluid can improve the mechanical function of joints by lubricating articulating surfaces, that is, to reduce friction between the articular cartilage of synovial joints during movement [57, 58]. Most of the applied load on human joints is supported by the articular cartilage, which contains about 75 wt. % of water, and is regarded as a gel-like elastic material. Synovial fluid is a natural and water-based lubricant with high efficiency. Normal synovial fluid contains 3–4 mg/ml hyaluronan (hyaluronic acid), a polymer of disaccharides composed of D-glucuronic acid and D-N-acetylglucosamine joined by alternating beta-1,4 and beta-1,3 glycosidic bonds. The hyaluronan is synthesized by the synovial membrane and secreted into the joint cavity to increase the viscosity and elasticity of articular cartilages and to lubricate the surfaces between synovium and cartilage [59]. Experimental work on the tribological properties is typically conducted with distilled water, NaCl solution, phosphate buffered saline (PBS) (Table 2.1) [60] or simulated body fluid (SBF) (Table 2.2) [61, 62]. Another frequently used fluid to mimic synovial fluid is bovine serum (BS) [63-66].

Table 2.1 Composition of phosphate buffered saline

Compound	Concentration (mmol/L)	Concentration (g/L)
NaCl	137	8.0
KCl	2.7	0.2
Na_2HPO_4	10	1.44
KH_2PO_4	1.8	0.24

Table 2.2 Composition of simulated body fluid (SBF)

Ion	Simulated body fluid (mmol/L)	Human blood plasma (mmol/L)
Na^+	142.0	142.0
K^+	5.0	5.0
Mg^{2+}	1.5	1.5
Ca^{2+}	2.5	2.5
Cl^-	148.8	103.0
HCO_3^-	4.2	27.0
HPO_4^{2-}	1.0	1.0
SO_4^{2-}	0.5	0.5

2.2 Approaches for aqueous lubrication

2.2.1 Hydration lubrication - definition and mechanism

Hydration lubrication is a special kind of lubrication, involving water and involving a surface layer of hydrophilic polymers fixed to the surface. It originates from hydration of the surface layers, and the lubricating mode is recognized as completely different from the classic mode of oils [67]. Distinct features [68] are:

1. On the approach of two bodies, pressure rises in the surface layer and a repulsive force arises between them and most of the applied load is supported by water.

2. Under sliding motion, the water molecules are sheared with low stress, whereas the polymers are fixed to the surface.

Hydration lubrication can be created by hydrated ions, polymer-brushes, amphiphilic surfactants under water and by liposomes. The latter is the case for the applications in biological systems like in human joints, because articular cartilage works based on hydration lubrication.

The use of water for tribological applications has attracted considerable attention in the past years [7, 9, 69-74], especially since the mechanisms and chemistry of hydration lubrication are understood at an engineering level.
Hydration lubrication starts with the hydrated layers, which are formed by the hydrophilic polymers and water on the interacting surfaces during sliding. Some polymers are grafted on to the surface and others are grafted from a water-based fluid on to the surface to create a boundary layer, well designed for friction control in aqueous environments [75]. When two surfaces approach, pressure rises in the surface layer and a repulsive force arises between them. Then water molecules attracted by the polymers are sheared, while the polymers are attached to the surface (see Fig. 2.3). Therefore, the applied compressive force is normally supported by the fluid [75].

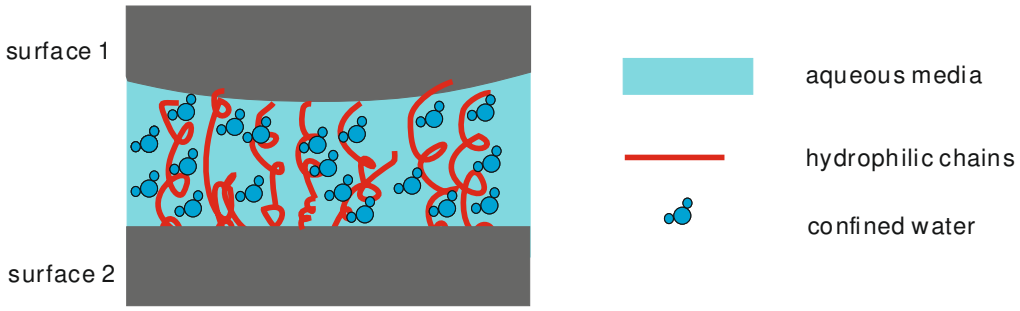

Fig. 2.3 The brush coatings in aqueous media

2.2.2 Water as a lubricating fluid

Some tribological properties of water can be attributed to the fluidity of water in confined thin films [76]. That is to say, when oils and some organic compounds slide relative to each other, the confined layers become solid-like [77, 78]. However, if confined water is on the surface, even a monolayer, water can retain the fluidity [79]. Long-ranged and short-ranged forces should be considered when two solid surfaces approach each other across a fluid. Long-ranged forces, van der Waals forces, are related to electrostatic repulsions. The forces are the sum of the attractive or repulsive forces between molecules (or between parts of the same molecule) or the electrostatic interaction of ions with one another or with neutral molecules or charged molecules. The forces are less than those forces related to covalent bonds or the hydrogen bonds [80]. The short-ranged forces sometimes are called steric forces or solvation forces which arise from the interactions of the adsorbed molecules of the confined liquids [81]. As mentioned before, the fluidity of water in very thin films is different from oils and organic solvents which solidify under the confinements. Normally there is a gap between the two surfaces, and the liquids tend to be adsorbed on the surface. There are several layers of molecules attached tightly to the very close surface. The density of these layers is higher than the bulk liquids. When the two surfaces slide very closely, the overlap even is thinner than the two layers of the liquid molecules and the layers become denser than the bulk liquids. For oils and organics, the solid phase is denser than the liquid phase, and then the adsorbed layers tend to solidify [82]. For water, on the other hand, the liquid phase is denser than the solid phase. Therefore, water retains the fluidity of the bulk liquid [83].

As is shown in Fig. 2.4, water has an electric dipole due to the electronegativity of hydrogen and oxygen. When water molecules surround charges in aqueous media to form hydration layers on the surface, the energy related to hydration of charges leads to hydration repulsion effects [84]. Normally the energy associated with charge hydration results in a strong and short-ranged repulsion of steric force. The fact that the hydration effect can lead to strong repulsion when two surfaces interact can also be proved by a high-concentration salt solution. This short-ranged repulsion is big enough by far to overcome the van der Waals force between the surfaces. There are several studies related to the estimate of the pressure caused by hydrated repulsion effect. When the liquid is an 0.1 M alkali metal salt solution, the pressure between the mica surface and the solution is measured up to around 10 MPa [85, 86]. This means that the hydration repulsion can support very high pressure to overcome the van der Waals force between the two surfaces.

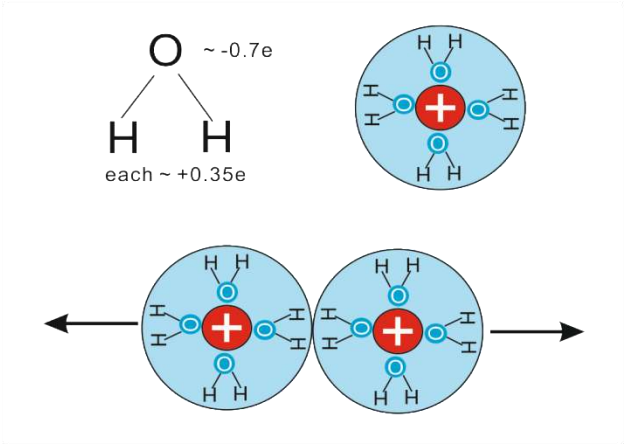

Fig. 2.4 The hydration shells of water and their repulsive interaction, extracted from [81]

2.2.3 Tribochemical aspects related to hydration lubrication

By studying the shear forces between charged polymer brushes in water, Raviv [72] discovered that the hydrated brushes can form boundary layers much more effectively than neutral polymer brushes. The brushes are also more robust than the adsorption brushes, and the coefficient of friction is measured as low as 0.0004 in pure water at around 8 MPa [9].

The mechanism of boundary lubrication by surfactants can be described as follows: the surfaces were coated with the monolayer of a polar group head and an alkyl tail when the surfaces were sliding past each other. Generally, the head

groups attach to the surface to form the boundary layers. Due to the weak shear strength of the van der Waals force between the layers, they can protect the substrates from contact and wear [87]. But when water is added to the system, it can penetrate the surfactant layers to hydrate the polar heads at each substrate surface. The surfaces of substrate like metals or micas generally possess negative charges. Then the charged head group layers can be hydrated and the lubrication changes to the hydration lubrication mechanism [88, 89]. Liposome can be seen as an emulsion given the similarities in boundary layer structure [90]. Hence, liposomes provide possibilities for biological and medical applications where most surfactants cannot be applied because of reasons of toxicity.

Another interesting example of the tribochemistry of water in hydration lubrication is found in the behaviour of synovial fluid. A typical hip or knee joint possesses a layer of articular cartilage which is like the coat of the articulating bones. The synovial fluid serves as an aqueous lubricant. Synovial fluids contain hyaluronic acid (HA), polysaccharide, aggrecan (Agg) and proteoglycan. In several experiments HA was adsorbed on mica, but the measured tribological properties are poor. This may be due to the relatively poor hydration of the negative charged groups ($-COO^-$ in HA and $-SO_3^-$ in Agg). The negative groups cannot adsorb on to the negative mica surface [91].

In summary, hydration layers are strongly attached by the charged water they surround, and can support contact pressures relevant to engineering applications, without being squeezed out. At the same time, hydration layers remain very rapidly relaxing and have a fluidic response to shear [81]. Therefore hydration lubrication provides a framework for understanding, controlling, and designing efficient boundary lubrication systems in aqueous media.

2.2.4 Current state-of-the-art in brush coatings and applications

Water-soluble polymers are widely used for hydrophilic coatings. Poly(L-lysine)-*graft*-(poly(ethylene glycol, PEG) can graft on to a surface to form a brush-like layer. It is shown that the solvent absorbed within the brush plays an important role in lubrication of a sliding contact [92]. An increase in the molecular weight of the PEG side chains and a reduction in grafting ratio result in an improvement of lubrication condition at low velocities, and an increase in the

solvent absorbed in the brush results in a lower friction force [93]. Poly(vinylalcohol) (PVA) can also be grafted on to polyethylene and this is used as a model for an artificial joint [94, 95]. Dimethylacrylamide (DMAA) hydrogel was coated on a polyethylene femoral head and then frictional behaviour against a stainless steel cup was studied [96]. Low friction forces are found which are attributed to the formation of a highly viscous zone through hydration of DMAA at the solid/liquid interface. Poly(2-methacryloyloxyethyl phosphorylcholine-co-n-butyl methacrylate) ([poly(MPC-co-BMA]) was evaluated as a potential coating material for vascular applications to provide smooth catheterization [97]. The coating on the polyurethane (PU) substrate gives rise to low friction forces in sliding because it enhances boundary lubrication due to the hydration of phosphoryleholine when compared to uncoated PU surfaces. These tribochemical observations of the [poly(MPC-co-BMA)] coating suggest that the overall efficacy of PU for clinical applications could increase.

Graft polymerization is the second strategy to produce a surface with a hydrogel layer or a polymer brush. It is reported that the coefficient of friction of a catheter with a graft polymerized brush surface in sliding contact with human tissue is very low because of the effect of hydration lubrication [98]. Due to the fact that the polymers are bonded chemically to the surface, normally a grafted surface layer is much stronger than an adsorbed one. A densely grafted surface can maintain a good lubrication condition for a short time. If the applied load increases, water is discharged from the surface layer and the friction force increases for several minutes until a new equilibrium condition is reached [99]. A biocompatible polymer was grafted on to the surface of artificial joints in order to prevent periprosthetic osteolysis [100]. By the use of surface-initiated atom transfer radical polymerization, a low-polydispersity poly(2-hydroxyethyl methacrylate) (pHEMA) was densely grafted on to the inner surfaces of silica monoliths [101]. The interaction of concentrated polymer brushes with proteins was chromatographically investigated. The inertness of the concentrated brush in the interaction with the large proteins improved the system's long-term stability against biofouling.

Polyzwitterionic brushes and liposomes can also be used as coatings effective in decreasing friction. Wei et al. reported a method of tuning friction using responsive polyelectrolyte brushes, and found that the friction of anionic brushes can be tuned by oppositely charged surfactants (tetraalkylammonium) with different lengths of lipophilic tails, multivalent metal ions, and protons [102]. Polyzwitterionic brushes were designed with a structure similar to the highly-hydrated phosphorylcholine head groups of phosphatidylcholine lipids. Such polyzwitterions are grown from a macroinitiator coating the substrate (mica) surface using atom transfer radical polymerization (ATRP) of 2(methacryloyloxy)ethyl phosphorylcholine (MPC) to form exceptionally robust poly(MPC) brushes [103]. Liposomes are also designed to be adsorbed as lubricants for the lubrication mechanism study. It is shown that the low friction is attributed to the hydration lubrication mechanism arising from rubbing of the highly hydrated phosphocholine-head group layers exposed at the outer surface of each liposome, and provides support for the conjecture that phospholipids may play a significant role in biological lubrication [104]. Quintana et al. reported some low fouling zwitterionic polymer brushes with diblock architecture which can enhance the stability in seawater [105]. Hydrophilic polymer brushes can also improve the wettability and antifouling behaviour of the surfaces [106]. The low adhesion force between the brush and the oil could contribute to the good antifouling and self-cleaning properties.

From the reported studies, it shows that normally the frictional behaviour was enhanced due to the hydrated layer. If the polymers are chemically bonded to the surface, the durability is satisfied for surfaces such as mica, silica wafer and steel [107].

Only a few applications have been found for stainless steel with hydrogels. Freeman et al. reported the tribological behaviour of synthesized poly(2-hydroxyethyl)methacrylate (pHEMA) hydrogels for biotribology research [108]. It shows that interactions between hydration and lubrication as well as hydration and crosslinking on wear were significant. Similarly, Bavaresco et al. used UHMWPE coated with pHEMA hydrogel as a pin, a stainless steel 316L as a disk, and distilled water as lubricant [109]. They found that as the crosslinking density of hydrogels increased, the capacity of absorption of water is reduced

and the dominant wear mechanism becomes abrasion. Ishikawa et al. studied the behaviour of a stainless steel acetabular cup against a polyethylene femoral head coated with dimethylacrylamide (DMAA) hydrogel, and hyaluronic acid (HA) as lubricant [96]. Lee et al. found that PLL-*g*-PEG behaves as a very unique and effective aqueous boundary lubricant additive for the sliding contact of thermoplastics against themselves as well as against many hydrophilic, polar materials, including metals (e.g. stainless steel) or ceramics [110].

2.3 Stainless steel and CoCrMo

2.3.1 The effect of stainless steel and CoCrMo on water lubrication

The aqueous environment differs greatly from an oil-based environment with respect to the risk of corrosion. Therefore non-metallic materials like ceramics and polymers are developed for sliding in aqueous systems. Yet, in some cases, corrosion resistance needs to be combined with mechanical strength, hardness and wear resistance. Stainless steel and CoCrMo surfaces are frequently used in tribological applications that require this type of combination of hardness, wear resistance and corrosion resistance. Examples within the scope of this thesis are found in a biomedical environment: hip joint replacements, implants and minimally invasive – medical – tools like catheters, endoscopes and cytoscopes. The second set of examples is found in industrial applications where environmental conditions require the use of minimal lubrication or preferably water lubrication: sliding parts in food processing equipment, outdoor equipment and maritime environments. Low friction and wear are needed in both of the applications, therefore a new lubrication concept has to be raised to overcome the limit of the applications nowdays.

The tribosystems in the latter applications are characterized by sliding contacts in the presence of water-based fluids and by the interaction either with biological material or with CoCrMo and stainless steel counter surfaces. The performance of these systems is determined greatly by friction. Friction is sometimes needed, for example, for grip during operation but friction can also initiate failure or can cause irritation during use. Friction control is required for constant performance during use. Material selection for engineering applications in a corrosive environment is typically based on materials that can withstand close and

prolonged contact with reducing environments such as water, or physiological fluids [111, 112]. Metallic biomaterials have been widely used in replacing the structural components of the human body because of their excellent mechanical properties such as tensile and fatigue strengths [113-115]. Metal-on-metal implants e.g. do not wear out as quickly as a combination of metallic and polymer materials. The metal - polymer implants wear at a rate of about 0.1 millimetres each year. Metal-on-metal implants wear at a rate of about 0.01 millimetres each year, about 10 times less than metal - polymer [116]. The lower wear rate of metal combinations than metal- or ceramic-on-Ultra High Molecular Weight Poly Ethylene (UHMWPE) combinations is shown in Fig. 2.5. Compared to metal-on-polymer materials, metal-on-metal joints could reduce wear-debris-triggered osteolysis and have better durability due to the associated lower specific wear rate, that is: in the case of fully lubrication conditions. Dry metallic contacts will cause catastrophic failure due to severe scratching and local solid phase welding. The most common metal alloys used in joint implants are stainless steels and cobalt-chromium alloys. Titanium alloys and other metallic alloys are out of the scope of the current work.

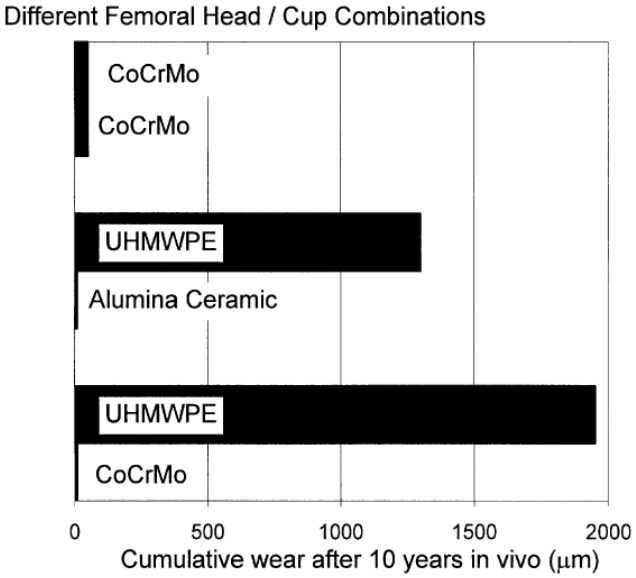

Fig. 2.5 Comparison of wear behaviour of different material combinations, extracted from [117]

2.3.1.1 Stainless steel

Based on the excellent mechanical properties, such as high tensile strength and toughness in combination with the required corrosion and wear resistance,

stainless steels have been widely used in roller bearing applications and replace e.g. standard ball bearing steel AISI 52100 for roller bearing applications [118]. Applications are found in mechanical components at sea, food processing equipment, medical devices for minimally invasive surgery, but also in joint replacement materials [119, 120]. Specifically, stainless steel is used for implants that are intended to help repair fractures, such as bone plates, bone screws, pins, and rods. Stainless steel consists mainly of Fe-C, alloyed with chromium, nickel and molybdenum to make it more resistant to corrosion. The stainless steels used for joint implants can resist the chemicals found in the human body. Stainless steel 316L / X5 CrNiMo17-12-2 is widely used in traumatological temporary devices such as fracture plates, screws and hip nails. The 'L' refers to low carbon content to increase the weldability of the material. The chemical composition and mechanical properties of 316L and CoCrMo alloy (ASTM F75) are shown in Table 2.3 and Table 2.4.

Table 2.3 Chemical composition (wt. %) of 316L stainless steel and a CoCrMo alloy

316L stainless steel		Co-28Cr-6Mo	
C	<=0.03	Cr	26-29
Mn	<=2.0	Mo	4.5-6.0
Si	<=1.0	C	0.20-0.35
S	<0.03	Ni	2.0-3.0
P	<=0.045	Fe	<0.75
Cr	16 - 18	Si	<1.0
Ni	10 - 14	Mn	<1.0
Mo	2.0 - 3.0	Co	Balance
Fe	Balance		

Table 2.4 Mechanical properties of 316L and a CoCrMo alloy.

	316L stainless steel	Co-28Cr-6Mo
Tensile strength, 0.2% (MPa)	280	270
Ultimate tensile strength (MPa)	635	1000
Ultimate elongation (%)	49	20
Young's modulus, *E* (GPa)	200	245

Poisson's ratio, *v*	0.3	0.3
Hardness	HRC 28 – 38	HRC 25 - 35

Stainless steel has resistance to a wide range of corrosive agents due to its high Cr content, therefore it is widely used in medical tools. The Cr in the stainless steel allows the formation of a film of chromium oxide on the surface of the steel at a molecular level which is passive, adhesive, tenacious and self-healing [112]. In spite of this fact, Singh & Dahotre [121] indicated that stainless steel implants are often degraded due to pitting, corrosion fatigue, fretting corrosion, stress corrosion cracking, and galvanic corrosion in the body. Worse corrosion resistance, as well as the danger of an allergic reaction in patients [112], restricts their application in an orthopaedic joint prosthesis. Moreover, the Young's modulus of stainless steel is about 200 GPa, which is much higher than that of bone. Due to its limited ability to withstand corrosion in the human body for a long time, stainless steel is not often used in joint replacement implants. It is more suited to being used for temporary implants such as fracture plates and screws. Water-based lubricants and O/W emulsions can be used for stainless steel for the study of sheet metal forming and corrosion protection. Besides, the lubrication of stainless steel has also been studied in seawater [122], tap water [123] and even vapour water and other aqueous systems [124].

2.3.1.1 CoCrMo alloys

Cobalt-chromium alloys are also strong, hard and corrosion resistant, even at elevated temperatures. Alloying elements, such as molybdenum, increase their strength [125]. They are used in a variety of joint replacement implants, as well as some fracture repair implants, that require a longer service life. The alloy composition used in orthopaedic implants is described in standard ASTM-F75 [126]: cobalt with 27 to 30 wt.% chromium, 5 to 7 wt.% molybdenum, and limits on other alloying elements such as manganese and silicon, less than 1 wt.%, iron, less than 0.75 wt.%, nickel, less than 0.5 wt.%, and carbon, nitrogen, tungsten, phosphorus, sulphur and boron. The typical chemical composition of cobalt chromium molybdenum alloy Stellite 21 is shown in Table 2.3 and the mechanical property is shown in Table 2.4.

CoCrMo can be used in aqueous systems and even in acidic systems [127]. Saramago et al. investigated friction and wear mechanisms in hip prostheses by comparing the tribological performance of several materials in water-based lubricants [128]. UMWPE was used as acetabular cup material and alumina, stainless steel or CoCrMo alloy for the femoral head. Four lubricants were used: Hanks' balanced salt solution (HBSS) and solutions of bovine serum albumin (BSA), of hyaluronic acid (HA) and of both components (BSA+HA) in HBSS. The results indicate that the presence of albumin in the lubricant avoids the adhesion and transfer of UHMWPE only for the least hydrophilic surfaces, which are the metallic ones. Gilbert et al. reported on the electrochemical response of CoCrMo to high-speed fracture of its metal oxide by using an electrochemical scratch test method [129]. The scratch or wear behaviour changed owing to the availability of oxygen from the hydrolysis of water. Better behaviour in the presence of albumin may have been due to barrier effects of the adsorbed protein preventing water from reaching the sample surface. The corrosion and dissolution of high- and low-carbon CoCrMo alloys, as used in orthopaedic joint replacements, were studied by immersing samples in phosphate-buffered saline (PBS), water, and synovial fluid by Lewis et al. [130]. Milošev et al. reported similar effects of biomolecules on the behaviour of CoCrMo alloy in some simulated physiological solutions [131].

Other research with CoCrMo and stainless steel focuses on synovial fluid-related lubrication. Synovial joints have excellent friction and wear properties. The friction and wear characteristics of cartilage surfaces are investigated e.g. by sliding of the cartilage of an adult rat femur against a stainless steel plate [132]. It is found that the outer surface of orthopaedic cartilage is covered by a substance capable of providing lubrication for limited periods when synovial fluid is unable to prevent contact between opposing cartilage surfaces. Serum (bovine or calf serum) can be used as an alternative for synovial fluid [133]. The corrosion resistance of CoCrMo alloys was compared in serum, synovial fluid, albumin, 2,2',2'',2'''-(Ethane-1,2-diyldinitrilo)tetraacetic acid (EDTA), and water [134]. It is found that the components of synovial fluid have been identified as possible causes for the lack of significant calcium phosphate deposition in this environment. The composition of synovial fluid includes hyaluronic acid (HA), proteoglycans, pyrophosphates, phospholipids, lubricin, and superficial zone

protein (SZP). HA can also be used for the research of the biotribosystem. When the behaviour of CoCrMo alloy was studied in two simulated physiological solutions, NaCl and Hanks' solutions with HA, it was found that the addition of hyaluronic acid shifts the corrosion potential and increases the value of polarization resistance [135-137].

2.3.2 Coatings for stainless steel and CoCrMo alloy

2.3.2.1 Inorganic coatings

There are several thin inorganic hard coatings available to potentially enhance the surface properties of CoCrMo alloys [138-140]. Most of the reported work is based on a trial-and-error approach. Liu et al. reported a modified metal-on-polymer (CoCrMo/UHMWPE) combination with diamond-like carbon (DLC) coated and with nitrogen implanted CoCrMo surfaces [138]. For this a DLC film was deposited on a CoCrMo artificial hip joint head by filtered cathodic vacuum arc technique (FCVA) with a thickness of approximately 600 nm. Alternatively, nitrogen ions were implanted into the CoCrMo artificial hip joint head by plasma immersion ion implantation (PIII) technology. The results show that only applying the surface modification (DLC film or nitrogen ion implantation) on the CoCrMo head does not improve the wear resistance of a metal-on-polymer (CoCrMo/UHMWPE) combination. A nanostructured diamond coated CoCrMo alloy for use in biomedical implants is also reported by Lawson et al., but the results of wear tests are not promising [141]. Yang et al. reported deposition of ZrO_2 coating on CoCrMo implant materials using plasma spraying, but no significant difference between the hardness of all coatings and substrates was observed [139]. TiN/AlN-coated CoCrMo has a higher surface hardness and modulus of elasticity [140].

Soft compliant coatings can also be generated on the surface of CoCrMo alloys. Wang et al. reported a hydroxyapatite coating, efficiently generated on CoCrMo implant alloys by employing an electrochemically-assisted deposition (ECAD) pre-treatment followed by chemical immersion in a supersaturated calcification solution [142]. CoCrMo was electrochemically treated in a calcium- and phosphate-containing solution and a thin layer of about 200nm thickness, consisting mainly of amorphous calcium phosphate, was formed on the surface of

the CoCrMo after the treatment. Then after the chemical immersion, a layer of octacalcium phosphate was formed on the surfaces. A layer of hydroxyapatite was formed subsequently. The results showed that the ECAD pre-treatment highly enhanced the capability of formation of hydroxyapatite on the CoCrMo surface, while only a small amount of CaP islands were formed on CoCrMo through traditional chemical treatment. A tensile test showed that the coating is tightly bonded to the substrate.

For stainless steel, research is focused on the modification of the mechanical properties in combination with enhanced corrosion protection [143-147]. The substrate hardness is not sufficient to apply thin hard coatings. Thick hard coatings can be made by a thermal spraying process, yet the porosity of the coatings makes it unsuitable for applications inside the human body.

2.3.2.2 Organic coatings

Research on organic coatings for stainless steel is typically related to corrosion protection. Poly(o-ethylaniline) coatings are electrochemically synthesized on 304-stainless steel by using cyclic voltammetry from an aqueous salicylate medium [148]. The performance of poly(o-ethylaniline) as protective coating on AISI 304 is evaluated in aqueous 3% NaCl. The results demonstrate that the poly(o-ethylaniline) coating provides protection to both local and general corrosion of 304-stainless steel. Deberry also reported a modification of the electrochemical and corrosion behaviour of stainless steels with an electroactive coating [149]. Similarly, poly(3-octylthiophene) and polystyrene blends are able to give corrosion protection of stainless steel 304 [150].

Modification of metallic surfaces with bioactive molecules and/or nanoparticles to develop biomaterials that can interact with a biological environment, e. g. for cardiovascular stents, has recently attracted great attention. Successful adsorption of antibodies and enzymes on micro/nanoporous 316L stainless steel is reported [151]. The experimental results show that the micro/nanoporous stainless steel surface produced by electrochemical erosion can adsorb a large amount of proteins. The protein-coated porous surface was hydrophilic. The proteins at the micro/nanoporous stainless steel surface retain their high biological activity. Recently Kang et al. reported a biocompatible surface

modification technology composed of removing surface asperities by surface electropolishing and subsequent carbohydrate polymer grafting, which can be applied to stainless steel [152]. The coating process consists of an acid treatment, silanization, and covalent attachment of chitosan and dextran. The surface was changed from lipophilic to hydrophilic and from rough to smooth. Okner et al. reported a design of electrochemical co-deposition of sol-gel films on stainless steel which can be used to control the chemical and physical coating properties of biomedical implants [153, 154]. Based on aminopropyltriethoxysilane (APTS) and other coupling agents, the electrodeposition of films has been accomplished by applying negative potentials. The application of this approach can be potentially used for a stainless steel coronary stent.

For other applications, it has been demonstrated that surfaces coated with poly(ethylene glycol) (PEG) are capable of reducing protein adsorption, bacterial attachment, and biofilm formation [155]. Specifically, 12-crown-4-ether and tri(ethylene glycol) dimethyl-ether was coated on stainless steel surfaces using a cold-plasma-enhanced process. Compared to the unmodified surfaces, they not only significantly reduce bacterial attachment and biofilm formation but also influence the chemical characteristics of the biofilm.

There are only a few reports on organic coatings for CrCoMo alloys and even fewer researches are related to biomedical applications. Wang et al. reported the fabrication of Co-Cr alloy plate that is prepared for photodynamic application [156]. The immobilized photosensitizer molecules on the surface of Co-Cr alloy plate still possess their optical and functional properties including reactive oxygen generation. To open the possibility for its application as a photodynamic material to a biological system, the fabricated photofunctional Co-Cr alloy is applied to the decomposition of smooth muscle cells.

Chapter III A new aqueous lubrication concept for biomedical applications

3.1 Brush coatings

From the presented work in Chapter II, it is shown that hydrophilic coatings are commonly used to create hydration lubrication in combination with aqueous fluids. Furthermore, the hydrophilic coatings must be able to bind water in their structure. This combination results in a lubricating layer such as illustrated by Fig. 2.3. The confined water is able to separate the rubbing surfaces during the sliding contact and then reduce the friction. Furthermore, coatings grafted on to substrate by adsorption are not always durable enough, whereas using chemical bonding, the coatings can be coated on the metal substrate.

Poly(acrylic acid) (PAA) is an anionic polymer of acrylic acid with the ability to absorb and retain water and to swell to many times their original volume. Poly(ethylene glycol) (PEG) is a water-soluble polymer with many applications: from industrial manufacturing to medicine. PAA and PEG are selected in this work because of the fact that the –COOH and –OH groups in the molecules can combine plenty of water. Both PAA and PEG can be chemically bonded to the surface. Modifications of the basic structure are made to create specific functionality. Polylactide (PLA) is a biodegradable thermoplastic aliphatic polyester derived from renewable resources, e.g. corn starch, tapioca roots, chips or sugar cane. It is a polymer that is non-soluble in water. PEG-lactide is a combination of water-soluble PEG and oil-soluble PLA, and it is selected because of the amphiphilic characteristics. PEG-lactide is designed specifically to function with O/W emulsions and interaction is expected with the oil part of the emulsion and with the water part of the emulsion.

3.2 Graphene oxide

The durability of the sliding surface under severe operational conditions is assumed to be served by the combination of a solid lubricant and a surface-active polymer brush. Graphite is a solid lubricant with an anisotropic crystal structure

consisting of strong covalent intralayer bonding and weaker interlayer dispersive interactions. It was selected since it can easily be converted to graphene oxide, a two-dimensional lattice of partially broken sp^2-bonded carbon networks with hydroxyl and epoxide groups on the basal planes and carboxylic acid groups at the edges. It can be produced onto various large area substrates with strong adhesion and it can be functionalized with hydrophilic polymer brushes as well. Moreover, carbon materials have been used in the treatment of soft and hard tissue injuries, and graphene and its derivatives have attracted much attention in numerous applications in biotechnology, indicating the biocompatibility of graphene oxide.

The combination of the graphene oxide coated substrate material and the polymer coatings is shown in Fig. 3.1; the hydrophilic coatings function at lower loads, while at higher loads, the graphene oxide layer provides protection.

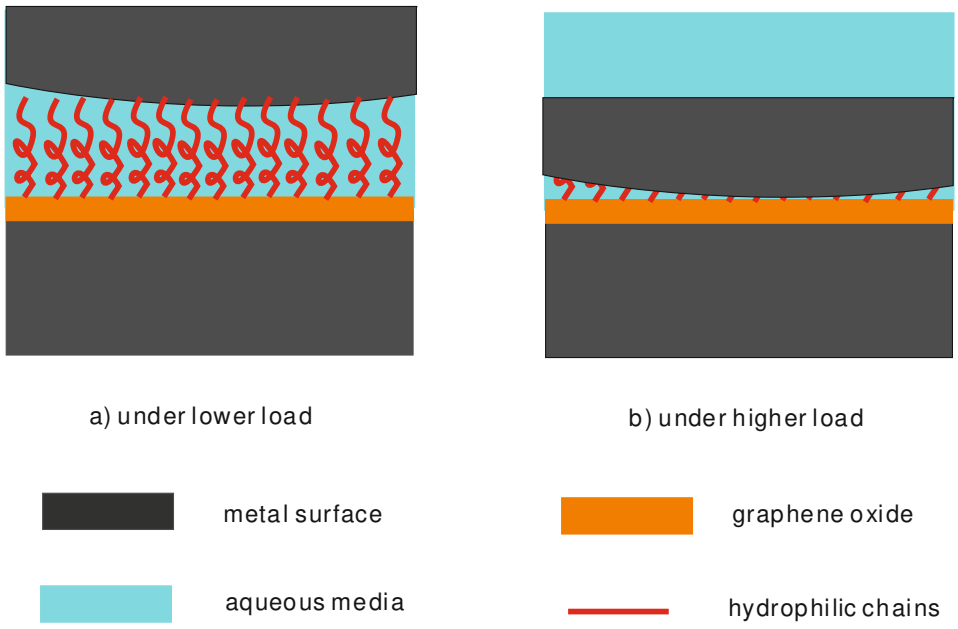

Fig. 3.1 The brush coatings with GO layer

3.3 Emulsion lubrication

3.3.1 Lubrication with an O/W emulsion

The lubricating action of O/W emulsions is typically explained using the plate-out theory. When an oil droplet is exposed to a metal surface, the layer

formed by the polar orientation of the emulsifier molecule induces droplets to adsorb onto the metal surface. Then, the droplet spreads and a layer of oil can be plated on the surface and work as a protection layer. As such, during running-in of the tribo system, water has a dominant role and the coefficient of friction COF does not depend on the dispersed oil or on the additives within the dispersed oil. Then, the droplets break and plate-out onto the surface. This process is schematically illustrated in Fig. 3.2. At the beginning, Stage I can be attributed to the transition of friction behaviour from the running-in period to the steady-state sliding. In Stage II oil droplets that dispersed in water adsorb and plate-out onto the metal surface. After the process of plate-out, the additives are adsorbed onto the metal surface and form the protection films, shown in Stage III.

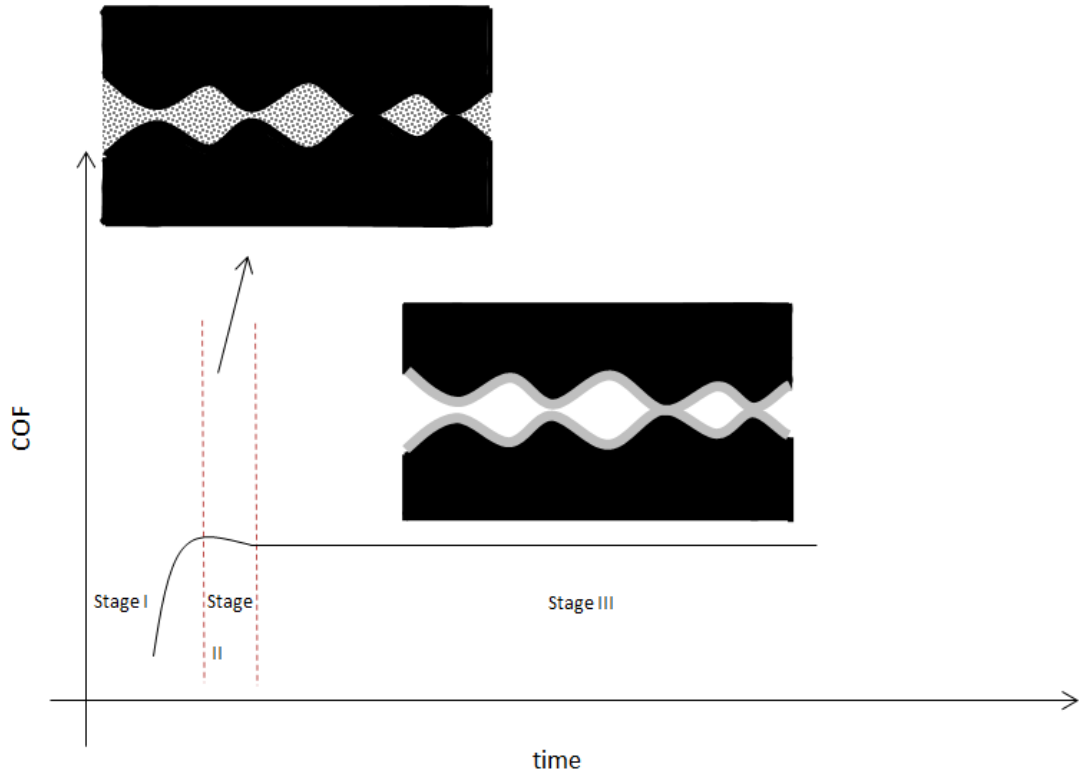

Fig. 3.2 Schematic friction curve and corresponding lubrication mechanism for an O/W emulsion

3.3.2 Emulsion lubrication of amphiphilic coatings

When hydrophilic coatings are used in combination with O/W emulsions, at first the hydrophilic chains extend due to the formation of hydrogen bonds with water (Fig. 3.3a). However, after the plate-out process, the oil component is adsorbed onto the surface and the hydrophilic chains collapse. In this situation, the chains may not work as a protection layer. This can possibly be overcome by introducing

an lipophilic part as well. For amphiphilic coatings, shown in Fig. 3.3b, before plating out, the surface is exposed to a water environment, the lipophilic chains collapse, while the hydrophilic chains extend due to the formation of hydrogen bonds with water. After plating out, the surface is covered by the oil component, the hydrophilic chains collapse, but the lipophilic chains extend because of the interaction between the lipophilic chain and the oil component.

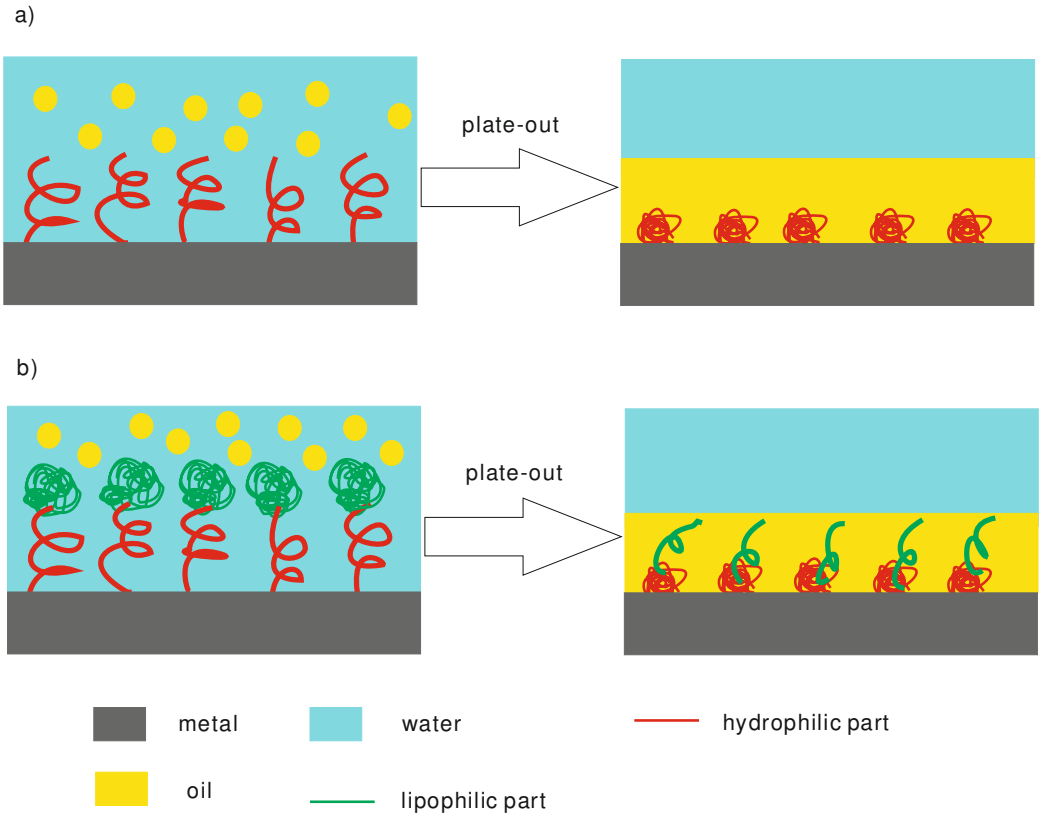

Fig. 3.3 Comparison of hydrophilic and amphiphilic coatings in emulsion lubrication.

3.4 Hydration lubrication based on O/W emulsions combined with graphene oxide

The aqueous lubrication concepts of this thesis can summarized as follows:

- First, CoCrMo is coated with a fully hydrophilic brush coating to form a hydrated layer on the substrate. The tribological response is measured and given in Section 4.3.2.

- Then, CoCrMo is coated with a layer of graphene oxide and subsequently coated with a fully hydrophilic brush coating to enhance the bonding strength of the layers or to create a layer that is able to withstand the higher pressure regime. The tribological response is measured and the synergy between graphene oxide and the brush coatings is discussed in Section 4.4.2.

- Finally, the amphiphilic coatings are combined with graphene oxide and used with the O/W emulsions. In this system at the hydration stage the hydrated layer works, while at the emulsion stage the plated-out oil layer works as lubricating layer. This is schematically drawn in Fig. 3.4. The tribological response is measured and given in Section 4.4.3.

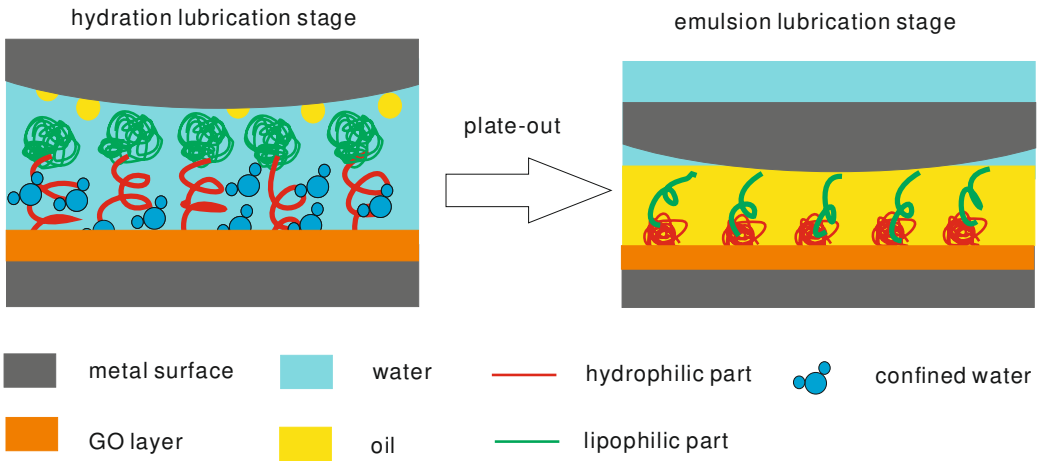

Fig. 3.4 Hydration lubrication based on O/W emulsions combined with graphene oxide

For reasons of comparison the interaction between the substrate metal and the O/W emulsions will be examined as well. The tribological response is measured and given in Section 4.2.2.

Chapter IV Measuring friction in the boundary lubrication regime

4.1 Reference measurements: the interaction between bearing steel and newly developed additives

In this section, the study on the tribological interactions between boron-containing additives and bearing steel were described.

4.1.1 Testing method and experimental details

The experiment method adopted in this measurement is Chinese national standard GB3142-82 which is similar to ASTM D-2783. The tribological performance, i.e. the friction-reducing and anti-wear capacities of the additives were measured by a four ball machine. The friction coefficients were automatically calculated from the friction signal and recorded. An optical microscope was used to measure the wear scar diameters (WSD). As such, a velocity of 1450 rpm was applied for 30 min at room temperature. The balls used for the experiments have a diameter of 12.7 mm which are made of AISI 52100 bearing steel. The balls are hardened to 59–61 HRC.

A commercial rapeseed oil, provided by Grease Factory of China, Lanzhou, China was used as the lubricating oil without any further treatment. Two boron-containing additives, tris (4-dodecylphenyl) borate (coded TDB) and 2-(2-(4-dodecylphenoxy)-1, 3, 6, 2-dioxazaborocan-6-yl) ethanol (coded DDB) were prepared which are detailed shown in Paper D. The lubricants were prepared by mixing 2.0 wt. % of the additives in rapeseed oil followed with stirring the solution at 50 ^{o}C for 1 hour.

After the tests, The samples used for X-ray absorption near edge structure spectroscopy (XANES) and X-Ray photoelectron spectroscopy (XPS) analysis were washed ultrasonically with petroleum ether and dried before the detection. XANES analysis was performed at Canadian Light Source Inc, Saskatoon, SK, Canada. Boron K-edge spectra were collected separately on the double-crystal

monochromator (DCM) covering an energy of 185–200 eV. The photo-adsorption spectra were collected with total electron yield (TEY) modes of detection, to provide chemical information on the bulk of the reaction film. XPS analysis was conducted with a PHI-5702 multifunctional X-ray electron spectrometer at the Lanzhou Institute of Chemical Physics, Lanzhou, China. The Mg Kα radiation was used as the excitation source with pass energy of 29.4 eV with a resolution of ±0.3 eV. The binding energy of C1s (284.6 eV) was used as the reference.

4.1.2 Friction-reducing and anti-wear properties

The coefficient of friction (COF) and WSD of rapeseed oil, 2.0 wt. % TDB and 2.0 wt. % DDB in rapeseed oil under the load of 294 N are shown in Fig. 4.1. The friction-reducing properties of the two boron-containing additives, TDB and DDB, are better than that of the base oil. At the same time, the COF with DDB is lower than that with TDB, revealing that different films are formed by the tribo-chemical reaction between the active elements in the additive molecules and the bearing steel surface. For the antiwear property, it can be seen that DDB can improve the anti-wear property of base oil and the performance of DDB is better at the same concentration than that of TDB. The difference is supposed to be related to their active element content and molecular structure which affect the adsorption ability and the tribo-chemical reaction activity. The interaction will be detailed discussed in the interaction section later. The synergetic effect of B and N elements in borate additives can both be found in friction-reducing as well as in antiwear properties, since TDB only contains B, while DDB contains both B and N.

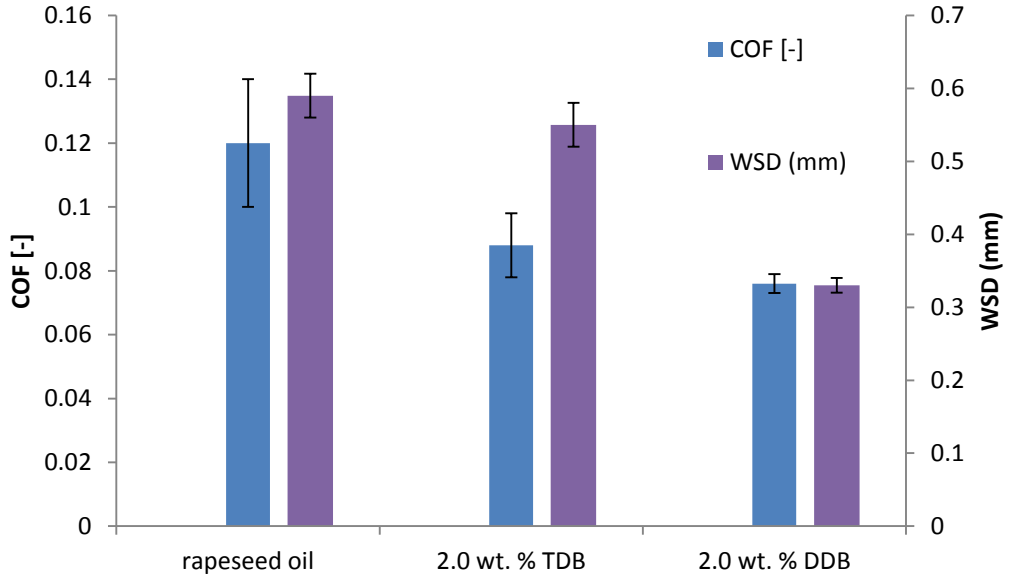

Fig. 4.1 The COF and WSD of rapeseed oil, 2.0 wt. % TDB and 2.0 wt. % DDB in rapeseed oil (four-ball machine, 294 N, rotation velocity of 1450 rpm for 30 min)

4.1.3 The interaction between bearing steel and the additives

As the interaction between bearing steel and the additives cannot be detected in situ yet, for a steel-steel combination, surface analysis after rubbing is typically selected and regarded as an effective method to explore the mechanism. XANES is recognized as a non-destructive method for the surface and can be used to investigate the chemical nature of boundary films generated in tribological contacts. XPS is also used to analyze the characteristics of the worn surface.

The B K-edge XANES (TEY) of tribofilms generated from different additives in rapeseed oil are shown in Fig. 4.2. The peak positions of each spectrum and model compounds are listed in Table 4.1. Peak b is the characteristic position of B_2O_3, and peaks a, c, d and e correspond to BN (more likely *h*-BN). Therefore, the tribofilm generated by 2.0 wt. % TDB mainly contains B_2O_3, and for DDB, the films are mainly composed of BN. The formation of B_2O_3 by TDB prevents the direct contact between the metal surfaces, and the melting point and shear strength of B_2O_3 are lower than that of metal surface, resulting in the friction reducing and wear resistance properties of TDB. For DDB, it can be adsorbed onto the metal surface and then the absorbed B and N can react with the metal surface under high load and triboheat to generate tribofilms. Associating these

results with tribological data, the conclusion can be drawn that the tribofilms which contains BN will get better AW performance than that contains B_2O_3.

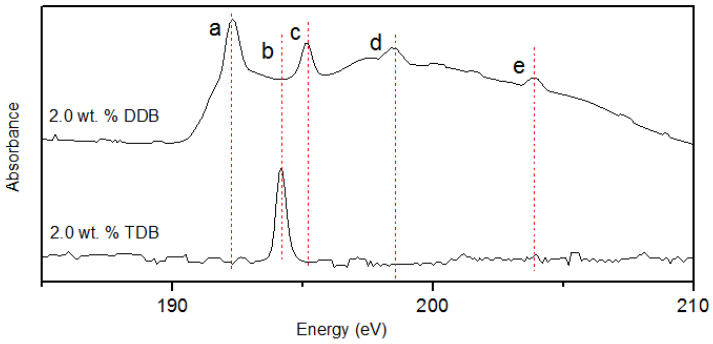

Fig. 4.2 B K-edge XANES spectra of the tribofilms

Table 4.1 Peak positions of the B K-edge (TEY) spectra of tribofilms generated from additives

	B K-edge (eV)				
peak	a	b	c	d	e
Sample					
2.0 wt. % TDB		194.1			
2.0 wt. % DDB	192.3		195.1	198.3	204.6
Compounds					
h-BN	192.4			198.7	204.6
c-BN			195.0	198.4	205.1
B_2O_3		194.0			

The peak positions of the N K-edge XANES (TEY) spectra of tribofilms generated from DDB in rapeseed oil are listed in Table 4.2. By comparison with the model compounds, the peaks at around 402.0 eV and 407.0 eV can also be attributed to *h*-BN which is in good agreement with the results of B spectra.

Table 4.2 Peak positions of the N K-edge (TEY) spectra of tribofilms generated from additives

	N K-edge (eV)	
Sample		
2.0 wt. % DDB	402.4	407.1
Compounds		
h-BN	402.2	407.3

From the XPS spectrum of TDB and DDB which is shown in detail in Paper D, it can also be found that the difference of the reaction films mainly lies in the

formation of BN. Associating with the tribological test results, the better performance of DDB than that of TDB reveals that BN plays a crucial role in reducing wear and friction, suggesting the importance of B-N synergetic effects.

4.2 Reference measurements: the interaction between stainless steel, CoCrMo alloy and newly developed additives

Phosphorous-nitrogen containing additives are known to create high performing boundary films on bearing steel. The same was concluded in Section 4.1 with respect to boron-containing additives that promote the formation of BN. This section explores the boundary lubrication capability of these additives for stainless steel and CoCrMo.

4.2.1 Testing method and experimental details

4.2.1.1 Test method

The experimental method used to measure the tribological performance is based on a ball on disk configuration by using a nanotribometer, provided by CSM-instruments. The detailed test conditions are listed in Table 4.3. Each COF is calculated based on 100 m sliding test and the average COF is recorded. Each test was repeated three times on the same specimen.

Table 4.3 Test conditions

Items	Nanotribometer
Diameter of ball	5 mm
Normal load	5 mN
Contact pressure	80-90 MPa
Velocity	35 mm/s, 10 mm/s
Sliding distance	100 m

The samples used for the surface analyses were washed with hexane and dried before the detection. The morphology of the wear scar was characterized by Keyence VK 9700 laser scanning microscope. X-ray Photoelectron Spectroscopy (XPS) analysis was conducted to determine the chemical state of the elements in the worn surface with a Quantera SXM (scanning XPS microprobe) from Physical

Electronics at the Materials Characterisation Department at Nanolab, University of Twente. The Al Kα monochromatic radiation was used as the excitation source with pass energy of 224.0 eV with a resolution of ±0.4 eV. The binding energy of C1s (284.8 eV) was used as the reference.

4.2.1.2 Materials

The CoCrMo alloy selected for this work, Stellite 21 (coded CoCrMo), contains 27.0 wt. % chromium, 5.5 wt. % molybdenum, 2.5 wt. % nickel and 0.3 wt. % carbon, balanced by cobalt. AISI 316 stainless steel, a 17 wt. % chromium, 12 wt. % nickel balanced by iron alloy (coded stainless steel) is taken as representative stainless steel for this study. AISI 52100 bearing steel (coded bearing steel) was selected as a reference material. This hardened steel contains 1.5 wt. % chromium balanced by iron. All of the alloys were used after polishing and without any further treatment. The hardness of the materials was tested on a DLH-200 Shimadzu Micro Hardness Tester. The roughness of the specimen was characterized by the Micromap 560 interference microscope. The centre line average roughness of the balls, $R_{a1,}$ and of the disks, R_{a2} values and hardness values are listed in Table 4.4.

Table 4.4 Description, roughness and hardness of the materials

Material code	Description	**R_{a1}**	**R_{a2}**	**Hardness [HV]**
CoCrMo	Stellite 21	70±20 nm	150±50 nm	375±3
Stainless Steel	AISI 316	70±20 nm	150±50 nm	247±6
Bearing Steel	AISI 52100	30±10 nm	150±50 nm	851±10

For the rapeseed oil used, the main chemical constituents of fatty acids in the rapeseed oil are as follows: 7.46 wt. % of saturated fatty acids, 64.06 wt. % of monounsaturated fatty acid and 28.48 wt. % of total polyunsaturated fatty acid. Phosphorous-nitrogen containing and boron-containing additives, dibutyl octadecylphosphoramidate (DBOP), 6-octadecyl-1,3,6,2-dioxazaborocan-2-ol calcium salt (ODOC) and 2-(4-dodecylphenoxy)-6-octadecyl-1,3,6,2-dioxazaborocane (DOB) were prepared according to [157]. The lubricants were prepared by mixing 2.0 wt. % of the additives in rapeseed oil followed with stirring the solution at 50^{o}C for 1 hour.

4.2.2 The tribological performance of additives on stainless steel

The COF of 2.0 wt. % DBOP, ODOC and DOB for stainless steel vs. bearing steel were respectively 0.065±0.005, 0.110±0.009 and 0.065±0.007. The friction reducing possibilities of the three additives can therefore be ranked qualitatively as ODOC < DBOP = DOB at a lubrication number value of about 1×10^{-4}. The specific wear rates for stainless steel vs. bearing steel were calculated as 1×10^{-7} $mm^3{\cdot}N^{-1}{\cdot}m^{-1}$, 4×10^{-7} $mm^3{\cdot}N^{-1}{\cdot}m^{-1}$ and 5×10^{-7} $mm^3{\cdot}N^{-1}{\cdot}m^{-1}$ for DBOP, ODOC and DOB respectively. The anti-wear performance is similar for ODOC, DBOP and DOB, which can also be reflected from the morphology of the wear scars in Fig. 4.3.

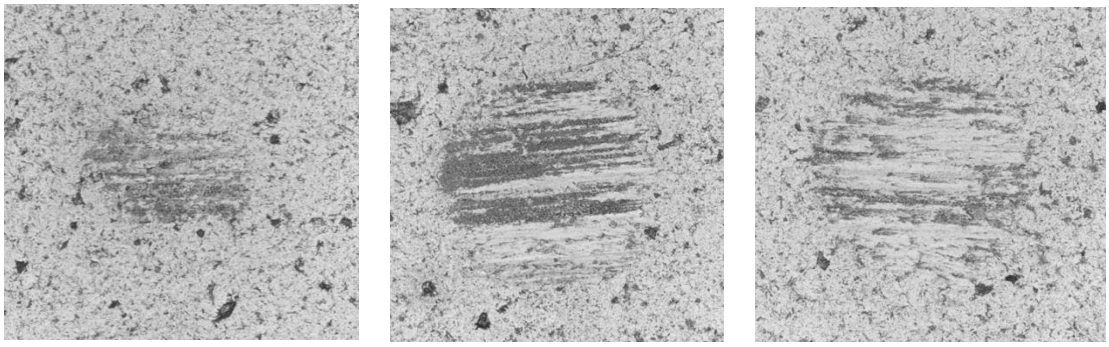

(a) (b) (c)

Fig. 4.3. The morphology of the wear scars on stainless steel balls; (a) DBOP, (b) ODOC, (c) DOB (2.0 wt. % additive in rapeseed oil, X50, sliding distance 2000 m)

4.2.3 The tribological performance of additives on CoCrMo

The COF of CoCrMo vs. CoCrMo lubricated by DBOP, ODOC and DOB doped rapeseed oil at a lubrication number of around 1×10^{-4} was calculated from the experimental work as 0.120±0.009, 0.097±0.006 and 0.110±0.010 respectively. The corresponding values for the specific wear rate were 6×10^{-7} $mm^3{\cdot}N^{-1}{\cdot}m^{-1}$, 3×10^{-7} $mm^3{\cdot}N^{-1}{\cdot}m^{-1}$ and 8×10^{-8} $mm^3{\cdot}N^{-1}{\cdot}m^{-1}$ respectively and the morphologies of the worn surface are shown in Fig. 4.4. The friction reduction property of the three additives is now ranked as ODOC > DOB > DBOP at the test condition.

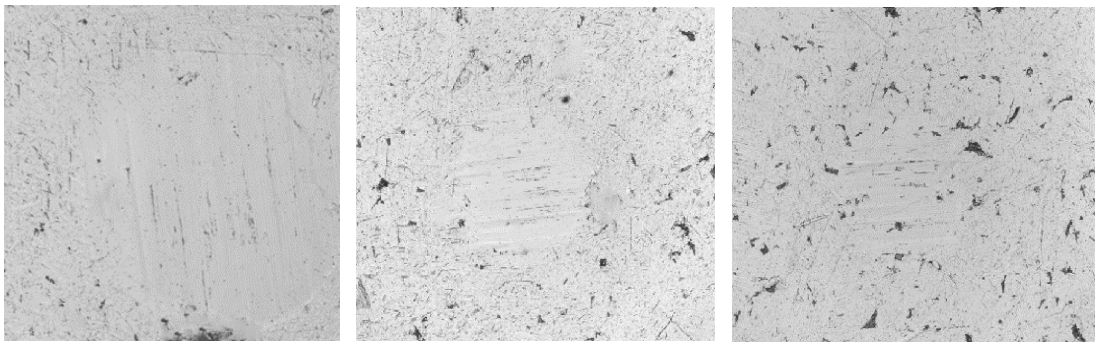

(a) (b) (c)

Fig. 4.4 The morphology of the wear scars on CoCrMo balls; (a) DBOP, (b) ODOC, (c) DOB (2.0 wt. % additive in rapeseed oil, X50, sliding distance 2000 m)

4.2.4 The interaction between the metals and the additives

XPS spectra of the elements in the worn surface were recorded to determine the chemical state of the elements and examine possible film forming mechanisms based on the known composition of the additives. The binding energies of some standard compounds containing Fe, O, P, B, N, and Ca are listed in Table 4.5 for comparison, which are obtained in NIST XPS Database.

Table 4.5 Binding energy of some standard compounds containing Fe, P, B, Ca, and N

Element	Compounds	Binding energy (eV)
Ferrum	Fe_2O_3	$Fe_{2p3/2}$(711.3); $Fe_{2p1/2}$(724.0); O_{1s}(529.8)
	Fe_3O_4	$Fe_{2p3/2}$(709.4); $Fe_{2p1/2}$(723.5); O_{1s}(529.7)
	FeO	Fe_{2p}(709.6); O_{1s}(530.1)
	FeOOH	$Fe_{2p3/2}$(711.5); $Fe_{2p1/2}$(724.3); O_{1s}(531.7)
	Fe(OH)O	Fe_{2p}(711-711.8); O_{1s}(531.2-531.8)
Phosphorous	$FePO_4$	Fe_{2p}(712.8); P_{2p}(133.7); O_{1s}(531.8)
Boron	Fe_xB_y	Fe_{2p}(706.9-707.4); B_{1s}(188.0)
	B_2O_3	B_{1s}(192.0); O_{1s}(532.5-533.8)
Calcium	CaO	Ca_{2p}(347.0); O_{1s}(531.3-531.5)
	$Ca(NO_3)_2$	Ca_{2p}(347.0); N_{1s}(407.6)
Nitrogen	N-containing organic	N_{1s}(399.7)
	NH_4NO_3	N_{1s}(403.1)

Because the wear scars were too small when using CoCrMo vs. CoCrMo, the XPS evaluation was only conducted for stainless steel vs. bearing steel. The XPS

spectra of the elements on bearing steel surface with the lubrication of DBOP, DOB and ODOC are given in Fig. 4.5.

The Fe_{2p} peaks appear at around 711.39eV and 724.49eV, which can be corresponded to iron oxides (Fe_2O_3, Fe_3O_4) and/or iron hydroxides (FeOOH, Fe(OH)O), indicating the lubricated surface is liable to oxidize during the friction process. When taking a look at the XPS spectra for O_{1s}, all the three additive based lubricating systems exhibit an intensive wide peak at around 533.67 eV (in the range of 531-534 eV). It further confirms the existence of FeOOH, Fe(OH)O and Fe_2O_3 on the bearing steel surfaces. In case of nitrogen, there is a wide peak

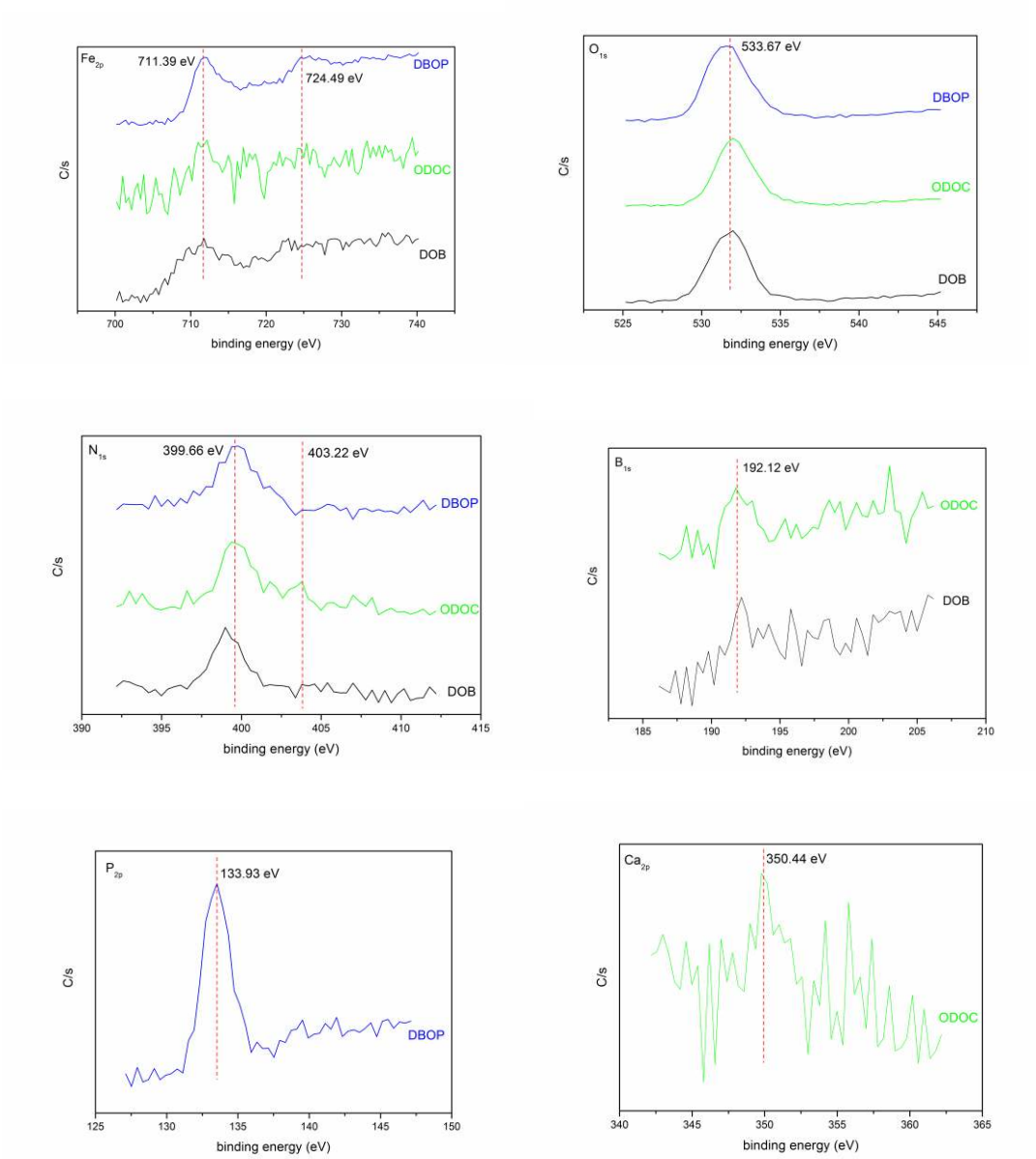

Fig. 4.5 XPS spectra of Fe_{2p}, O_{1s}, N_{1s}, B_{1s}, Ca_{2p} and P_{2p} on the worn surfaces for stainless steel vs. bearing steel lubricated with 2.0 wt. % additives in rapeseed oil

at around 399.66eV for all the three surfaces, suggesting that the N element is still in organic state. It may be the complex compounds of metal surface with the decomposed additives like organic amine, organic amide, nitrile and other N-containing compounds. The B_{1s} spectra show peak at around 192.12eV, corresponding to B_2O_3, which is in good accordance with the result of O_{1s} spectra and also indicates there is no Fe_xB_y formed on the surface. The binding energy of P_{2p} at 133.93eV further confirms the existence of $FePO_4$, and there may be also other organic phosphorous compounds formed on the worn surface. The wide Ca_{2p} peak at around 350.44eV can be identified as $Ca(NO_3)_2$ and CaO.

Therefore, the above surface analysis results demonstrate that under the boundary lubrication condition, the active additive molecule first adsorb on the metal surface, and then decompose and react with the metal surface during the rubbing process to form stable lubricating films on the rubbed surfaces. The lubricating films are complex and consist of adsorption layer and reaction layer (see Table 4.6). The adsorption layer is formed mainly by the coordination bonding of nitrogen-containing groups with the metal surface resulting from the decomposed products from the additives. The reaction layer originates from the tribochemical reaction of the active elements contained in the additives, which resulting in the formation of boron oxide, nitrate, phosphate and other oxidized compounds. The main difference on the films formed by these three additives lies in the reaction layer.

Table 4.6 The main composition of the films on the scar

Additive	Adsorption film	Reaction film
DBOP	N-containing organic compounds	Iron oxides, iron hydroxides, phosphate
ODOC	N-containing organic compounds	Iron oxides, iron hydroxides, B_2O_3, CaO, nitrate
DOB	N-containing organic compounds	Iron oxides, iron hydroxides, B_2O_3

4.3 The interaction between uncoated metallic substrates and O/W emulsions

To apply the functional oil-based additives into aqueous system, one approach could be the incorporation of the additives into O/W emulsion.

4.3.1 Experimental details

The experimental method used to measure the tribological performance is based on a ball on disk configuration and the details are similar to 4.2.1. The O/W emulsions were prepared by by milling and mixing 2.0 wt. % of the additive, 6.0 wt. % of Polysorbate 80 and 6.0 wt. % of the rapeseed oil together, then adding water gradually and stirring (800 r/min) for 30 minutes.

4.3.2 The friction and wear behaviour

The effect of choosing stainless steel, ball bearing steel or CoCrMo on friction is shown in Fig. 4.6, in which 2.0 wt. % DOB-based emulsion was used as a lubricant for different material combinations, i.e. stainless steel vs. ball bearing steel, ball bearing steel vs. ball bearing steel and CoCrMo vs. CoCrMo. The data is presented using the dimensionless lubrication number based on the viscosity η of the lubricant, the sliding velocity v, the average contact pressure P and the composite roughness of the surfaces, R_a. The composite roughness R_a is defined as

$$R_a = \sqrt{R_{a1}^2 + R_{a2}^2} \quad (1)$$

In which R_{a1} and R_{a2} are the surface roughness based on the area of the surfaces 1 (ball) and 2 (ring). The lubrication number range, i.e. from around 5×10^{-3} to around 1×10^{-5}, predicts boundary lubrication conditions [158]. For the base O/W emulsion without 2.0 wt. % DOB, the COF of bearing steel vs. bearing steel, CoCrMo vs. CoCrMo and stainless steel vs. bearing steel was 0.120±0.010, 0.120±0.010 and 0.170±0.020 with the lubrication number of around 1×10^{-5}. For the results in the emulsion with 2.0 wt. % DOB, it can be seen from Fig. 4.6 that for boundary lubrication conditions the COF of bearing steel vs. bearing steel varies from 0.045±0.005 to 0.092±0.012, and for CoCrMo vs. CoCrMo, the COF varies between 0.110 and 0.120. When the material is changed to stainless steel vs. bearing steel, the COF is around 0.150. The results suggest that compared to standard ball bearing steel, the COF for boundary lubrication conditions is higher for the CoCrMo alloy. The COF in combination with stainless steel (stainless steel vs. bearing steel) is the highest. The different COF may be attributed to the different boundary layers.

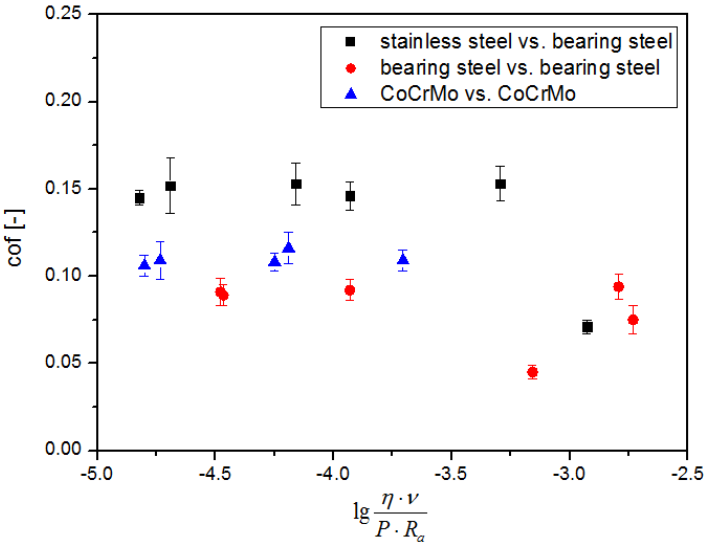

Fig. 4.6 The COF as a function of the materials (2.0 wt. % DOB-based emulsion).

The wear rate for stainless steel vs. bearing steel in 2.0 wt. % DOB-based emulsion is at a level of 3 $\times 10^{-7}$ $mm^3 \cdot N^{-1} \cdot m^{-1}$. Under the same condition for bearing steel vs. bearing steel and CoCrMo vs. CoCrMo, the wear rate is 8 $\times 10^{-8}$ $mm^3 \cdot N^{-1} \cdot m^{-1}$ and 8 $\times 10^{-7}$ $mm^3 \cdot N^{-1} \cdot m^{-1}$ respectively. The tendency is also reflected in the topographies shown in Fig. 4.7.

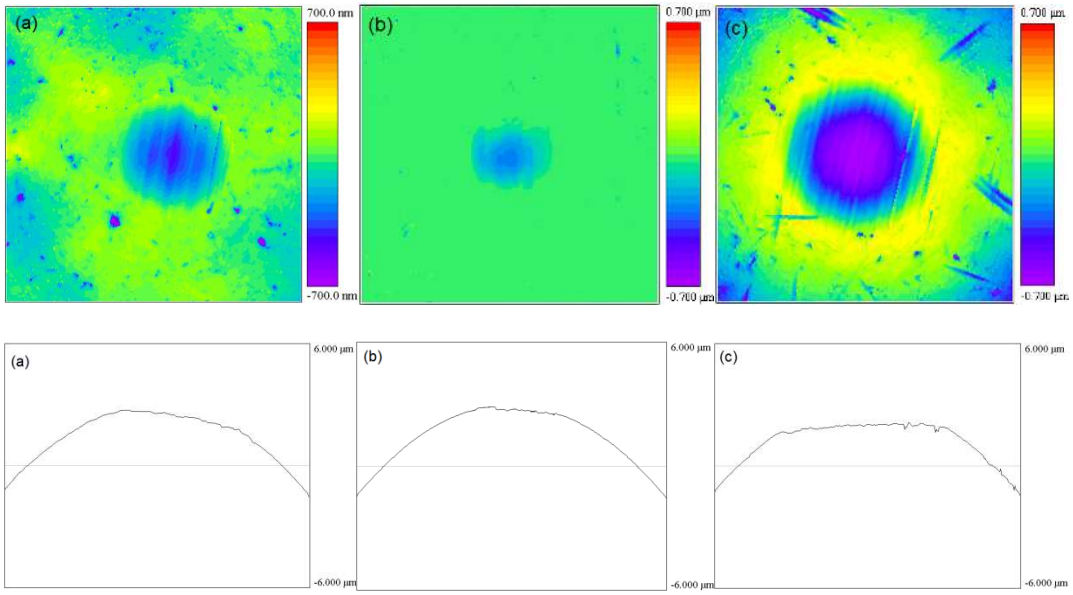

Fig. 4.7 The morphology and wear profile of the wear scars for different materials (2.0 wt. % DOB-based emulsion, sliding distance 2000m, 10X, the scales are all shown as height in µm, all of the morphology areas are 300µm×300 µm based on curvature mode, all of the wear profile length is 300 µm in the centre based on plane mode) (a) stainless steel vs. bearing steel (b) bearing steel vs. bearing steel (c) CoCrMo vs. CoCrMo

The friction profiles of CoCrMo vs. CoCrMo lubricated by different additive-based emulsions are shown in Fig. 4.8. The COF of base fluid without additives is 0.120±0.015 and is shown in the figure as a reference. The friction reduction property of the three additives is ranked as DBOP ~ ODOC > DOB under the tested conditions. The average COF found in combination with the three emulsions is 0.100±0.010, 0.100±0.008 and 0.120±0.009 respectively. The COF is higher at the beginning of the test and after around 600 seconds the curve becomes stable for DBOP. For ODOC and DOB, the curves show a slight increase afterwards. The wear rate of DBOP, ODOC and DOB based emulsions for CoCrMo vs. CoCrMo is 4×10^{-7} $mm^3 \cdot N^{-1} \cdot m^{-1}$, 4×10^{-7} $mm^3 \cdot N^{-1} \cdot m^{-1}$ and 8×10^{-7} $mm^3 \cdot N^{-1} \cdot m^{-1}$ respectively.

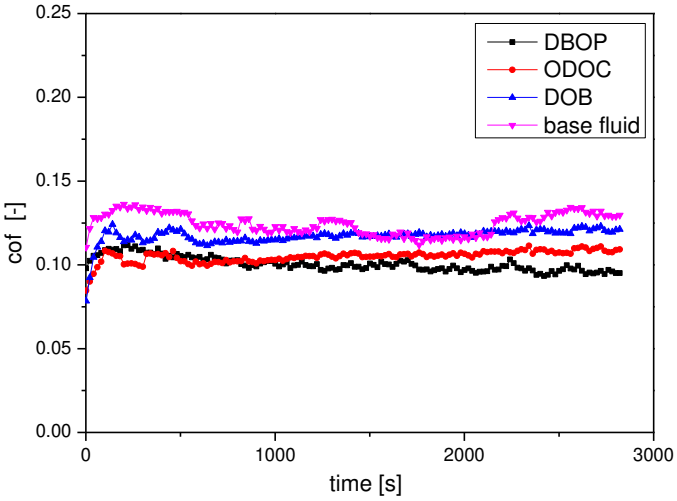

Fig. 4.8 The COF for 2.0 wt. % DBOP, ODOC and DOB-based emulsions in combination with CoCrMo vs. CoCrMo with time

4.3.3 The interaction between the metallic surfaces and the additives

The XPS spectra of Fe_{2p}, O_{1s}, N_{1s}, B_{1s}, Ca_{2p} and P_{2p} on the worn surfaces for stainless steel lubricated with 2.0 wt. % DBOP, ODOC and DOB-based emulsions

are depicted in Fig. 4.9. The summarized results are shown in Table 4.7.

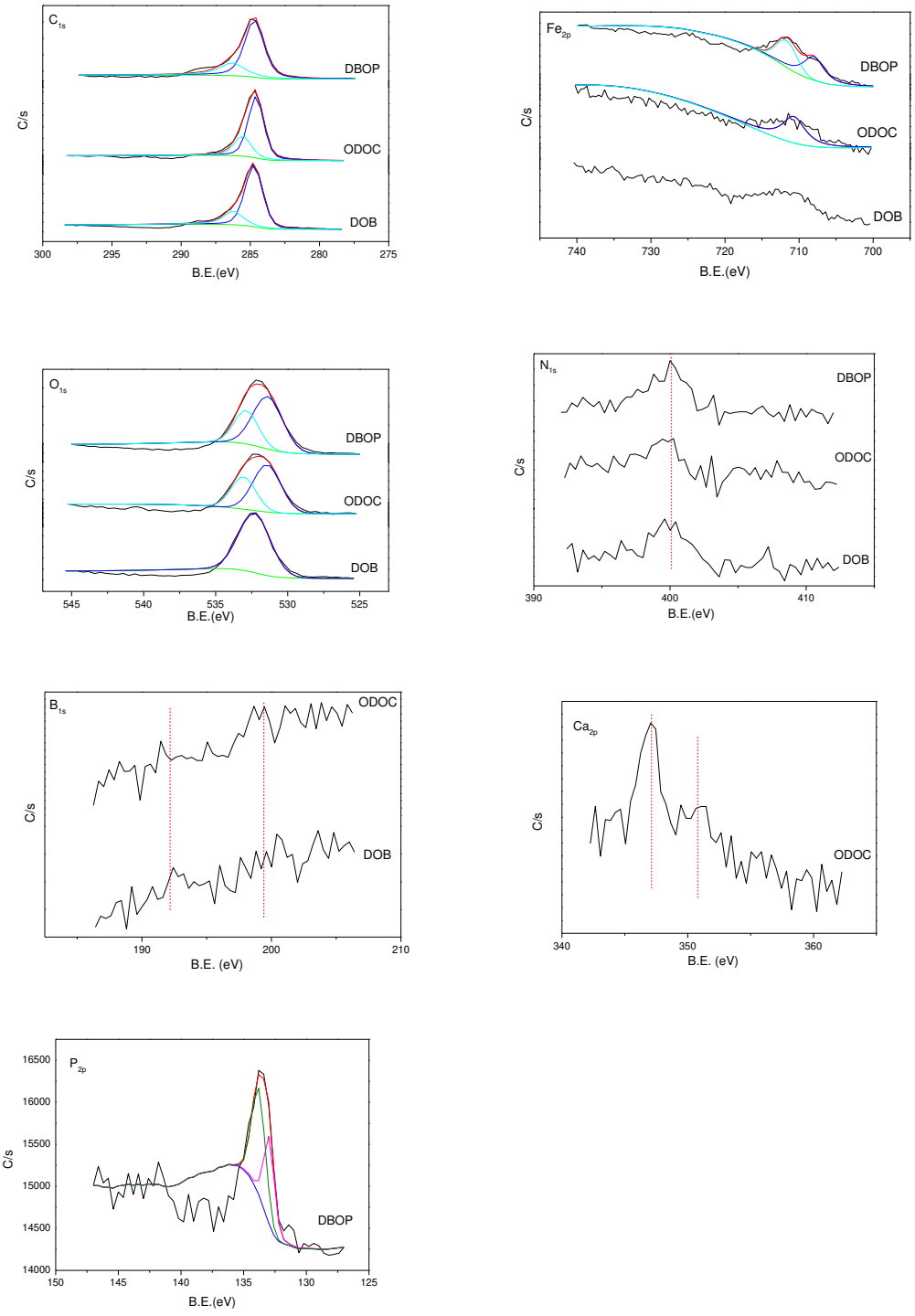

Fig. 4.9. XPS spectra of C_{1s}, Fe_{2p}, O_{1s}, N_{1s}, B_{1s}, Ca_{2p} and P_{2p} on the worn surfaces for stainless steel lubricated with 2.0 wt. % additives

Table 4.7 The fitted results of binding energy of the samples

	Binding energy (eV)						
Additive-based emulsion	Fe_{2p}	N_{1s}	Ca_{2p}	P_{2p}	B_{1s}	C_{1s}	O_{1s}
DBOP	706.58, 710.56, 719.68, 723.66	399.38		132.70, 133.54		284.76, 286.47	531.39, 533.70
ODOC	710.58, 723.68	399.59	347.14, 350.86		192.00	284.79, 286.57	531.89, 533.33
DOB	710.80, 723.90	399.89			192.10	284.85, 286.59	532.45

The Fe_{2p} peaks appear at around 711.70eV and 723.80eV, which can be ascribed to iron oxides (Fe_2O_3) and/or iron hydroxides (FeOOH), indicating that the lubricated surface is oxidized during the friction process. Interestingly, it can be seen from the spectra that the intensity of Fe_{2p} for DBOP is the highest, while for ODOC and DOB, the intensity is slightly weaker. The higher intensity for DBOP may lie in that phosphorous can easily react with iron. Generally phosphorous is proved to be an active element during the rubbing process [159]. The other interesting difference for DBOP is that there are peaks around 706.58eV and 719.68eV which can be attributed to the formation of renascent iron surface during rubbing. For other elements like nitrogen, there is a wide peak at around 399.60eV for all of the three additive lubricated surfaces, suggesting that the N element is still in the state of organic N-containing compounds. It may be the complex compounds of metal surface with the decomposed additives like organic amine, organic amide and other N-containing compounds [102]. The C_{1s} spectra confirm the existence of the organic compounds because of the sp^2 peak (C–C), which is around 284.80 eV, and the C–O group which is around 286.50 eV [106]. The B_{1s} spectra show peak at around 192.10eV, corresponding to B_2O_3 and/or some borates. The binding energy of P_{2p} at 132.70eV and 133.54eV suggests the existence of $FePO_4$ formed on the worn surface. The wide Ca_{2p} peak at around 347.14eV and 350.86eV can be identified as $CaCO_3$ and CaO with the peak distance about 3.5eV. When taking a look at the XPS spectra for O_{1s}, all of the three additive lubricated systems exhibit an intensive wide peak in the range of

530-535eV. Firstly, it further confirms the existence of FeOOH and Fe_2O_3 on the stainless steel surfaces. For DBOP, it confirms the existence of $FePO_4$ with the characteristic peak at 531.39eV and 533.70eV. As for ODOC, CaO and $CaCO_3$ can exist because its characteristic peak is at 531.3-531.5eV. It is obvious that the peak for DOB is located in a higher binding energy area compared to that of DBOP, which can be attributed to the formation of B_2O_3. The detailed compositions of the adsorption layer and reaction layer are listed in Table 4.8.

Table 4.8 Main composition of boundary films found at the surface of the wear scar

Additive	Adsorption film	Reaction film
DBOP	N-containing organic compounds	Iron oxides, iron hydroxides, phosphate
ODOC	N-containing organic compounds	Iron oxides, iron hydroxides, CaO, $CaCO_3$
DOB	N-containing organic compounds	Iron oxides, iron hydroxides, B_2O_3

4.3.4 Comparison of O/W system with an oil system

The tribological performance of the additives in an oil-based system (2.0 wt. % additives in rapeseed oil as lubricants) for stainless steel vs. bearing steel was examined in Paper A. A summary of the COF and wear rate for the oil-based systems and for the O/W emulsion-based system is given in Table 4.9. The COF in the oil system is lower than that in the water system for DBOP and DOB. This can be attributed to the different viscosity and the oil content. On the one hand, it is reported that the coefficient of friction decreases with the increase of viscosity in a boundary lubrication regime [20]. In oil system, the overall viscosity of the lubricant (around 90×10^{-3} Pa·s) is higher than that of the O/W emulsion (around 30×10^{-3} Pa·s). On the other hand, in an oil-based system, both the additives and the base oil can be adsorbed onto the metal surface to form a stable and compact protection layer. The difference can be related to the different structure of the additive-based emulsions. From the chemical compositions of the additives, ODOC is an ionic compound and Polysorbate 80 is a compound with hydroxyl groups. Therefore, the polarity of the additives and the emulsifier can be ranked as ODOC > Polysorbate 80 > DOB and DBOP. The polarity of the additives is different, and the structure of the oil droplet is different. So within one oil droplet, there are different domains: for DOB and DBOP containing emulsions, DOB and

DBOP are in the core of the oil droplet because of the similar polarity to oil, while for ODOC-based emulsion, ODOC is at the interface of the oil droplet and works as the co-emulsifier. Therefore, ODOC can be easier to adsorb onto the metal surface to form the protective layer, demonstrating similar friction-reducing performance to that of an ODOC oil system.

Table 4.9 Comparison of the COF and wear rate for oil lubricated and for O/W emulsions lubricated systems

	COF		**Wear rate ($mm^3 \cdot N^{-1} \cdot m^{-1}$)**	
Additive	in oil	in O/W emulsion	in oil	in O/W emulsion
DBOP	0.065±0.005	0.130±0.010	1×10^{-7}	3×10^{-7}
ODOC	0.110±0.009	0.120±0.007	4×10^{-7}	4×10^{-7}
DOB	0.065±0.007	0.150±0.020	5×10^{-7}	3×10^{-7}

4.4 Tribological performance of graphene oxide combined with brush coatings in aqueous systems at the macro scale

4.4.1 Experimental method

Besides the preparation of the coatings, the materials and testing methods are similar to Section 4.2.1. The disks are in two different roughness which is shown in Table 4.10. For the coating materials, 3-Aminopropyltrimethoxysilane (APTMS) was obtained from Aldrich. Poly(acrylic acid) (PAA) with Mn of 5.5 kg/mol was obtained from Acros Organics. Amino-terminated poly(ethylene glycol) (PEG, Mn = 5.0 kg/mol) and amino-terminated poly(ethylene oxide-lactide) (PEG-lactide, PEG Mn = 10.0 kg/mol, lactide Mn = 1.4 kg/mol) were obtained from Polymer Source Inc. Graphite was 30 μm in diameter powder and obtained from Shanghai Chemicals.

A typical Hummers method [160] was used to prepare graphene oxide (GO) by using graphite powder as the starting material. The detailed procedure of the coating preparation is given in Paper C. The abbreviations of the coatings are shown in Fig. 4.10. Attenuated total reflectance Fourier transform infrared (ATR–FTIR) spectra and XPS were used to characterized the coated samples.

Table 4.10 Test conditions used in this work

Items	Nanotribometer
Diameter of ball	5 mm
Normal force	5 mN
Velocity	35 mm/s
Sliding distance	100 m
Surface roughness (ball)	70±20 nm
Surface roughness (disk smooth)	30±10 nm
Surface roughness (disk rough)	150±50 nm

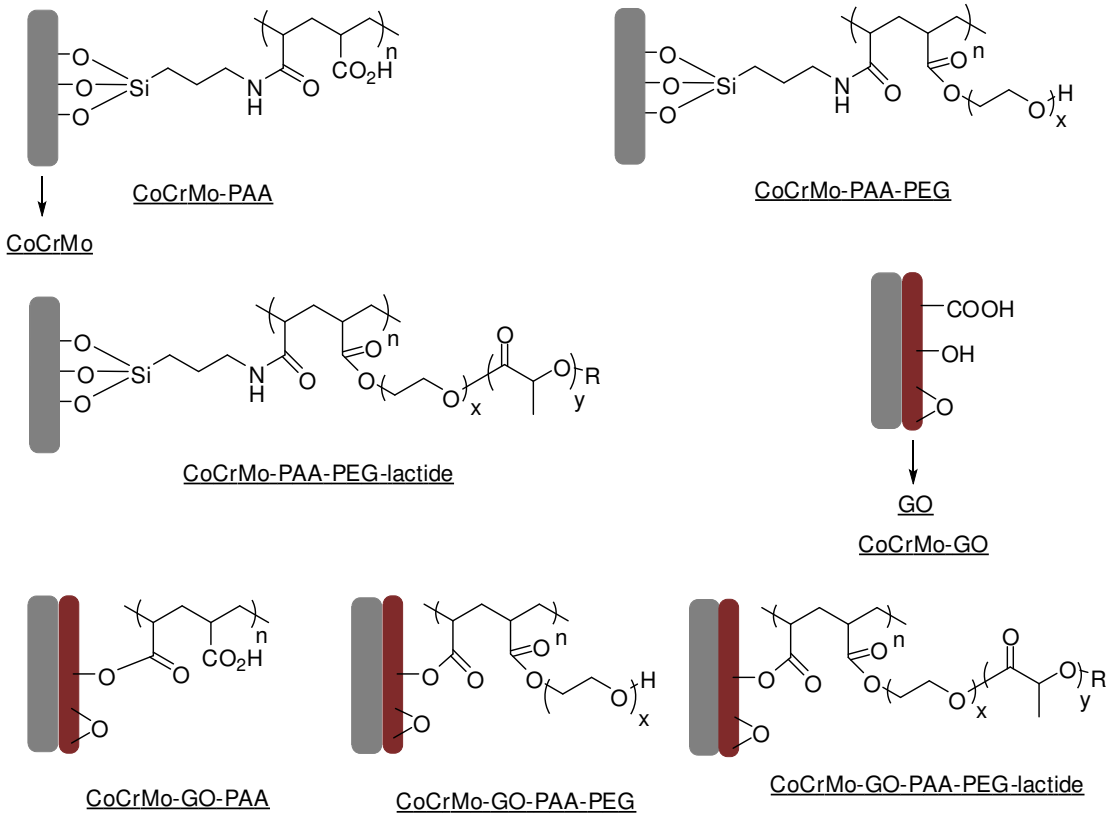

PAA: Poly(acrylic acid), Mn = 5.5 kg/mol
PEG: Amino-terminated poly(ethylene glycol), Mn = 5.0 kg/mol
PEG-lactide: poly(ethylene oxide-lactide)(PEG-lactide, PEG Mn = 10.0 kg/mol, lactide Mn = 1.4 kg/mol)
GO: graphene oxide

Fig. 4.10 The schematic structure and abbreviations of the coatings

4.4.2 Tribological performance of graphene oxide combined with brush coatings in aqueous systems

For the aqueous media, the behaviour with 100 % water is the starting point. Fig. 4.11 shows the COF of different coatings in water. It can be seen from the figure that CoCrMo reveals a high COF of 0.300±0.030 and that CoCrMo with coatings always shows a lower COF in water. The COF for CoCrMo-PAA, CoCrMo-PAA-PEG and CoCrMo-PAA-PEG-lactide in water is 0.230±0.020, 0.240±0.020 and 0.260±0.040 respectively. When there is a GO layer in between, the COF for CoCrMo-GO and CoCrMo-GO-PAA is 0.210±0.030 and 0.180±0.010. For the CoCrMo-GO-PAA-PEG and CoCrMo-GO-PAA-PEG-lactide, the COF is largely reduced to 0.180±0.030 and 0.120±0.040, indicating GO layer has a strong influence on the friction behaviour of the coated materials as demonstrated in Fig. 3.1 and 3.2.

The effect of surface roughness can be seen from Fig. 4.11 as well. For the smoother surface, CoCrMo reveals a COF of 0.210±0.030. The COF for CoCrMo-PAA and CoCrMo-PAA-PEG in water is 0.220±0.010 and 0.200±0.050, respectively. When there is a GO layer in between, the COF for CoCrMo-GO and CoCrMo-GO-PAA is 0.210±0.050 and 0.170±0.010. For the CoCrMo-GO-PAA-PEG, the COF is reduced to 0.160±0.030. From the data, it can be seen that the GO layer has a strong influence on the friction behaviour of the polymer coated materials. It can be also seen that the rough surface always show higher friction values than compared to the same tribosystem with a smoother surface.

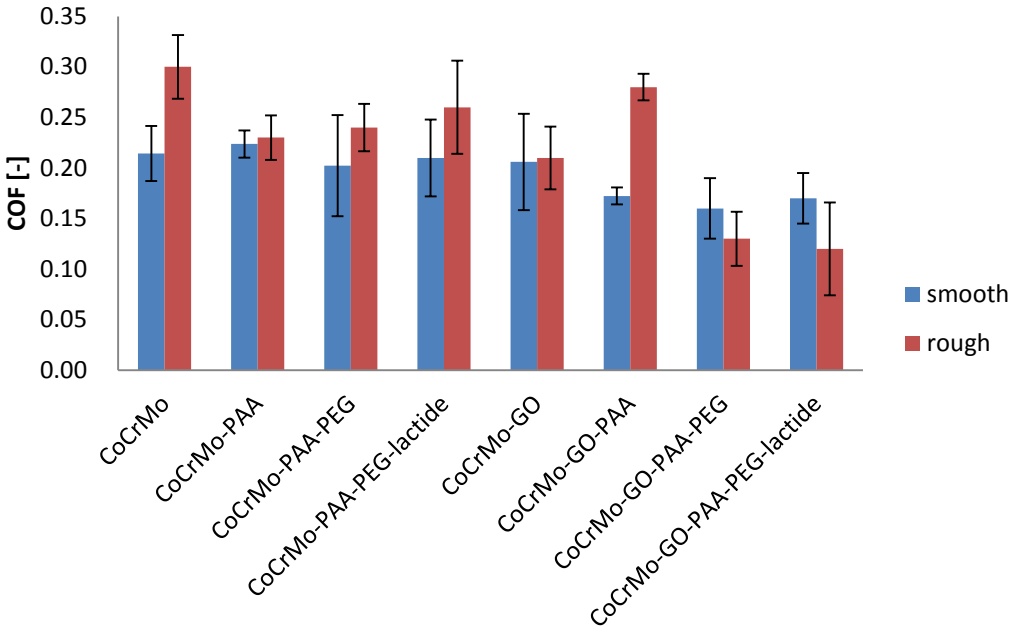

Fig. 4.11 The COF for different coatings in water

The coefficient of friction of CoCrMo-PAA-PEG and CoCrMo-GO-PAA-PEG in different aqueous media is shown in Fig. 4.12. The friction coefficient of the coatings with GO layer is lower than that without GO layer for all the tested aqueous media, indicating the effectiveness of incorporating the GO layer.

For the PAA-PEG coated CoCrMo surface, it can be seen that it performs better in bovine serum (BS) and 2.0 wt. % DBOP based emulsion than that in water, phosphate buffered saline (PBS) and 0 wt. % emulsion. For the CoCrMo surface coated with GO-PAA-PEG, the COF is ranked as 0 wt. % emulsion>PBS≥BS ≥water>2.0 wt. % emulsion. The data clearly suggest that the aqueous medium plays a significant role on the friction performance. It can be seen that the coatings perform slightly better in water than in PBS. When tested under emulsion without additive (O/W 0%), the friction coefficient is the highest among all the media. The performance of the hydrophilic polymers in BS and in emulsion with additive (O/W 2%) is in both cases better than the performance with water.

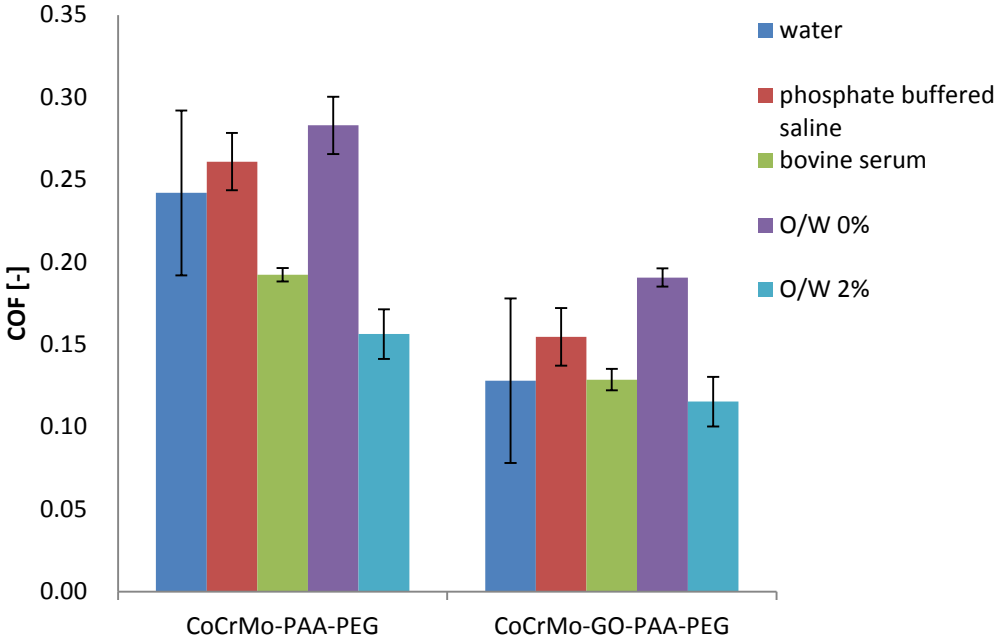

Fig. 4.12 The coefficient of friction of CoCrMo-PAA-PEG and CoCrMo-GO-PAA-PEG in different aqueous media

4.4.3 The interaction between emulsions and an amphiphilic coating

Since PEG-lactide contains both long alkyl chains (lipophilic) and PEG chains (hydrophilic), it is assumed that when used in O/W emulsion, the hydrophobic part may interact with the oil component of the emulsion and the hydrophilic part will interact with water. Fig. 4.13 shows the coefficient of friction of CoCrMo-PAA-PEG-lactide and CoCrMo-GO-PAA-PEG-lactide in emulsions. The performance of CoCrMo-PAA-PEG and CoCrMo-GO-PAA-PEG is also shown for reasons of comparison. From the figure, it can be seen again that the coatings with GO perform better than those without GO. For the same coating, the COF in the emulsion with 2.0 wt. % additive (O/W 2%) is lower than that without additive (O/W 0%). When using an emulsion with additive, the COF of the coating with lactide is almost the same as without lactide, suggesting that the additive effect is predominantly due to the formation of protective boundary layers from the additive. When using an emulsion without additive, the coating with lactide always performs better than that without lactide, which may be attribute to the different response of amphiphilic coatings to the O/W emulsion at different stages of the friction process as illustrated in Fig. 3.2 and 3.4.

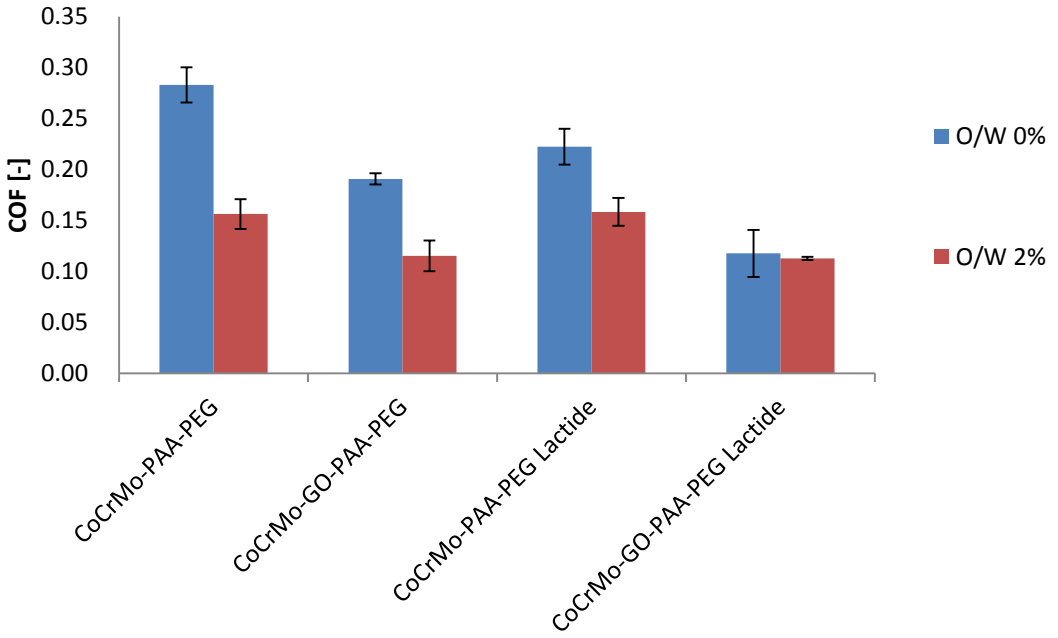

Fig. 4.13 The coefficient of friction of CoCrMo-PAA-PEG-lactide and CoCrMo-GO-PAA-PEG-lactide in emulsions

According to the friction profile as shown in Fig. 4.14, the COF of experimental work with the coatings in water increases with time, while in 0% additive emulsion the COF increases before 600 seconds and after that the COF drops and then increases gradually with time.

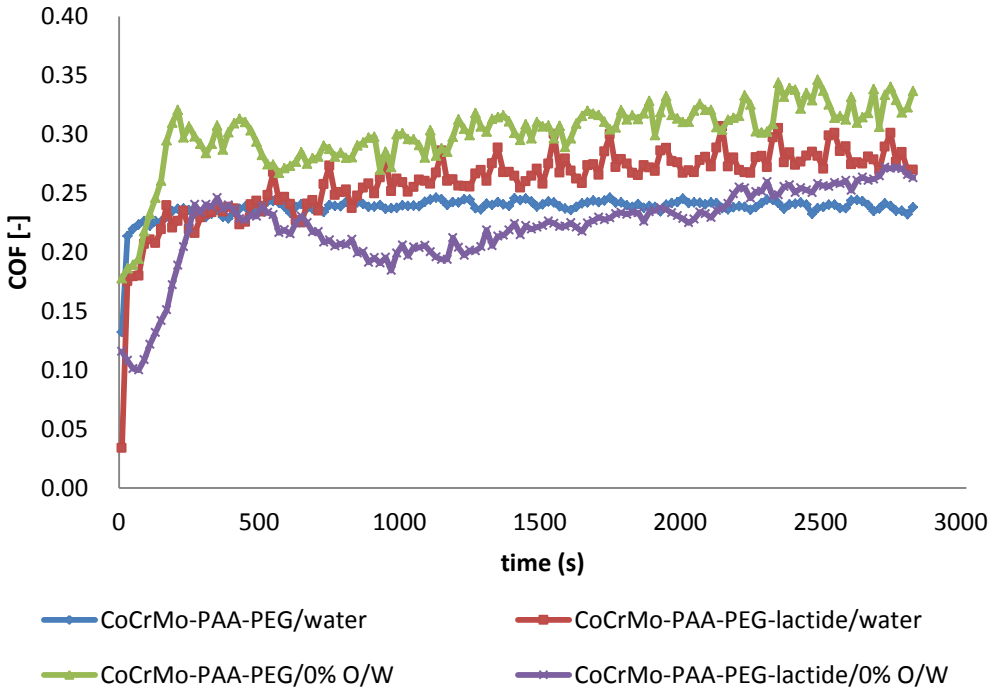

Fig. 4.14 The variations of COF with time for different coatings in different lubricants

By comparing the friction profile, the interaction between the PEG-lactide coating and water is quite different compared to the interaction between the PEG-lactide coating and an O/W emulsion. In water, the COF increases with time, while in the emulsion, the friction profile shows the three stage phenomena as described in detail in Section 3.3.1. At the beginning of the test, after the first stage of running-in, water plays the dominant role and a higher COF can be found in stage two. After 500 to 600 seconds, the droplets broke and plated-out onto the surface to form protection layer in stage three resulting in lower friction.

The tribological performance of PEG-lactide coating in the 0% O/W emulsion is better than that of the PEG coating. This is in-line with the proposed lubrication mechanism with amphiphilic coatings, see Fig. 3.2 and 3.3, i.e. interaction between the hydrophilic group with the water phase at stage two, and interaction between lipophilic group with the oil phase at stage three. The tribological interaction between PEG-lactide coating and emulsions is schematically shown in Section 3.4. At stage two, the surface is exposed to a water environment, the lipophilic chains in PEG-lactide collapse, while the hydrophilic chains extend due to the formation of hydrogen bonds with water. At stage three, the surface is covered by the oil component, the hydrophilic chains in PEG-lactide collapse, but the lipophilic chains extend because of the interaction between the lipophilic chain and the oil component.

4.5 Micro scale tribological performance of graphene oxide combined with brush coatings in aqueous systems

4.5.1 Outlook on tribological phenomena at the micro scale

Macro scale tribological study has been used to prove the lubrication concept. The measurements showed the effectiveness of the newly developed lubrication concept. In this section, micro scale tribological experiments were performed to understand the interactions at the asperity scale. The experiments were conducted in phosphate buffered saline (PBS), a water-based salt solution containing sodium phosphate, potassium chloride and potassium phosphate. It is

widely used in biomedical research because the osmolarity and ion concentrations of the solutions match those of the human body.

Atomic force microscopy (AFM) is used for this section to study the micro scale friction behaviour, and AFM can also be used to undertake adhesion study and imaging which is helpful to understand the hypothesis in Chapter III. The tip of the AFM used in sliding on a smooth surface could represent a single asperity contact. Most AFM measurements in a solution are carried out in PBS [161-164]. Therefore, PBS is used as a start to examine the micro scale tribological behaviour.

4.5.2 Searching and defining an experimental method

The material and aqueous media used in this section are similar to Section 4.4.1 with the smooth surface. The microtribological properties of different film samples were measured using a Nanoscope III a multimode atomic force microscope (AFM, Veeco) in contact mode. Triangular silicon nitride cantilevers with a normal force constant of 3 N/m were employed for AFM measurements. The scanning frequency is 1.969 Hz and the scan size is 500 nm which means the sliding velocity is 1.969 μm/s. No attempt was made to calibrate the torsional force constant, and the same cantilever was applied in all measurements. The output voltages were directly used as the relative frictional force. A series of measurements of friction–load relationship was conducted from friction loops obtained from at least three separate locations on each sample surface. All experiments were carried out under ambient conditions of 25 ^{o}C and 30% relative humidity.

4.5.3 Preliminary measurements

As the lateral spring constant of the cantilevers and the lateral sensitivity of the optical detector were not measured, the absolute frictional force could not be obtained directly. The output voltages were directly used as the relative frictional force. The friction forces on various surfaces can be compared with one another when the same AFM tip is employed. The friction-versus-load curves for different surfaces in PBS were plotted in Fig. 4.15. It is apparent that the curves can be fitted by straight lines. The relative coefficient of friction (RCOF), i.e., the slope of

the fitted line, is introduced to compare with each other [165, 166]. The results of at least three tests are shown in Fig. 4.16 by taking the RCOF of CoCrMo as 1.

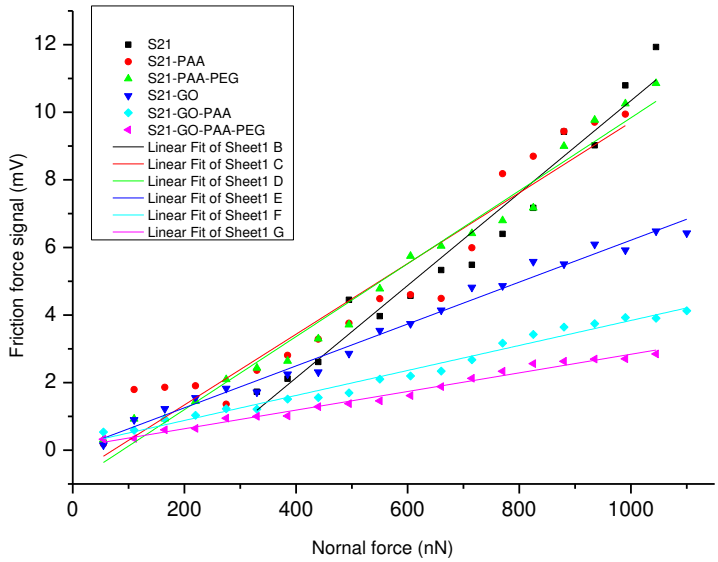

Fig. 4.15 Friction force signal as a function of normal force in PBS for smooth surface

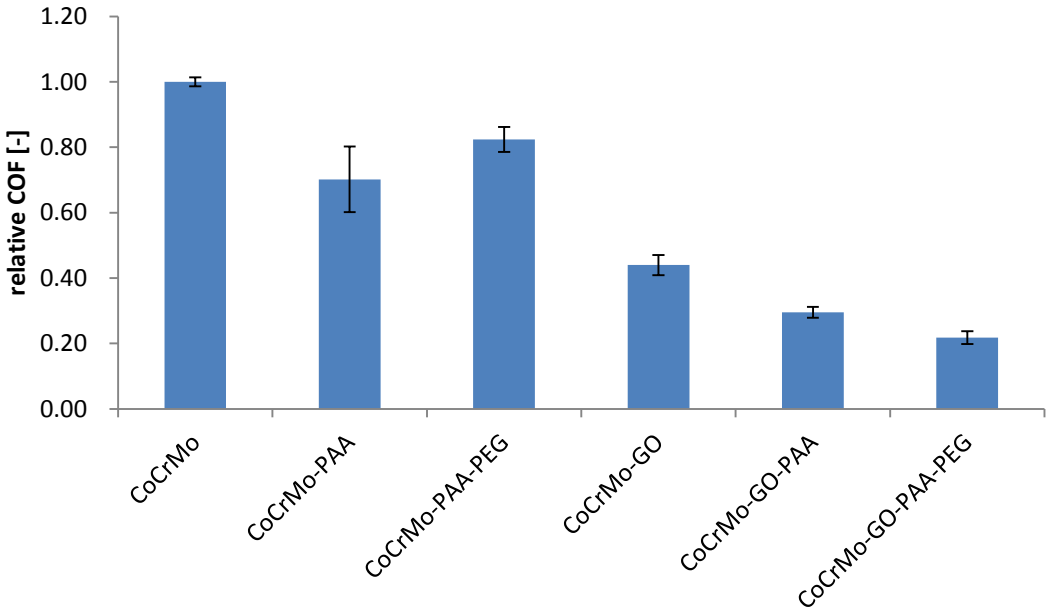

Fig. 4.16 Relative COF of the coatings in PBS for smooth surface

As is shown in the figures, it can be seen that the RCOF is ranked as CoCrMo substrate>CoCrMo-PAA-PEG>CoCrMo-PAA, indicating the function of hydrophilic coatings. Furthermore, when GO was coated, the RCOF decreased largely and the ranking is in the sequence of CoCrMo substrate>>CoCrMo-GO>CoCrMo-GO-PAA> CoCrMo-GO-PAA-PEG. The tendency suggests the same synergy effect of GO with

the hydrophilic coatings and similar trend to macro scale friction results in Section 4.4.2.

Chapter V Conclusions and recommendations

New lubrication concepts for aqueous environments were studied and, more specifically, the tribochemical mechanisms that determine the tribological response of poly(ethylene glycol)-*graft*-poly(acrylic acid) (PEG-*g*-PAA) coatings on engineering surfaces of stainless steel and CoCrMo-alloys were studied in detail. The research included the role of hydration with water only, and the effect of 2.0 wt. % additives oil in water (O/W) emulsions and the effect of graphene oxide. New additives based on boron chemistry were investigated on their functionality in combination with stainless steel and CoCrMo. The conclusions are listed below grouped per chapter, followed by the recommendations for future study.

5.1 Conclusions

Oil-based lubricants have some major drawbacks such as poor biodegradability and high toxicity for humans. As such, oil-based lubricants cannot be used for applications with a high risk of polluting the environment or for applications that involve a bio-medical environment, respectively. Water-based lubricants, can potentially overcome these problems. The tribological performance, however limits the current use of water based lubricants. From a literature review on Lubrication in an aqueous environment it showed that:

- Oil lubrication is widely used for mechanical components. New additives such as phosphorus–nitrogen additives with lower phosphorus content, borate esters and borate calcium are successfully used for boundary lubrication of ball bearing steel.

- Water-based lubrication makes use of the cooling capability, low toxicity and fire resistance properties of aqueous fluids, yet water has poor lubricating properties related to the low viscosity.

    - Alternatively, oil-in-water emulsion are widely used in metal forming operations such as rolling, cutting, ironing or grinding especially for food related industry. For the emulsion, researchers have conventionally attributed the effectiveness in lubricating contacts to

the ‘plate out’ mechanism.

- Synovial fluids is a natural and water-based lubricant with high efficiency. Experimental work on the tribological properties is typically conducted with water, PBS, SBF and BS.

- One of the approaches of aqueous lubrication is hydration lubrication It involves water and a surface layer of hydrophilic polymers fixed to the surface. The hydrated layers formed by the hydrophilic polymers and water on the interacting surfaces during sliding create a boundary layer which is used for friction control in aqueous environments.

  - Some tribological properties of water can be attributed to the fluidity of water in confined thin films. The hydration repulsion originated from the confined water can support very high pressure to overcome the Van der Waals force between the two surfaces.

  - Hydration lubrication is found in the behaviour of synovial fluid. A typical hip or knee joint possesses a layer of articular cartilage which is like the coat of the articulating bones. The synovial fluid serves as an aqueous lubricant.

  - Water-soluble polymers such as PAA and PEG are widely used as hydrophilic coatings. The polymers are chemically bonded to the surface, and the durability is satisfied for surfaces such as mica, silica wafer and steel.

- Stainless steel and CoCrMo are frequently used in tribological applications that require a combination of hardness, wear resistance and corrosion resistance. Therefore, they are most common used in joint implants and can be found in some researches on the development of synovial fluid based lubricants. Furthermore, a few inorganic hard coatings like DLC and ZrO_2 are applied to enhance the surface properties of CoCrMo alloys. The modification of stainless steel and CoCrMo with biomaterials like enzymes can extend their application in a biological environment.

New aqueous lubrication concepts for biomedical applications

This thesis contains four aqueous lubrication concepts for engineering surfaces from CoCrMo:

- O/W emulsion lubrication with tailored additives for use with CoCrMo surfaces and a biomedical environment.
- A fully hydrophilic brush coating to form a hydrated layer on the engineering contact surfaces.
- A layer of graphene oxide, subsequently coated with a fully hydrophilic brush coating to enhance the bonding strength of the layers or to create a layer that is able to withstand high pressure.
- An amphiphilic coating combined with graphene oxide and used with the O/W emulsions. In this system at the hydration stage the hydrated layer is thought to work, while at the emulsion stage the plated-out oil layer is thought to work as lubricating layer.

Measuring friction in boundary lubrication regime

- The XPS and XANES analysis of TDB and DDB suggests that different reaction films were generated on bearing steel. The tribofilms which contains BN formed by DDB are more helpful for AW properties than B_2O_3 formed by TDB.
- For the interaction between stainless steel, CoCrMo alloy and newly developed additives, XPS results show that the lubricating films are consist of an adsorption layer and a reaction layer. The adsorption layer is formed by the coordination of nitrogen-containing additives on the metal surface. The reaction layer originates from the tribochemical reaction of the active elements in the additives and the main difference on the films lies in the reaction layer.
- For the interaction between uncoated metallic substrates and O/W emulsions, the main difference between the tribological performances of the films formed by the additives also originates from the reaction layer.
    - More specifically for ODOC, besides iron oxide and iron hydroxide, calcium oxide was also generated, all of which are demonstrated to be

helpful for friction-reducing. For DBOP, besides iron oxides and iron hydroxides, the existence of $FePO_4$ and the freshly exposed iron, which is proved to be reactive with the additives, could be related to the better performance.

- The friction profiles generated by different additive-based emulsions suggest that the water phase may play the dominant role at the beginning, while after the droplet of the emulsion is broken, the additives will adsorb onto and react with the metal surface.

- The differences in friction and wear performance between the oil-based system and the O/W emulsion-based system with the same functional additives are related to the chemical structure of the reaction layer formed at the surface.

- From the tribological performance of graphene oxide combined with brush coatings in aqueous systems at the macro scale, a surface of higher roughness showed higher friction values compared to the same tribosystem with a smoother surface.

  - The tribological performance of the surface-active polymer coatings with or without GO was evaluated in different aqueous media, i.e. water, PBS, BS and O/W emulsions. Synergetic effects have been observed between GO and surface-active polymers. From the preliminary work at the micro scale, the synergy effect between graphene and the polymeric coatings was also confirmed by using AFM in PBS.

  - The tribological behaviour of PEG-lactide coating in emulsion was better than that of PEG coating, indicating the advantage of using hydrophilic and hydrophobic group containing surface-active polymers for emulsion lubrication.

- From the results it showed that CoCrMo performs poorly in water at low sliding velocity and moderate contact pressure: the measurements revealed a high COF of 0.30 in water. CoCrMo with a polymeric brush coating always showed a lower COF when measured at the same operational conditions and in water. The COF for CoCrMo-PAA in water at the selected operational

conditions was 0.23. When there is a GO layer in between, the COF for CoCrMo-GO-PAA was reduced to 0.18. For CoCrMo-GO-PAA-PEG-lactide in O/W emulsion, the COF was even reduced to 0.11. The reduction in friction of about 63 % demonstrated the potential of the novel lubrication concept.

5.2 Recommendations for future study

- The presented friction behaviour can be enhanced further towards super low friction:

    - Surface active polymers grafted onto one of the interacting surfaces have proved to be functional in reducing friction for rough engineering surfaces in this study. Systematic research on tailoring potential surface active polymers onto both interacting surfaces with respect to surface roughness and interacting environment is vital for the real application of surface active polymers into industries. The optimum thickness and density for reducing friction on rough surface may be predicted and designed by modeling and establishing the relationship among surface coating parameters (grating density, grafting thickness, etc.), surface roughness parameters and frictional behaviour of surface coating. “Grafting-from” method can be used to control and tailor the surface coating parameters.

    - Both graphene oxide and O/W emulsion have been proved to have promising boundary lubrication capability for stainless steel and CoCrMo alloy in aqueous system. Instead of coating graphene oxide onto the substrate surface, and instead of using surfactant as the emulsifier for making O/W emulsion, pickering emulsion by using graphene oxide as the emulsifier, is expected to not only generate promising synergetic boundary lubrication performance due to the incorporating of lubricious graphene oxide, but also reduce the potential toxicity of surfactant compared to traditional O/W emulsion. With careful development steps this could potentially grow to a new methodology for extending the life of prosthetic articular joints.

- The developed aqueous lubrication concepts are based on metal surfaces, i.e.

bearing steel, stainless steel and CoCrMo alloy, and should be extended to other engineering surfaces, like various polymeric materials, i.e. UHMWPE in joint implant, fibers used in medical textiles. The scope of the hydrophilic coatings can be enlarged as well to for instance hydrogels.

- The scientific knowledge of the mechanisms that control the novel lubrication concepts can be further developed by studying the micro scale friction behaviour, by studying the adhesion aspects related to the layer as well as by advanced imaging of chemistry of the layer. Especially, surface-modified CoCrMo and stainless steel can be studied in more detail during and after friction process to reveal differences in the composition, thickness and structure of the surface layers formed as a function of solution composition.

- Efforts should be made to transfer the results obtained in the laboratory to practical applications in bio-, medical-, and mechanical engineering. The lubrication concept might be applied to machine elements in a water environment.

Bibliography

[1] Lee S, Spencer ND. Aqueous lubrication of polymers: Influence of surface modification. Tribology International. 2005;38:922-30.
[2] Wei QB, Cai MR, Zhou F. Progress on surface grafted polymer brushes for biomimetic lubrication. Acta Polymerica Sinica. 2012:1102-7.
[3] Dowson D. History of tribology: Longman London; 1979.
[4] de Vicente J, Stokes JR, Spikes HA. Lubrication properties of non-adsorbing polymer solutions in soft elastohydrodynamic (EHD) contacts. Tribology International. 2005;38:515-26.
[5] Campos JM, Stamford TLM, Sarubbo LA, de Luna JM, Rufino RD, Banat IM. Microbial Biosurfactants as Additives for Food Industries. Biotechnology Progress. 2013;29:1097-108.
[6] Klein J. Polymers in living systems: from biological lubrication to tissue engineering and biomedical devices. Polymers for Advanced Technologies. 2012;23:729-35.
[7] Briscoe WH, Titmuss S, Tiberg F, Thomas RK, McGillivray DJ, Klein J. Boundary lubrication under water. Nature. 2006;444:191-4.
[8] Li JJ, Zhang CH, Luo JB. Superlubricity Behavior with Phosphoric Acid-Water Network Induced by Rubbing. Langmuir. 2011;27:9413-7.
[9] Chen M, Briscoe WH, Armes SP, Klein J. Lubrication at Physiological Pressures by Polyzwitterionic Brushes. Science. 2009;323:1698-701.
[10] Chen BB, Wang JZ, Yan FY. Friction and Wear Behaviors of Several Polymers Sliding Against GCr15 and 316 Steel Under the Lubrication of Sea Water. Tribology Letters. 2011;42:17-25.
[11] Ku ISY, Reddyhoff T, Wayte R, Choo JH, Holmes AS, Spikes HA. Lubrication of Microelectromechanical Devices Using Liquids of Different Viscosities. Journal of Tribology-Transactions of the ASME. 2012;134.
[12] Wang J, Li T, Peng J, Chen Z. Water lubrication of mechanical frictional pairs - current research and future development trends. Proceedings of the International Conference on Gearing, Transmissions, and Mechanical Systems, ed. D.Z. Su. 2000;761-768.
[13] Hamrock BJ, Schmid SR, Jacobson BO. Fundamentals of fluid film lubrication: CRC press; Vol. 169, 2004.
[14] Stribeck R. Die Wesentlichen Eigenschaften der Gleit- und Rollenlager. Z Verein Deut Ing. 1902;46:1341-8.
[15] de Gee A, Rowe G. Glossary of Terms and Definitions in the Field of Friction, Wear, and Lubrication: Tribology. IRG-OECD. 1969.
[16] Klein J. Shear of liquid films confined to molecular dimensions. Journal of non-crystalline solids. 1998;235:422-7.
[17] Mate CM, McClelland GM, Erlandsson R, Chiang S. Atomic-scale friction of a tungsten tip on a graphite surface. Scanning Tunneling Microscopy: Springer; 1993. p. 226-9.
[18] Salomon G. Application of Systems Thinking to Tribology. ASLE Transactions. 1974;17:295-9.
[19] Czichos H. Tribology: a systems approach to the science and technology of friction, lubrication, and wear: a systems approach to the science and technology of friction, lubrication, and wear: Elsevier; 2009.
[20] Dowson D. Tribological principles in metal-on-metal hip joint design. Proceedings of the Institution of Mechanical Engineers, Part H: Journal of Engineering in Medicine. 2006;220:161-71.

[21] Hosford W, Duncan J. Sheet metal forming: A review. JOM. 1999;51:39-44.
[22] Chen S, Doolen GD. Lattice Boltzmann method for fluid flows. Annual Review of Fluid Mechanics. 1998;30:329-64.
[23] Rudnick LR. Lubricant additives: chemistry and applications: CRC Press; 2010.
[24] Ii M, Eda H, Imai T, Nishimura M, Kawasaki T, Shimizu J, et al. Development of high water-content cutting fluids with a new concept - Fire prevention and environmental protection. Precision Engineering-Journal of the International Societies for Precision Engineering and Nanotechnology. 2000;24:231-6.
[25] Yao JB. Antiwear function and mechanism of borate containing nitrogen. Tribology International. 1997;30:387-9.
[26] Shen GQ, Zheng Z, Wan Y, Xu XD, Cao LL, Yue QX, et al. Synergistic lubricating effects of borate ester with heterocyclic compound. Wear. 2000;246:55-8.
[27] Zheng Z, Shen GQ, Wan Y, Cao LL, Xu XD, Yue QX, et al. Synthesis, hydrolytic stability and tribological properties of novel borate esters containing nitrogen as lubricant additives. Wear. 1998;222:135-44.
[28] Li JS, Xu XH, Wang YG, Ren TH. Tribological studies on a novel borate ester containing benzothiazol-2-y1 and disulfide groups as multifunctional additive. Tribology International. 2010;43:1048-53.
[29] Betton CI. Lubricants and Their Environmental Impact. In: Mortier RM, Fox MF, Orszulik ST, editors. Chemistry and Technology of Lubricants: Springer Netherlands; 2010. p. 435-57.
[30] Bakunin VN, Suslov AY, Kuzmina GN, Parenago OP. Synthesis and application of inorganic nanoparticles as lubricant components - a review. Journal of Nanoparticle Research. 2004;6:273-84.
[31] Xu SF, Chen AM, Ni ZM, Zhao SF. Synthesis and Characterization of OA Modified Calcium Borate Nanoplatelets. Rare Metal Materials and Engineering. 2010;39:340-3.
[32] Martin JM, Onodera T, Bouchet MID, Hatakeyama N, Miyamoto A. Anti-wear Chemistry of ZDDP and Calcium Borate Nano-additive. Coupling Experiments, Chemical Hardness Predictions, and MD Calculations. Tribology Letters. 2013;50:95-104.
[33] Tas AC. Porous, biphasic CaCO3-calcium phosphate biomedical cement scaffolds from calcite (CaCO3) powder. International Journal of Applied Ceramic Technology. 2007;4:152-63.
[34] Hori M, Kiriya D, Takeuchi S, Ieee. inorganic/parylene composite thin film toward 3d robust structures. 2012 Ieee 25th International Conference on Micro Electro Mechanical Systems2012.
[35] Wang YG, Li JS, Ren TH. Tribological study of a novel borate ester containing S, P with high hydrolytic stability as a multifunctional lubricating additive. Tribology Transactions. 2008;51:160-5.
[36] Li JC, Li ZP, Ren TH, Zeng XQ, van der Heide E. Hydrolytic stability and tribological properties of N-containing heterocyclic borate esters as lubricant additives in rapeseed oil. Tribology International. 2014;73:101-7.
[37] Skaer RJ, Peters PD, Emmines JP. The Localization of Calcium and Phosphorus in Human Platelets. Journal of Cell Science. 1974;15:679-92.
[38] Plaza S, Margielewski L, Celichowski G, Wesolowski RW, Stanecka R. Tribological performance of some polyoxyethylene dithiophosphate derivatives water solutions. Wear. 2001;249:1077-89.
[39] Ma HB, Qiao R, Li YL, Chen H, Ren TH. XANES characteristics of tribofilms generated by dithiophosphate additive in water at different test temperatures and durations. Surface and Interface Analysis. 2009;41:779-84.

[40] Ma HB, Peng LL, Liang PP, Qiao R, Ren TH. X-ray absorption near-edge structure analysis of tribofilms generated by highly efficient, friction-reducing additive in water-polyglycol-glycol lubricant. Lubr Sci. 2009;21:297-304.
[41] Benito JM, Cambiella A, Lobo A, Gutierrez G, Coca J, Pazos C. Formulation, characterization and treatment of metalworking oil-in-water emulsions. Clean Technologies and Environmental Policy. 2010;12:31-41.
[42] Tieu AK, Kosasih PB. Experimental and numerical study of O/W emulsion lubricated strip rolling in mixed film regime. Tribology Letters. 2007;25:23-32.
[43] Azushima A, Inagaki S, Ohta H. Starvation Behavior in Cold Rolling of Aluminum with Oil-in-Water Emulsion. Tribology Transactions. 2009;52:744-9.
[44] Liu JY, Han RD, Wang Y. Research on difficult-cut-material in cutting with application of water vapor as coolant and lubricant. Industrial Lubrication and Tribology. 2010;62:251-62.
[45] Schmid SR, Zhou J. Flow factors for lubrication with emulsions in ironing. Journal of Tribology-Transactions of the Asme. 2001;123:283-9.
[46] Dubey SP, Sharma GK, Shishodia KS, Sekhon GS. A study of lubrication mechanism of oil-in-water (O/W) emulsions in steel cold rolling. Industrial Lubrication and Tribology. 2005;57:208-12.
[47] Wang WX, Liu P, Yao GQ. Study on Lubrication Properties of Emulsion for Aluminum Cold-rolling. In: Gao QJ, editor. Machinery, Materials Science and Engineering Applications, Pts 1 and 22011. p. 321-6.
[48] Cambiella A, Benito JM, Pazos C, Coca J, Ratoi M, Spikes HA. The effect of emulsifier concentration on the lubricating properties of oil-in-water emulsions. Tribology Letters. 2006;22:53-65.
[49] Schmid SR, Wilson WRD. Lubrication mechanisms for oil-in-water emulsions. Lubrication Engineering. 1996;52:168-75.
[50] Ma LR, Zhang CH, Luo JB. Investigation of the film formation mechanism of oil-in-water (O/W) emulsions. Soft Matter. 2011;7:4207-13.
[51] Fujita N, Kimura Y. Plate-out efficiency related to oil-in-water emulsions supply conditions on cold rolling strip. Proceedings of the Institution of Mechanical Engineers, Part J: Journal of Engineering Tribology. 2012.
[52] Ma L, Zhang C, Luo J. Investigation of the film formation mechanism of oil-in-water (O/W) emulsions. Soft Matter. 2011;7:4207-13.
[53] Kumar A, Schmid SR, Wilson WRD. Particle behavior in two-phased lubrication. Wear. 1997;206:130-5.
[54] Abdul-Raouf ME, Abdul-Raheim ARM, Maysour NE, Mohamed H. Synthesis, Surface-Active Properties, and Emulsification Efficiency of Trimeric-Type Nonionic Surfactants Derived From Tris(2-aminoethyl)amine. Journal of Surfactants and Detergents. 2011;14:185-93.
[55] Mohlin K, Holmberg K. Nonionic ortho ester surfactants as cleavable emulsifiers. Journal of Colloid and Interface Science. 2006;299:435-42.
[56] Hvattum E, Yip WL, Grace D, Dyrstad K. Characterization of polysorbate 80 with liquid chromatography mass spectrometry and nuclear magnetic resonance spectroscopy: Specific determination of oxidation products of thermally oxidized polysorbate 80. Journal of Pharmaceutical and Biomedical Analysis. 2012;62:7-16.
[57] Pavlovich RI, Lubowitz J. Current concepts in synovial tissue of the knee joint. Orthopedics. 2008;31:160-5.

[58] Vanwanseele B, Lucchinetti E, Stussi E. The effects of immobilization on the characteristics of articular cartilage: current concepts and future directions. Osteoarthritis and Cartilage. 2002;10:408-19.
[59] Hui AY, McCarty WJ, Masuda K, Firestein GS, Sah RL. A systems biology approach to synovial joint lubrication in health, injury, and disease. Wiley Interdisciplinary Reviews-Systems Biology and Medicine. 2012;4:15-37.
[60] Mavraki A, Cann PM. Friction and lubricant film thickness measurements on simulated synovial fluids. Proceedings of the Institution of Mechanical Engineers Part J-Journal of Engineering Tribology. 2009;223:325-35.
[61] Julian LC, Munoz AI. Influence of microstructure of HC CoCrMo biomedical alloys on the corrosion and wear behaviour in simulated body fluids. Tribology International. 2011;44:318-29.
[62] Marques MRC, Loebenberg R, Almukainzi M. Simulated Biological Fluids with Possible Application in Dissolution Testing. Dissolution Technologies. 2011;18:15-28.
[63] Saxne T, Palladino MA, Heinegard D, Talal N, Wollheim FA. Detection of tumor necrosis factor-alpha but not tumor necrosis factor-beta in rheumatoid-arthritis synovial-fluid and serum. Arthritis and Rheumatism. 1988;31:1041-5.
[64] Kaur H, Halliwell B. Evidence for nitric oxide-mediated oxidative damage in chronic inflammation - nitrotyrosine in serum and synovial-fluid from rheumatoid patients. Febs Letters. 1994;350:9-12.
[65] Farrell AJ, Blake DR, Palmer RMJ, Moncada S. Increased concentrations of nitrite in synovial-fluid and serum samples suggest increased nitric-oxide synthesis in rheumatic diseases. Annals of the Rheumatic Diseases. 1992;51:1219-22.
[66] Houssiau FA, Devogelaer JP, Vandamme J, Dedeuxchaisnes CN, Vansnick J. Interleukin-6 in synovial-fluid and serum of patients with rheumatoid-arthritis and other inflammatory arthritides. Arthritis and Rheumatism. 1988;31:784-8.
[67] Gaisinskaya A, Ma L, Silbert G, Sorkin R, Tairy O, Goldberg R, et al. Hydration lubrication: exploring a new paradigm. Faraday discussions. 2012;156:217-33.
[68] Ikeuchi K. Origin and future of hydration lubrication. Proceedings of the Institution of Mechanical Engineers Part J-Journal of Engineering Tribology. 2007;221:458-.
[69] Goren T, Crockett R, Spencer ND. Influence of Solutes on Hydration and Lubricity of Dextran Brushes. Chimia. 2012;66:192-5.
[70] Nalam PC, Ramakrishna SN, Espinosa-Marzal RM, Spencer ND. Exploring Lubrication Regimes at the Nanoscale: Nanotribological Characterization of Silica and Polymer Brushes in Viscous Solvents. Langmuir. 2013;29:10149-58.
[71] Perkin S, Goldberg R, Chai L, Kampf N, Klein J. Dynamic properties of confined hydration layers. Faraday Discussions. 2009;141:399-413.
[72] Raviv U, Giasson S, Kampf N, Gohy JF, Jerome R, Klein J. Lubrication by charged polymers. Nature. 2003;425:163-5.
[73] Liu GQ, Wang XL, Zhou F, Liu WM. Tuning the Tribological Property with Thermal Sensitive Microgels for Aqueous Lubrication. Acs Applied Materials & Interfaces. 2013;5:10842-52.
[74] Wang QZ, Zhou F, Ding XD, Zhou ZF, Zhang WJ, Li LKY, et al. Influences of ceramic mating balls on the tribological properties of Cr/a-C coatings with low chromium content in water lubrication. Wear. 2013;303:354-60.
[75] Klein J, Kumacheva E, Mahalu D, Perahia D, Fetters LJ. Reduction of frictional forces between solid-surfaces bearing polymer brushes. Nature. 1994;370:634-6.

[76] Raviv U, Perkin S, Laurat P, Klein J. Fluidity of Water Confined Down to Subnanometer Films. Langmuir. 2004;20:5322-32.
[77] Israelachvili JN, Mcguiggan PM, Homola AM. Dynamic Properties of Molecularly Thin Liquid Films. Science. 1988;240:189-91.
[78] Klein J, Kumacheva E. Confinement-Induced Phase Transitions in Simple Liquids. Science. 1995;269:816-9.
[79] Raviv U, Laurat P, Klein J. Fluidity of water confined to subnanometre films. Nature. 2001;413:51-4.
[80] Cappella B, Dietler G. Force-distance curves by atomic force microscopy. Surface Science Reports. 1999;34:1-3:1-3, 5-104.
[81] Klein J. Hydration lubrication. Friction. 2013;1:1-23.
[82] Cui ST, Cummings PT, Cochran HD. Molecular simulation of the transition from liquidlike to solidlike behavior in complex fluids confined to nanoscale gaps. Journal of Chemical Physics. 2001;114:7189-95.
[83] Jagla EA. Boundary lubrication properties of materials with expansive freezing. Physical Review Letters. 2002;88.
[84] Israelachvili JN, Adams GE. Measurement of forces between two mica surfaces in aqueous electrolyte solutions in the range 0-100 nm. Journal of the Chemical Society, Faraday Transactions 1: Physical Chemistry in Condensed Phases. 1978;74:975-1001.
[85] Leng YS. Hydration Force between Mica Surfaces in Aqueous KCl Electrolyte Solution. Langmuir. 2012;28:5339-49.
[86] Pashley RM. Hydration forces between mica surfaces in aqueous-electrolyte solutions. Journal of Colloid and Interface Science. 1981;80:153-62.
[87] Hardy W, Bircumshaw I. Bakerian Lecture. Boundary Lubrication. Plane Surfaces and the Limitations of Amontons' Law. Proceedings of the Royal Society of London Series A, Containing Papers of a Mathematical and Physical Character. 1925;108:1-27.
[88] Briscoe WH, Klein J. Friction and adhesion hysteresis between surfactant monolayers in water. Journal of Adhesion. 2007;83:705-22.
[89] Briscoe BJ, Evans DCB. The Shear Properties of Langmuir-Blodgett Layers. Proceedings of the Royal Society of London A Mathematical and Physical Sciences. 1982;380:389-407.
[90] Goldberg R, Schroeder A, Silbert G, Turjeman K, Barenholz Y, Klein J. Boundary Lubricants with Exceptionally Low Friction Coefficients Based on 2D Close-Packed Phosphatidylcholine Liposomes. Advanced Materials. 2011;23:3517-21.
[91] Klein J. Repair or Replacement--A Joint Perspective. Science. 2009;323:47-8.
[92] Müller M, Lee S, Spikes H, Spencer N. The Influence of Molecular Architecture on the Macroscopic Lubrication Properties of the Brush-Like Co-polyelectrolyte Poly(L-lysine)-g-poly(ethylene glycol) (PLL-g-PEG) Adsorbed on Oxide Surfaces. TriL. 2003;15:395-405.
[93] Müller MT, Yan X, Lee S, Perry SS, Spencer ND. Lubrication Properties of a Brushlike Copolymer as a Function of the Amount of Solvent Absorbed within the Brush. Macromolecules. 2005;38:5706-13.
[94] Komoto T, Tanaka K, Hironaka S. Poly (vinyl alcohol)-grafted polyethylene as a model for an artificial joint. Sen'i Gakkaishi. 1984;40:T125-T8.
[95] Hironaka S, Tanaka K, Komoto T. Frictional Behavior of Poly(vinyl alcohol)-Grafted Polyethylene in Water. Journal of The Japan Petroleum Institute. 1985;28:168-71.

[96] Ishikawa Y, Sasada T. Lubrication properties of hydrogel-coated polyethylene head. Materials Transactions. 2004;45:1041-4.
[97] Ho SP, Nakabayashi N, Iwasaki Y, Boland T, LaBerge M. Frictional properties of poly(MPC-co-BMA) phospholipid polymer for catheter applications. Biomaterials. 2003;24:5121-9.
[98] Uyama Y, Tadokoro H, Ikada Y. Low-frictional catheter materials by photoinduced graft-polymerization. Biomaterials. 1991;12:71-5.
[99] Ikeuchi K, Takii T, Norikane H, Tomita N, Ohsumi T, Uyama Y, et al. Water lubrication of polyurethane grafted with dimethylacrylamide for medical use. Wear. 1993;161:179-85.
[100] Moro T, Takatori Y, Ishihara K, Konno T, Takigawa Y, Matsushita T, et al. Surface grafting of artificial joints with a biocompatible polymer for preventing periprosthetic osteolysis. Nature Materials. 2004;3:829-36.
[101] Yoshikawa C, Goto A, Tsujii Y, Ishizuka N, Nakanishi K, Fukuda T. Sur-face interaction of well-defined, concentrated poly,(2-hydroxyethyl methacrylate) brushes with proteins. J Polym Sci Pol Chem. 2007;45:4795-803.
[102] Wei QB, Cai MR, Zhou F, Liu WM. Dramatically Tuning Friction Using Responsive Polyelectrolyte Brushes. Macromolecules. 2013;46:9368-79.
[103] Chen M, Briscoe WH, Armes SP, Cohen H, Klein J. Polyzwitterionic brushes: Extreme lubrication by design. European Polymer Journal. 2011;47:511-23.
[104] Goldberg R, Klein J. Liposomes as lubricants: beyond drug delivery. Chemistry and Physics of Lipids. 2012;165:374-81.
[105] Quintana R, Gosa M, Janczewski D, Kutnyanszky E, Vancso GJ. Enhanced Stability of Low Fouling Zwitterionic Polymer Brushes in Seawater with Diblock Architecture. Langmuir. 2013;29:10859-67.
[106] Kobayashi M, Terayama Y, Yamaguchi H, Terada M, Murakami D, Ishihara K, et al. Wettability and Antifouling Behavior on the Surfaces of Superhydrophilic Polymer Brushes. Langmuir. 2012;28:7212-22.
[107] Yang WJ, Cai T, Neoh KG, Kang ET, Dickinson GH, Teo SLM, et al. Biomimetic Anchors for Antifouling and Antibacterial Polymer Brushes on Stainless Steel. Langmuir. 2011;27:7065-76.
[108] Freeman ME, Furey MJ, Love BJ, Hampton JM. Friction, wear, and lubrication of hydrogels as synthetic articular cartilage. Wear. 2000;241:129-35.
[109] Bavaresco VP, Zavaglia CAC, Reis MC, Gomes JR. Study on the tribological properties of pHEMA hydrogels for use in artificial articular cartilage. Wear. 2008;265:269-77.
[110] Lee S, Spencer ND. Poly(L-lysine)-graft-poly(ethylene glycol): a versatile aqueous lubricant additive for tribosystems involving thermoplastics. Lubr Sci. 2008;20:21-34.
[111] Farag MM. Quantitative Methods of Materials Selection. Handbook of Materials Selection: John Wiley & Sons, Inc.; 2007. p. 1-24.
[112] Navarro M, Michiardi A, Castano O, Planell JA. Biomaterials in orthopaedics. Journal of the Royal Society Interface. 2008;5:1137-58.
[113] Holzapfel BM, Reichert JC, Schantz JT, Gbureck U, Rackwitz L, Noth U, et al. How smart do biomaterials need to be? A translational science and clinical point of view. Advanced Drug Delivery Reviews. 2013;65:581-603.
[114] Grimm MJ. Selection of Materials for Biomedical Applications. Handbook of Materials Selection: John Wiley & Sons, Inc.; 2007. p. 1165-94.
[115] Shang S, Woo L. Selecting Materials for Medical Products. Handbook of Materials Selection: John Wiley & Sons, Inc.; 2007. p. 1195-222.

[116] Wilches LV, Uribe JA, Toro A. Wear of materials used for artificial joints in total hip replacements. Wear. 2008;265:143-9.
[117] Long M, Rack HJ. Titanium alloys in total joint replacement - a materials science perspective. Biomaterials. 1998;19:1621-39.
[118] Kelly J. Stainless Steels. Handbook of Materials Selection: John Wiley & Sons, Inc.; 2007. p. 67-88.
[119] Reclaru L, Lerf R, Eschler PY, Meyer JM. Corrosion behavior of a welded stainless-steel orthopedic implant. Biomaterials. 2001;22:269-79.
[120] Venugopalan R, Trepanier C. Assessing the corrosion behaviour of Nitinol for minimally-invasive device design. Minimally Invasive Therapy & Allied Technologies. 2000;9:67-73.
[121] Singh R, Dahotre NB. Corrosion degradation and prevention by surface modification of biometallic materials. Journal of Materials Science-Materials in Medicine. 2007;18:725-51.
[122] Liu N, Wang JZ, Chen BB, Yan FY. Tribochemical aspects of silicon nitride ceramic sliding against stainless steel under the lubrication of seawater. Tribology International. 2013;61:205-13.
[123] Uchidate M, Iwabuchi A, Shimizu T, Liu HB. Tribological properties of stainless steel under water lubricated conditions - Effects of dissolved ions in tap water. Journal of Japanese Society of Tribologists. 2004;49:173-80.
[124] Liu JY, Liu HP, Han RD, Wang Y. The study on lubrication action with water vapor as coolant and lubricant in cutting ANSI 304 stainless steel. International Journal of Machine Tools & Manufacture. 2010;50:260-9.
[125] Gradzka-Dahlke M, Dabrowski JR, Dabrowski B. Modification of mechanical properties of sintered implant materials on the base of Co-Cr-Mo alloy. Journal of Materials Processing Technology. 2008;204:199-205.
[126] Standard Specification for Cobalt-28 Chromium-6 Molybdenum Alloy Castings and Casting Alloy for Surgical Implants. ASTM Standard. 2012;F75.
[127] Zhang XQ, Li YP, Tang N, Onodera E, Chiba A. Corrosion behaviour of CoCrMo alloys in 2 wt% sulphuric acid solution. Electrochimica Acta. 2014;125:543-55.
[128] Gispert MP, Serro AP, Colaço R, Saramago B. Friction and wear mechanisms in hip prosthesis: Comparison of joint materials behaviour in several lubricants. Wear. 2006;260:149-58.
[129] Goldberg JR, Gilbert JL. Electrochemical response of CoCrMo to high-speed fracture of its metal oxide using an electrochemical scratch test method. Journal of Biomedical Materials Research. 1997;37:421-31.
[130] Lewis AC, Kilburn MR, Papageorgiou I, Allen GC, Case CP. Effect of synovial fluid, phosphate-buffered saline solution, and water on the dissolution and corrosion properties of CoCrMo alloys as used in orthopedic implants. Journal of Biomedical Materials Research Part A. 2005;73A:456-67.
[131] Milošev I. The effect of biomolecules on the behaviour of CoCrMo alloy in various simulated physiological solutions. Electrochimica Acta. 2012;78:259-73.
[132] Stachowiak GW, Batchelor AW, Griffiths LJ. Friction and wear changes in synovial joints. Wear. 1994;171:135-42.
[133] Vidal CV, Juan AO, Munoz AL. Adsorption of bovine serum albumin on CoCrMo surface: Effect of temperature and protein concentration. Colloids and Surfaces B-Biointerfaces. 2010;80:1-11.

[134] Lewis AC, Kilburn MR, Heard PJ, Scott TB, Hallam KR, Allen GC, et al. The entrapment of corrosion products from CoCr implant alloys in the deposits of calcium phosphate: A comparison of serum, synovial fluid, albumin, EDTA, and water. Journal of Orthopaedic Research. 2006;24:1587-96.
[135] Milošev I, Hmeljak J, Cor A. Hyaluronic acid stimulates the formation of calcium phosphate on CoCrMo alloy in simulated physiological solution. Journal of Materials Science-Materials in Medicine. 2013;24:555-71.
[136] Hua ZK, Gu P, Zhang JH. Tribological and electrochemical studies on biomimetic synovial fluids. Science China-Technological Sciences. 2010;53:2996-3001.
[137] Yan Y, Neville A, Blowson D. Biotribocorrosion of CoCrMo orthopaedic implant materials - Assessing the formation and effectof the biofilm. Tribology International. 2007;40:1492-9.
[138] Liu HJ, Leng YX, Tang JL, Wang S, Xie D, Sun H, et al. Tribological performance of ultra-high-molecular-weight polyethylene sliding against DLC-coated and nitrogen ion implanted CoCrMo alloy measured in a hip joint simulator. Surface & Coatings Technology. 2012;206:4907-14.
[139] Yang YZ, Ong JL, Tian J. Deposition of highly adhesive ZrO2 coating on Ti and CoCrMo implant materials using plasma spraying. Biomaterials. 2003;24:619-27.
[140] Goldberg JR, Gilbert JL. The electrochemical and mechanical behavior of passivated and TiN/AlN-coated CoCrMo and Ti6Al4V alloys. Biomaterials. 2004;25:851-64.
[141] Lawson TR, Catledge SA, Vohra YK. Nanostructured diamond coated CoCrMo alloys for use in biomedical implants. In: Li P, Zhang K, Colwell CW, editors. Bioceramics, Vol 172005. p. 1015-8.
[142] Wang LN, Luo JL. Preparation of hydroxyapatite coating on CoCrMo implant using an effective electrochemically-assisted deposition pretreatment. Materials Characterization. 2011;62:1076-86.
[143] Dallaire S, Legoux JG, Levert H. Abrasion wear-resistance of arc-sprayed stainless-steel and composite stainless-steel coatings. Journal of Thermal Spray Technology. 1995;4:163-8.
[144] Liang P, Xu HF, Liu M, Lu L, Fu J. Electrochemical Performance Testing and Characterization of Silver-Plated and Graphite-Coated 316L Stainless Steel Bipolar Plates. Acta Physico-Chimica Sinica. 2010;26:595-600.
[145] Park TJ, Kong JP, Uhm SH, Woo IS, Lee JS, Kang CY. Effect of Al-Si coating layer on the penetration and microstructures of ferritic stainless steel, 409L GTA welds. Journal of Materials Processing Technology. 2011;211:415-23.
[146] Tian RJ. Chromium nitride/Cr coated 316L stainless steel as bipolar plate for proton exchange membrane fuel cell. Journal of Power Sources. 2011;196:1258-63.
[147] Wang HL, Turner JA, Li XN, Teeter G. Process modification for coating SnO_2 : F on stainless steels for PEM fuel cell bipolar plates. Journal of Power Sources. 2008;178:238-47.
[148] Chaudhari S, Sainkar SR, Patil PP. Poly(o-ethylaniline) coatings for stainless steel protection. Progress in Organic Coatings. 2007;58:54-63.
[149] Deberry DW. Modification of the electrochemical and corrosion behavior of stainless-steels with an electroactive coating. Journal of the Electrochemical Society. 1985;132:1022-6.
[150] Leon-Silva U, Nicho ME. Poly(3-octylthiophene) and polystyrene blends thermally treated as coatings for corrosion protection of stainless steel 304. Journal of Solid State Electrochemistry. 2010;14:1487-97.
[151] Yu ZJ, Chen YQ, Yang XD. Effective Adsorption of Functional Biological Macromolecules on Stainless Steel Surface with Micro/Nanoporous Texture. Acta Physico-Chimica Sinica. 2013;29:1595-602.

[152] Kang CK, Lee YS. Carbohydrate polymer grafting on stainless steel surface and its biocompatibility study. Journal of Industrial and Engineering Chemistry. 2012;18:1670-5.
[153] Okner R, Favaro G, Radko A, Domb AJ, Mandler D. Electrochemical codeposition of sol-gel films on stainless steel: controlling the chemical and physical coating properties of biomedical implants. Physical Chemistry Chemical Physics. 2010;12:15265-73.
[154] Okner R, Domb AJ, Mandler D. Electrochemically deposited poly(ethylene glycol)-based sol-gel thin films on stainless steel stents. New Journal of Chemistry. 2009;33:1596-604.
[155] Denes AR, Somers EB, Wong ACL, Denes F. 12-crown-4-ether and tri(ethylene glycol) dimethyl-ether plasma-coated stainless steel surfaces and their ability to reduce bacterial biofilm deposition. Journal of Applied Polymer Science. 2001;81:3425-38.
[156] Wang KK, Kim BJ, Lee MH, Kwon BJ, Choi DH, Park JC, et al. Photofunctional Co-Cr Alloy Generating Reactive Oxygen Species for Photodynamic Applications. International Journal of Photoenergy. 2013.
[157] Yan JC, Zeng XQ, van der Heide E, Ren TH. The tribological performance and tribochemical analysis of novel borate esters as lubricant additives in rapeseed oil. Tribology International. 2014;71:149-57.
[158] Jin ZM, Stone M, Ingham E, Fisher J. Biotribology. Current Orthopaedics. 2006;20:32-40.
[159] Yan JC, Bu JM, Bai XF, Li J, Ren TH, Zhao YD. The tribological study of novel phosphorous-nitrogen type phosphoramidate additives in rapeseed oil. Proceedings of the Institution of Mechanical Engineers Part J-Journal of Engineering Tribology. 2012;226:377-88.
[160] Marcano DC, Kosynkin DV, Berlin JM, Sinitskii A, Sun ZZ, Slesarev A, et al. Improved Synthesis of Graphene Oxide. Acs Nano. 2010;4:4806-14.
[161] Lubarsky GV, Browne MM, Mitchell SA, Davidson MR, Bradley RH. The influence of electrostatic forces on protein adsorption. Colloids and Surfaces B-Biointerfaces. 2005;44:56-63.
[162] Boyd AR, Meenan BJ, Leyland NS. Surface characterisation of the evolving nature of radio frequency (RF) magnetron sputter deposited calcium phosphate thin films after exposure to physiological solution. Surface & Coatings Technology. 2006;200:6002-13.
[163] Ehrensberger MT, Gilbert JL. A time-based potential step analysis of electrochemical impedance incorporating a constant phase element: A study of commercially pure titanium in phosphate buffered saline. Journal of Biomedical Materials Research Part A. 2010;93A:576-84.
[164] Thyparambil AA, Wei Y, Latour RA. Determination of Peptide-Surface Adsorption Free Energy for Material Surfaces Not Conducive to SPR or QCM using AFM. Langmuir. 2012;28:5687-94.
[165] Ou J, Wang J, Liu S, Mu B, Ren J, Wang H, et al. Tribology Study of Reduced Graphene Oxide Sheets on Silicon Substrate Synthesized via Covalent Assembly. Langmuir. 2010;26:15830-6.
[166] Ou J, Wang Y, Wang J, Liu S, Li Z, Yang S. Self-assembly of octadecyltrichlorosilane on graphene oxide and the tribological performances of the resultant film. The Journal of Physical Chemistry C. 2011;115:10080-6.

Acknowledgements

I would like to thank all my colleagues, families and friends for your support during my PhD study.

Firstly, I would like to acknowledge the support of the “EU Marie Curie CIG” (grant no. PCIG10-GA-2011 -303922) which provided financial support for this research.

My supervisors prof. dr. ir. Emile van der Heide, prof. dr. Tianhui Ren and dr. Xiangqiong Zeng must be thanked for their guidance, support as well as the patience. Emile, thanks for the wonderful project and discussion of the research, and also I came to know about so many new things besides the research work. Xiangqiong, I appreciate the daily supervising and care for so many aspects of the work, and for the help related to living in Enschede. Also thanks to prof. Ren for his great consideration of me. I am really thankful to them.

Next, I would like to thank each member of my thesis advisory committee, prof. dr. ir. E. van der Heide, prof. dr. T. Ren, dr. X. Zeng, prof. dr. G.J. Vancso, prof. dr. ir. G.J. Verkerke, prof. dr. Z. Jin and prof. dr. rer. nat. A. Pich for accepting and reading the final thesis draft and also for their comments.

I am grateful to prof. dr. ir. D.J. Schipper, dr. ir. R. Bosman, dr. ir. M.A. Masen and dr. ir. M.B. de Rooij for their advice on the research, papers and thesis. I would also like to thank Erik, Walter, Laura, Dedy, Gerard, Jacob, Nadia, Clemens, Peter, Sissi and Xueling for their assistance during the experimental work. I want to thank Belinda and Debbie for all arrangements for conferences and helps during my work. I would also like to thank my colleagues in the group: Mahdiar, Adeel, Dinesh, Martijn, Agnieszka, Natalia, Piet, Adriana, Ellen, Julien, Milad, Sheng, Yibo, Aydar, Febin, Duriash, Mariana, Michael and Matthijs. Indeed I had a very nice time with you guys, so many sweet memories with you. I want to thank my friends Shaojie, Peter, Bo and Wenqi for the help. Also my project could not be accomplished without the help of my colleagues in Shanghai: Jianchang, Zhipeng, Yawen and Gangqiang.

Lastly, I owe my gratitude to my family who support me without any hesitation.

Thank you all.

Jincan Yan

Part II

Paper A: J. Yan, X. Zeng, T. Ren and E. van der Heide. Boundary lubrication of stainless steel and CoCrMo alloy materials based on three ester-based additives. Tribology International, 2014, 73, 88-94.

Paper B: J. Yan, X. Zeng, T. Ren and E. van der Heide. Boundary lubrication of stainless steel and CoCrMo alloys based on phosphorous and boron compounds in an oil-in-water emulsion. Applied Surface Science, 2014, 315, 415-424..

Paper C: J. Yan, X. Zeng, T. Ren and E. van der Heide. The synergy between graphene oxide and surface-active polymers in aqueous lubrication of CoCrMo alloys. Submitted to Scientific Reports, 06-2014.

Paper D: J. Yan, X. Zeng, E. van der Heide and T. Ren. The tribological performance and tribochemical analysis of novel borate esters as lubricant additives in rapeseed oil. Tribology International, 2014, 71, 149–157.

Paper A

Boundary lubrication of stainless steel and CoCrMo alloy materials based on three ester-based additives

Jincan Yan, Xiangqiong Zeng, Tianhui Ren, Emile van der Heide. Tribology International, 2014, 73, 88-94

Boundary lubrication of stainless steel and CoCrMo alloy materials based on three ester-based additives

Jincan Yan, Xiangqiong Zeng, Tianhui Ren, Emile van der Heide

Abstract

Material selection and lubricant additive development are two important aspects for engineering applications. This work explores the possibilities of three different ester-based additives (DBOP, ODOC and DOB) to generate boundary films on two corrosion and wear resistant materials, stainless steel AISI 316 (A3) and CoCrMo alloy (S21) surfaces. The tribological performance of the materials and the additives were investigated. The different performance is proved to be related to the different adsorption and reaction film on the surfaces. XPS analysis on the A3 surface further confirms that at the boundary lubrication condition, the reaction layer originates from the tribochemical reaction of the active elements in the additives with the material surfaces.

Keywords: Ester-based additives, Calcium-containing additive, Borate based additive, P-N type additive, Boundary lubrication

1. Introduction

Material selection for engineering applications in a corrosive environment is typically based on materials that can withstand close and prolonged contact with the environments such as water, or physiological fluids [1-3]. Stainless steel and CoCrMo-alloy have been widely used in replacing standard ball bearing steel AISI 52100 for mechanical component with sliding contacts operating in such environments based on their excellent mechanical properties such as high tensile strength and toughness in combination with the required corrosion and wear resistance [4]. Applications are found in mechanical components at sea, food processing equipment, medical devices for minimally invasive surgery, but also in joint replacement materials [5-7].

Control over friction and wear during sliding is needed to ensure the proper functioning of the tribological system. One of the approaches is to use well selected and carefully formulated lubricants for the metal-on-metal sliding

contacts, especially at boundary lubrication conditions. At these conditions chemically reactive constituents of the lubricant react with the contact surface, forming a highly resistant tenacious layer which is capable of supporting the load and accommodate the difference in sliding velocity without adhesive wear or scuffing. Boundary layers have a dominant role in the frictional response of low sliding velocity tribological contacts. For the generally used lubricants, phosphorus–nitrogen additives (P-N type additive) with lower phosphorus content have been used extensively as multi-functional additives for boundary lubrication of ball bearing steel AISI 52100. The boundary film formed with P-N type additive consists mainly of $FePO_4$ [8]. Especially CoCrMo-based alloys are suspected not to function properly with this class of additives, as they require the abundant presence of Fe at the rubbing surface. The specific nature of maritime, food processing and bio-applications in which stainless steels and CoCrMo alloys are used, enhances the need for low toxic, environmental friendly additives. Organic borate esters, for example, have received extensive attention because of the expected high anti wear and extreme pressure, low toxicity, and pleasant odor [9-11].

In the course of developing new lubricant additives especially for sliding contacts with CoCrMo-alloys, it becomes necessary to analyse the tribo-chemical interactions of the additives with the metallic surfaces. This work, explores the possibilities of three ester-based additives in generating high performing boundary films on stainless steel and CoCrMo-surfaces at mildly loaded and low sliding velocities. The results are compared with the tribological performance of the same additives in combination with standard ball bearing steel.

2. Experiments

2.1 Materials

The CoCrMo-alloy selected for this work, Stellite 21 (coded S21), contains 27.0 wt. % chromium, 5.5 wt. % molybdenum, 2.5 wt. % nickel and 0.3 wt. % carbon, balanced by cobalt. AISI 316, a 17 wt. % chromium, 12 wt. % nickel balanced by iron alloy (coded A3) is taken as representative stainless steel for this study. AISI 52100 bearing steel (coded A5) was selected as a reference material. This hardened steel contains 1.5 wt. % chromium. The CoCrMo alloy is purchased from Kennametal and complies with the standard ASTM F–75. The carbides in

Stellite 21 are usual type which contain intergranular and interdendritic carbides. The AISI 316 stainless steel and 52100 bearing steel are purchased from SKF. All of the alloys were used without further treatment. The hardness of the materials was tested on DLH-200 Shimadzu Micro Hardness Tester. The roughness of the specimen and the morphology of the wear scar were characterized by the Micromap 560 interference microscope and the Keyence VK 9700 laser scanning microscope, respectively. The centre line average roughness R_{a1} (the balls) and R_{a2} (the disks) values based on surface and hardness values are listed in Table 1.

Table 1

Description, roughness and hardness of the materials

Material code	**Description**	**R_{a1} (roughness of balls)**	**R_{a2} (roughness of disks)**	**Hardness [HV]**
S21	Stellite 21	50-100 nm	100-200 nm	375
A3	AISI 316	50-100 nm	100-200 nm	247
A5	AISI 52100	20-50 nm	100-200 nm	851

2.2 Additives

A commercial rapeseed oil, provided by Grease Factory of Lanzhou, China was used as the lubricating base oil without any additional treatment. The main chemical constituents of the rapeseed oil are as follow: 7.46 wt. % of saturated fatty acids, 64.06 wt. % of monounsaturated fatty acid and 28.48 wt. % of total polyunsaturated fatty acid. For the lubricant, the P-N type and recently developed borate based additives were synthesized according to [8, 12]. The prepared additives, dibutyl octadecylphosphoramidate (DBOP), 6-octadecyl-1,3,6,2-dioxazaborocan-2-ol calcium salt (ODOC) and 2-(4-dodecylphenoxy)-6-octadecyl-1,3,6,2-dioxazaborocane (DOB) are depicted in Fig. 1. All of the compounds were characterized by Infra-Red spectroscopy and elemental analysis. The lubricants are prepared by adding 2.0 wt. % of the additive into the rapeseed oil and heated to 50^{o}C, ultrasonic for 30 min.

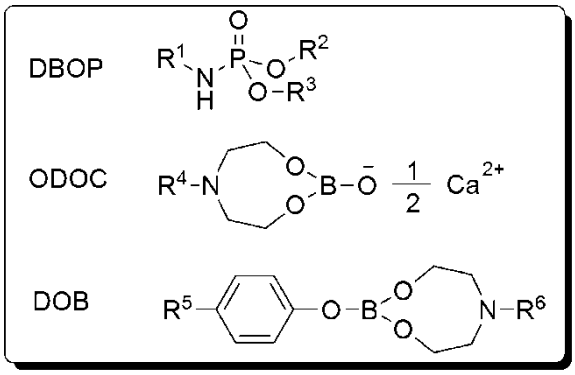

$R^1 = C_{18}H_{37}$, $R^2 = R^3 = C_4H_9$, $R^4 = R^6 = C_{17}H_{35}$, $R^5 = C_{12}H_{25}$

Fig.1. The chemical structure of the additives

2.3 Test conditions

The experimental work is conducted based on a nano-tribometer and a pin–on–disk machine, both manufactured by CSM–instruments. An overview of the test conditions is given in Table 2.

Table 2

Test conditions

	Nanotribometer	**Pin-on-disk**
Diameter of ball	5 mm	80 mm
Normal load	5 mN	1 N
Contact pressure	80-90 MPa	80-90 MPa
Velocity	35 mm/s, 10 mm/s	35 mm/s, 240 mm/s

2.4 Analysis of the worn surface and the wear scar

The samples used for the surface analyses are washed ultrasonically with acetone and dried before the detection. X-ray Photoelectron Spectroscopy (XPS) analysis is conducted to determine the chemical state of the elements at the worn surface with a Quantera SXM (scanning XPS microprobe) from Physical Electronics. The Al Kα monochromatic radiation is used as the excitation source with pass energy of 224.0 eV with a resolution of ±0.4 eV. The binding energy of C1s (284.8 eV) is used as the reference.

3. Results and discussions

3.1 The influence of materials

The effect of the material selection on the coefficient of friction (COF) is shown in Figure 2, in which 2.0 wt. % DOB containing lubricant was used for the material combination of A3 vs. A5, A5 vs. A5 and S21 vs. S21. The results are plotted against the lubrication number, L^+, defined as [13]

$$L^+ = \frac{\eta \cdot v}{P \cdot R_a} \qquad (1)$$

In which η is the viscosity of the lubricant, v is the velocity used in the tests, P is the average contact pressure and R_a is the composite roughness of the surface. The composite roughness R_a is defined as

$$R_a = \sqrt{R_{a1}^2 + R_{a2}^2} \qquad (2)$$

In which R_{a1} *and* R_{a2} are the centre line average roughness of the surfaces 1 (balls) and 2 (disks).

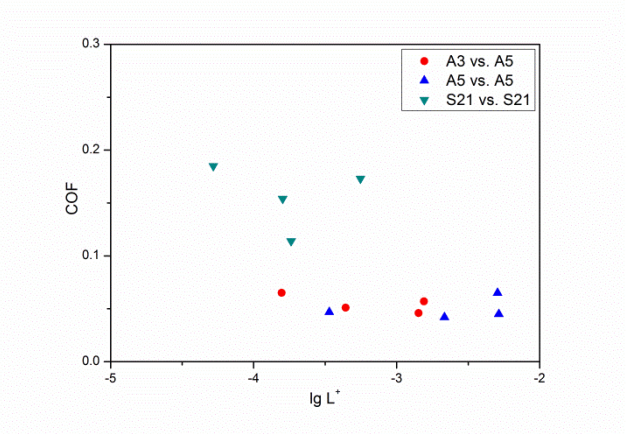

Fig. 2. The COF as a function of the lubrication number for three material combinations (rapeseed oil with 2.0 wt. % DOB, the results of A3 vs. A5 and A5 vs. A5 are based on the pin-on-disk machine, and the results of S21 vs. S21 are based on nanotribometer, sliding distance 100m)

From Figure 2, it can be seen that the COF of A3 vs. A5 changes from 0.046 to 0.065, and the average of the COF is about 0.055. For A5 vs. A5, the COF varies between 0.042 and 0.065 and with the average of 0.051. However, the COF changes from 0.114 to 0.185 for S21 vs. S21 and the average COF is 0.163. The

results suggest a similar COF for stainless steel (A3 vs. A5) compared to standard ball bearing steel (A5 vs. A5). The COF at boundary lubrication conditions is higher for the CoCrMo alloy (S21 vs. S21). This may be attributed to the different reaction activity of the materials. According to the position of Fe and Co in the periodic table of elements, Fe is easier to lose electrons and form positive ions than Co, indicating the reactivity of Fe is higher than that of Co. The balance between forming of the boundary layer by a tribo-chemical reaction and removal of the layer in the friction process determines the long term stability of the friction and wear properties in sliding contacts. The Fe-based surface can react easier with the additives and the process will probably be faster and possibly form a stronger chemical reaction layer. This could explain the lower COF of A3 and A5 in the presences of the currently selected additives. For S21, the additives cannot react easily with the metal surface and thus will not form enough chemical reaction layer, due to the small amount of Fe and low reactivity of Co in S21. Furthermore, due to the difference in reactivity, the thickness of the chemical reaction boundary layer is different. In general, as the thickness of a boundary film increases, the COF decreases accordingly [14]. Given the low reactivity of Co, a thinner film is expected and consequently higher COF.

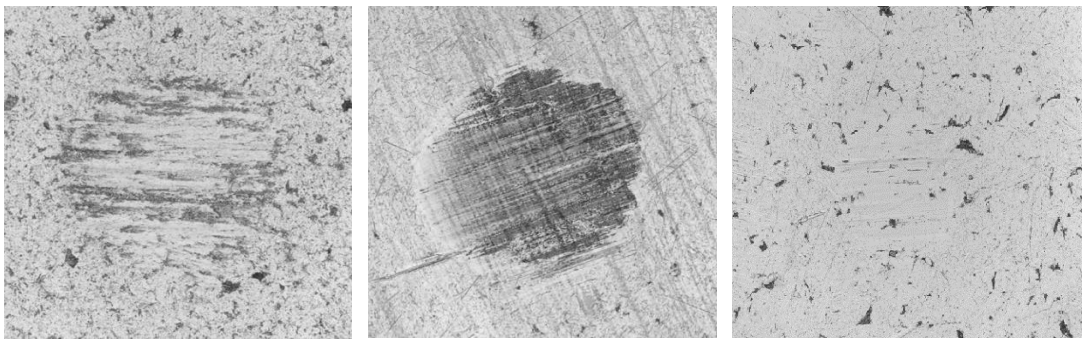

(a) (b) (c)

Fig. 3. The morphology of the worn surface (2.0 wt. % DOB in rapeseed oil, X50, sliding distance 2000m); (a) A3 vs. A5 (b) A5 vs. A5 (c) S21 vs. S21

Wear rates (k) are calculated based on the wear scar diameter (WSD) of the upper balls and 2000m of sliding distance [15]. For A3 vs. A5, the wear rate was 5×10^{-7} $mm^3 \cdot N^{-1} \cdot m^{-1}$. For A5 vs. A5, the wear rate was at about 2×10^{-7} $mm^3 \cdot N^{-1} \cdot m^{-1}$. For S21 vs. S21, a small wear scar was found and the wear rate was 8×10^{-8} $mm^3 \cdot N^{-1} \cdot m^{-1}$. The tendency can also be clearly seen from the topography of the different ball materials after sliding tests shown in Fig. 3. The WSD of A3 vs. A5

and A5 vs. A5 is similar which is shown in Fig. 3(a) and Fig. 3(b), furrows can be detected on the surface of A3 andA5. When the material was changed to S21, a small and smooth wear scar can be observed in Fig. 3(c). The results indicate that compared to standard ball bearing steel and stainless steel, Stellite 21 CoCrMo alloy possesses better anti-wear property. This is in accordance with the differences in hardness: the specific wear rate increases with the reduction of hardness [16].

3.2 The influence of additives

3.2.1 Stainless steel AISI 316

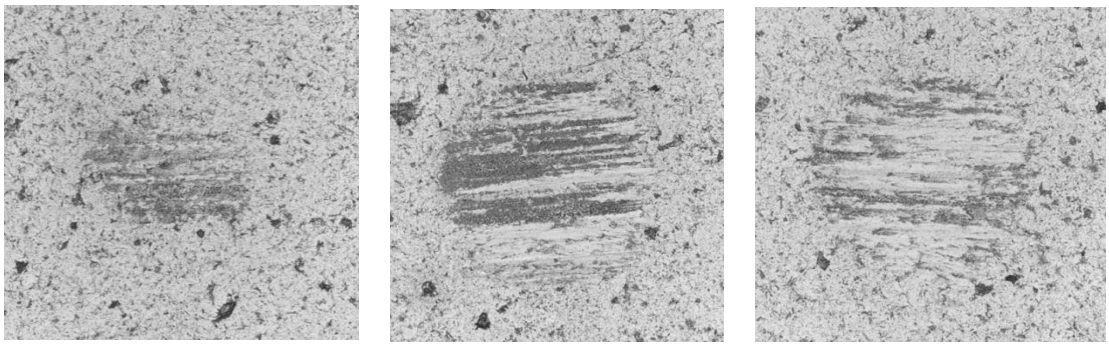

(a) (b) (c)

Fig. 4. The morphology of the wear scars on A3 balls; (a) DBOP, (b) ODOC, (c) DOB (2.0 wt. % additive in rapeseed oil, X50, sliding distance 2000 m)

The COF of 2.0 wt. % DBOP, ODOC and DOB for A3 vs. A5 were respectively 0.065, 0.114 and 0.065. The friction reducing possibilities of the three additives can therefore be ranked qualitatively as ODOC < DBOP = DOB at a lubrication number value of about 1×10^{-4}. The specific wear rates for A3 vs. A5 were calculated as 1×10^{-7} $mm^3\cdot N^{-1}\cdot m^{-1}$, 4×10^{-7} $mm^3\cdot N^{-1}\cdot m^{-1}$ and 5×10^{-7} $mm^3\cdot N^{-1}\cdot m^{-1}$ for DBOP, ODOC and DOB respectively. The anti-wear performance is similar for ODOC, DBOP and DOB, which can also be reflected from the morphology of the wear scars in Fig. 4.

The different COF can be attributed to the formation of different adsorption film and/or tribochemical reaction film by the additives at the interacting metal

surfaces. The reaction time and thickness of the films are dependent on the reaction activity, the active elements and the molecular structure of the additives. From the molecular structure, it can be concluded that the reaction activity of ODOC is the highest among the three additives. Firstly, ODOC is a salt with high polarity which can be easily absorbed onto the metal surface. Secondly, ODOC contains the most types of active elements including B, O, N and Ca. Thirdly, the content of each active element is also the highest among the three additives, with about 2.84% B, 12.37% O, 3.61% N and 5.15% Ca. While the highest reaction activity does not necessarily lead to the best tribological performance of ODOC. On the contrary, the friction-reducing property of ODOC is qualitatively the poorest among the three additives. This may be because the reaction activity is too high so that corrosion occurred. The active elements in DBOP are O, N and P, which typically result in the formation of iron oxides and phosphate [8]. DOB consists of B, O and N, which may generate iron oxides, boron oxide and/or BN on the rubbing surfaces [17-18]. From the experimental work, the friction reducing and anti-wear properties of DOB and DBOP are similar, indicating the boron containing film as well as the phosphorous film can be effective boundary films. . Detailed information on the composition of the films formed on the rubbing surfaces is presented in Section 3.3 based on XPS analysis.

3.2.2 CoCrMo-alloy

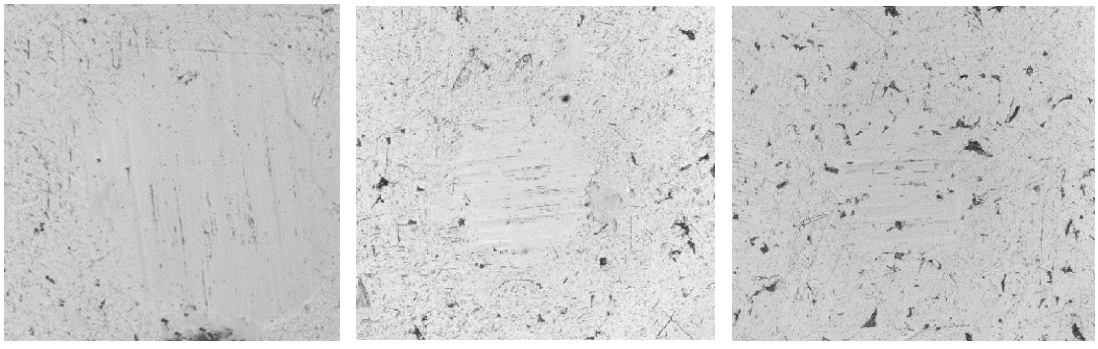

(a) (b) (c)

Fig. 5. The morphology of the wear scars on S21 balls; (a) DBOP, (b) ODOC, (c) DOB (2.0 wt. % additive in rapeseed oil, X50, sliding distance 2000 m)

The COF of S21 vs. S21 lubricated by DBOP, ODOC and DOB doped rapeseed oil at a lubrication number of about 1×10^{-4} was calculated from the experimental work

as 0.123, 0.097 and 0.114 respectively. The corresponding values for the specific wear rate were 6×10^{-7} $mm^3\cdot N^{-1}\cdot m^{-1}$, 3×10^{-7} $mm^3\cdot N^{-1}\cdot m^{-1}$ and 8×10^{-8} $mm^3\cdot N^{-1}\cdot m^{-1}$ respectively. The friction reduction property of the three additives is now ranked as ODOC > DOB > DBOP at the test condition.

The polarity of ODOC is higher than that of DBOP and DOB. Therefore, more ODOC can be adsorbed on the metal surface to form the adsorption layer than that of DBOP and DOB. This could well explain the enhanced friction reducing properties of ODOC for the case of the CoCrMo surface. In addition, the adsorption film formed by DOB will be more stable than that established by DBOP due to the existence of aromatic group in DOB. This could explain the difference in boundary lubrication friction for DOB and DBOP. The anti-wear properties of DBOPand ODOC are similar, and DOB performs better. The morphologies of the wear scars on the S21 balls for different additives are shown in Fig. 5. Although there are fewer possibilities for the additives to interact with the CoCrMo alloy, a certain amount of tribochemical reaction film can still be generated on the S21 surface. This is because of the existence of certain amount of Fe in the alloy and the increase of metal reactivity, since the formation of freshly exposed metallic surface during the rubbing process. Therefore, the better anti-wear performance of DOB results from both the formation of adsorption and tribochemical reaction films.

3.3 XPS analysis

XPS spectra of the elements in the worn surface were recorded to determine the chemical state of the elements and examine possible film forming mechanisms based on the known composition of the additives. The binding energies of some standard compounds containing Fe, O, P, B, N, and Ca are listed in Table 3 for comparison, which are obtained in NIST XPS Database.

Because the wear scars were too small when using S21 vs. S21, the XPS evaluation was only conducted for A3 vs. A5. The XPS spectra of the elements on A3 surface with the lubrication of DBOP, DOB and ODOC are given in Fig. 6.

Table 3

Binding energy of some standard compounds containing Fe, P, B, Ca, and N

Element	Compounds	Binding energy (eV)
Ferrum	Fe_2O_3	$Fe_{2p3/2}$(711.3); $Fe_{2p1/2}$(724.0); O_{1s}(529.8)
	Fe_3O_4	$Fe_{2p3/2}$(709.4); $Fe_{2p1/2}$(723.5); O_{1s}(529.7)
	FeO	Fe_{2p}(709.6); O_{1s}(530.1)
	FeOOH	$Fe_{2p3/2}$(711.5); $Fe_{2p1/2}$(724.3); O_{1s}(531.7)
	Fe(OH)O	Fe_{2p}(711-711.8); O_{1s}(531.2-531.8)
Phosphorous	$FePO_4$	Fe_{2p}(712.8); P_{2p}(133.7); O_{1s}(531.8)
Boron	Fe_xB_y	Fe_{2p}(706.9-707.4); B_{1s}(188.0)
	B_2O_3	B_{1s}(192.0); O_{1s}(532.5-533.8)
Calcium	CaO	Ca_{2p}(347.0); O_{1s}(531.3-531.5)
	$Ca(NO_3)_2$	Ca_{2p}(347.0); N_{1s}(407.6)
Nitrogen	N-containing organic	N_{1s}(399.7)
	NH_4NO_3	N_{1s}(403.1)

The Fe_{2p} peaks appear at around 711.39eV and 724.49eV, which can be corresponded to iron oxides (Fe_2O_3, Fe_3O_4) and/or iron hydroxides (FeOOH, Fe(OH)O), indicating the lubricated surface is liable to oxidize during the friction process. For DBOP, the peak is a little bit shifting towards the high binding energy direction, which may be due to the formation of $FePO_4$. And for DOB, the peak is wide and extending towards the low binding energy direction, which can be due to the existence of Fe_xB_y and FeO.

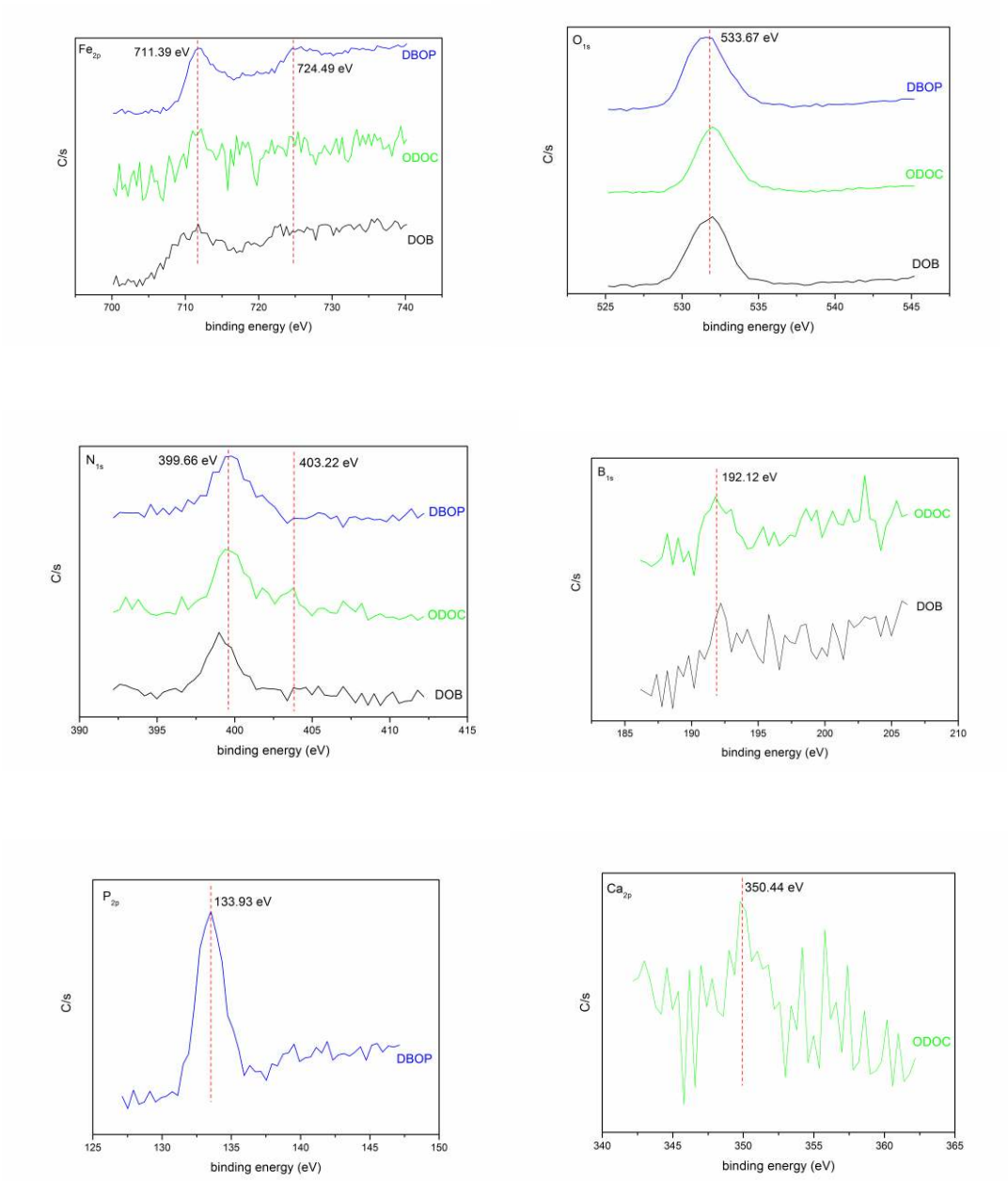

Fig. 6. XPS spectra of Fe_{2p}, O_{1s}, N_{1s}, B_{1s}, Ca_{2p} and P_{2p} on the worn surfaces for A3 vs. A5 lubricated with 2.0 wt. % additives in rapeseed oil

When taking a look at the XPS spectra for O_{1s}, all the three additive based lubricating systems exhibit an intensive wide peak at around 533.67 eV (in the range of 531-534 eV). Firstly, it further confirms the existence of FeOOH, Fe(OH)O and Fe_2O_3 on the A3 surfaces. For DBOP, $FePO_4$ with the characteristic peak at 531.8eV could also be present on the surface. As for ODOC, CaO can exist because its characteristic peak is at 531.3-531.5 eV. It is obvious that the peaks for DOB and ODOC are located in higher binding energy area compared to that of

DBOP, which can be attributed to the formation of B_2O_3 by the lubrication of DOB and ODOC, and the formation of $Ca(NO_3)_2$ by the lubrication of ODOC.

In case of nitrogen, there is a wide peak at around 399.66eV for all the three surfaces, suggesting that the N element is still in organic state. It may be the complex compounds of metal surface with the decomposed additives like organic amine, organic amide, nitrile and other N-containing compounds [19]. While for ODOC, there are small peaks at high binding energy (around 403.22 eV and around 408.00 eV) which can be related to the formation of nitrate.

The B_{1s} spectra show peak at around 192.12eV, corresponding to B_2O_3, which is in good accordance with the result of O_{1s} spectra and also indicates there is no Fe_xB_y formed on the surface. The binding energy of P_{2p} at 133.93eV further confirms the existence of $FePO_4$, and there may be also other organic phosphorous compounds formed on the worn surface. The wide Ca_{2p} peak at around 350.44eV can be identified as $Ca(NO_3)_2$ and CaO.

In summary, the above surface analysis results demonstrate that under the boundary lubrication condition, the active additive molecule first adsorb on the metal surface, and then decompose and react with the metal surface during the rubbing process to form stable lubricating films on the rubbed surfaces. The lubricating films are complex and consist of adsorption layer and reaction layer (see Table 4). The adsorption layer is formed mainly by the coordination bonding of nitrogen-containing groups with the metal surface resulting from the decomposed products from the additives. The reaction layer originates from the tribochemical reaction of the active elements contained in the additives, which resulting in the formation of boron oxide, nitrate, phosphate and other oxidized compounds. The main difference on the films formed by these three additives lies in the reaction layer. In particular, the reaction layer for DBOP consists of iron oxides, iron hydroxides and phosphate, and the reaction layer for DOB is composed of iron oxides, iron hydroxides and boron oxide. Related to the tribological performance in section 3.2.1, the friction reducing performance and anti-wear property of these two additives are similar, indicating that boron oxide containing film and phosphate containing film are both effective boundary films under current test conditions. As for ODOC, besides iron oxides, iron hydroxides and boron oxide, calcium oxide and nitrate was also generated at the surface. The formation of nitrate will consume nitrogen in the molecule structure, resulting in

less stable and less compact adsorption film. In addition, it may cause corrosive wear. The less functional adsorption layer and reaction layer formed by ODOC is likely causing the higher friction force and wear rate compared to the other two additives.

Table 4

The main composition of the films on the scar

Additive	Adsorption film	Reaction film
DBOP	N-containing organic compounds	Iron oxides, iron hydroxides, phosphate
ODOC	N-containing organic compounds	Iron oxides, iron hydroxides, B_2O_3, CaO, nitrate
DOB	N-containing organic compounds	Iron oxides, iron hydroxides, B_2O_3

4. Conclusions

1) This work gives a clear indication that the chemical and physical properties of the surface boundary films generated on the surface of CoCrMo vs. CoCrMo material combination are different from the films generated on the surface of AISI 316 vs. AISI 52100 material combination. This is related to the difference in the reactivity of cobalt and iron.

2) For the friction reducing properties of the additives, DOB and DBOP performed better than ODOC for stainless steel AISI 316, while for CoCrMo, DOB and ODOC performed better than DBOP. The boundary lubrication performance of the three additives can be explained from the chemical composition of the adsorption and reaction film on the interacting surfaces.

3) XPS results show that at the boundary lubrication conditions, the active additive molecules first adsorb on the metal surface, and then decompose and react with the metal surface during the rubbing process to form stable lubricating films on the rubbed surfaces. The lubricating films are complex and consist of an adsorption layer and a reaction layer. The adsorption layer is formed mainly by the coordination of nitrogen-containing groups with the metal surface resulting from the decomposed products from the additives. The reaction layer originates from the tribochemical reaction of the active elements contained in the additives and the main difference on the films formed by these three

additives lies in the reaction layer.

Acknowledgements

The authors are grateful to EU Marie Curie CIG (grant no. PCIG10-GA-2011-303922) and the Natural Science Foundation of China (NSFC grant No. 21272157) for the financial support.

References

[1] Grimm MJ. Selection of Materials for Biomedical Applications. In: Kutz M, editors. Handbook of Materials Selection, New York: John Wiley & Sons, 2002, p. 1165–94.

[2] Navarro M, Michiardi A, Castaño O, Planell JA. Biomaterials in orthopaedics. J R Soc Interface 2008;5(27):1137–58.

[3] Nielsen K. Corrosion of metallic implants. Corros Eng, Sci Technol 1987;22(4):272-8.

[4] Nishimura T, Katayama H, Noda K, Kodama T. Effect of Co and Ni on the corrosion behavior of low alloy steels in wet/dry environments. Corros Sci 2000;42(9:)1611–21.

[5] Reclaru, L, Lerf R, Eschler PY, Meyer JM. Corrosion behavior of a welded stainless-steel orthopedic implant. Biomaterials 2001;22(3):269–79.

[6] Sinnett-Jones PE, Wharton JA, Wood RJK. Micro-abrasion–corrosion of a CoCrMo alloy in simulated artificial hip joint environments. Wear 2005;259(7-12):898–909.

[7] Venugopalan R., Trépanier C. Assessing the corrosion behaviour of Nitinol for minimally-invasive device design. Minim Invasiv Ther 2000;9(2):67-73.

[8] Yan JC, Bu JM, Ren TH. The tribological study of novel phosphorous–nitrogen type phosphoramidate additives in rapeseed oil. Proc IMechE Part J: J Engineering Tribology 2012;226(5):377–88.

[9] Hao LF, Li JS, Xu XH, Ren TH. Preparation, characterization, and tribological evaluation of triethanolamine monooleate-modified lanthanum borate nanoparticles. Proc IMechE Part J: J Engineering Tribology 2010;224(J11):1163–71.

[10] Wang YG, Li JS, Ren TH. Using a novel disulphide compound containing boron as a potential substitute for sulphurized olefins in lubricants. Proc IMechE Part J: J Engineering Tribology 2007;221(J5):553–9.

[11] Li JS, Xu XH, Wang YG, Ren TH. Tribological studies on a novel borate ester containing benzothiazol-2-yl and disulfide groups as multifunctional additive. Tribol Int 2010;43(5-6):1048–53.

[12] Zheng Z, Shen GQ, Wan Y, Cao LL, Xu XD, Yue QX, Sun TJ. Synthesis, hydrolytic stability and tribological properties of novel borate esters containing nitrogen as lubricant additives. Wear 1998;222(2):135–44.

[13] Schipper DJ. Transitions in the lubrication of concentrated contacts, PhD thesis, 1988,

University of Twente, The Netherlands.

[14] Allen CM, Drauglis E. Boundary layer lubrication: monolayer or multilayer. Wear 1969;14(5):363–84.

[15] Qu J, Truhan JJ. An efficient method for accurately determining wear volumes of sliders with non-flat wear scars and compound curvatures. Wear 2006;261(7-8):848–55.

[16] Saka N, Pamies-Teixeira JJ, Suh NP. Wear of two-phase metals. Wear 1977;44(1):77–86.

[17] Yao JB. Antiwear function and mechanism of borate containing nitrogen. Tribol Int 1997;30(6):387–9.

[18] Shen GQ, Zheng Z, Wan Y, Xu XD, Cao LL. Synergistic lubricating effects of borate ester with heterocyclic compound. Wear 2000;246(1-2):55–8.

[19] Zeng XQ, Wu H, Yi HL, Ren TH. Tribological behavior of three novel triazine derivatives as additives in rapeseed oil. Wear 2007;262(5-6):718-26.

Paper B

Boundary lubrication of stainless steel and CoCrMo alloy based on phosphorous and boron compounds in oil-in-water emulsion

Jincan Yan, Xiangqiong Zeng, Tianhui Ren, Emile van der Heide. Applied Surface Science, 2014, 315, 415-424.

Boundary lubrication of stainless steel and CoCrMo alloy based on phosphorous and boron compounds in oil-in-water emulsion

Jincan Yan, Xiangqiong Zeng, Tianhui Ren, Emile van der Heide

Abstract

Emulsion lubrication is widely used in metal forming operations and has potential applications in the biomedical field, yet the emulsion lubrication mechanism is not well understood. This work explores the possibilities of three different oil-in-water (O/W) emulsions containing dibutyl octadecylphosphoramidate (DBOP), 6-octadecyl-1,3,6,2-dioxazaborocan-2-ol calcium salt (ODOC) and 2-(4-dodecylphenoxy)-6-octadecyl-1,3,6,2-dioxazaborocane (DOB) to generate boundary films on stainless steel AISI 316 and CoCrMo alloy surfaces. Experimental results show lower friction values for the emulsions in combination with CoCrMo compared to AISI 316. The different performance of the additives is related to the composition of the adsorption and reaction film on the interacting surfaces, which was shown to be dependent on the active elements and molecular structure of the additives. The friction profile of the emulsions indicates that the emulsion appears to be broken during the rubbing process, then the additives adsorb onto the metal surface to form protecting boundary layers. The XPS analysis shows that for boundary lubrication conditions, the additive molecules in the emulsion first adsorb on the metal surface after the droplet is broken, and then decompose and react with the metal surface during the rubbing process to form stable lubricating films on the rubbed surfaces.

Keywords Boundary lubrication; Oil-in-water emulsion; Calcium-containing additive; Borate-based additive; P-N type additive

1. Introduction

Water-based lubrication is seen as an attractive alternative to oil-based lubrication for hydraulic fluids [1], cutting fluids [2, 3], rolling fluids [4] and lubricants used in open systems that potentially could pollute the environment [5]. Clearly, water-based lubrication has the advantage of cooling capabilities,

reduced cleaning costs, lower toxicity and fire resistance. Recently, water-based lubrication has drawn considerable attention in biomedical engineering in reducing friction for systems that combine stainless steel or CoCrMo-based surfaces in the presence of bodily fluids, like synovia [6]. The potential utilization of water-based lubrication is typically limited by the poor lubricating properties of water. One possibility to enhance the tribological performance of water-based fluids is to use functional additives with defined active elements which can enhance the frictional response in combination with iron containing metallic surfaces [7]. Some of the functional additives can, however, only be dissolved in oil directly. Hence, an oil-in-water (O/W) emulsion is used in this work to incorporate the functional additives. An O/W emulsion is generally regarded as a two-phase heterogeneous mixture of oil and water, where the oil component remains in the dispersed phase while water forms the continuous phase. The oil phase contains base oil, lubricating additives, and an emulsifier. The emulsifier contains hydrophilic and lipophilic ends. The hydrophilic end consists of polar bonds and is soluble in water, whilst the lipophilic end is soluble in oil [8]. Frequently-used emulsifiers in lubrication technology are nonionic surfactants [9]. Researchers have conventionally attributed emulsion effectiveness to the idea that droplets 'plate out' onto exposed metal surfaces [10].

In recent years, phosphorous-nitrogen (P-N type) additives, calcium-containing and borate esters were recognized as good replacements for traditional additives in advanced formulation of additives [11-13]. Phosphorous, calcium and boron elements have a positive impact on the development of cells and tissues [14]. The biocompatibility of phosphorous, boron and calcium-based additives has not been proved at all, yet it is regarded in this work as a start for developing materials that can be used in a biomedical environment as well.

Metallic materials have been widely used in replacing the structural components of the human body or as sliding surfaces for medical tools because of their excellent mechanical properties, such as tensile and fatigue strengths [15, 16]. For the metal, stainless steel is considered as a high-strength alloy with low cost, and is often used in implants which intend to help repair fractures. Cobalt-chromium alloys are also strong, hard and corrosion resistant. As such, stainless steels and cobalt-chrome-molybdenum alloys are frequently chosen,

either for metal-tissue sliding contacts or for metal-on-metal sliding contacts [17]. The interaction of metallic surfaces and additives determines to a great extent the effectiveness of boundary layers [18]. In this study, the interactions between metals and O/W emulsions are studied. As metallic surfaces, stainless steel and CoCrMo alloy were chosen as test samples. Three additives containing P, Ca or B were selected for the preparation of the O/W emulsions in the study. The results are compared with the performance in combination with standard ball bearing steel.

2. Experiments

2.1. Materials

The CoCrMo alloy selected for this work, Stellite 21 (coded S21), contains 27.0 wt. % chromium, 5.5 wt. % molybdenum, 2.5 wt. % nickel and 0.3 wt. % carbon, balanced by cobalt. AISI 316 stainless steel, a 17 wt. % chromium, 12 wt. % nickel balanced by iron alloy (coded A3) is taken as representative stainless steel for this study. AISI 52100 bearing steel (coded A5) was selected as a reference material. This hardened steel contains 1.5 wt. % chromium balanced by iron. The CoCrMo alloy was purchased from Kennametal and complies with the standard ASTM F–75. The carbides in Stellite 21 are intergranular and interdendritic, according to the information of the supplier. AISI 316 stainless steel and 52100 bearing steel were purchased from SKF. All of the alloys were used after polishing and without any further treatment. The hardness of the materials was tested on a DLH-200 Shimadzu Micro Hardness Tester. The roughness of the specimen was characterized by the Micromap 560 interference microscope. The centre line average roughness of the balls, $R_{a1,}$ and of the disks, R_{a2} values and hardness values are listed in Table 1.

2.2. Lubricants

A commercial rapeseed oil, provided by Grease Factory of Lanzhou, China, was used with no further treatment. The main chemical constituents of fatty acids in the rapeseed oil are as follow: 7.46 wt. % of saturated fatty acids, 64.06 wt. % of monounsaturated fatty acid and 28.48 wt. % of total polyunsaturated fatty acid.

For the additives, the phosphorous–nitrogen additives and the borate ester additives were synthesized according to [11, 13]. The prepared additives, dibutyl

Table 1

Description, roughness and hardness of the materials

Material code	Description	R_{a1} (roughness of balls)	R_{a2} (roughness of disks)	Hardness [HV]	Main composition (%)
S21	Stellite 21	70±20 nm	150±50 nm	375±3	Co62.25 Cr27 Mo5.5 Ni2.5
A3	AISI 316	70±20 nm	150±50 nm	247±6	Fe70 Cr17 Ni12
A5	AISI 52100	30±10 nm	150±50 nm	851±10	Fe97.0 Cr1.5

octadecylphosphoramidate (DBOP), 6-octadecyl-1,3,6,2-dioxazaborocan-2-ol calcium salt (ODOC) and 2-(4-dodecylphenoxy)-6-octadecyl-1,3,6,2-dioxazaborocane (DOB) are depicted in Fig. 1. All of the compounds were characterized by Infra-Red spectroscopy and elemental analysis. Polyoxyethylene (20) sorbitan monooleate (Polysorbate 80) is a nonionic surfactant and emulsifier derived from polyethoxylated sorbitan and oleic acid [19]. Polysorbate 80 and other chemicals were purchased from Sigma-Aldrich and used without further treatment. The O/W emulsions are prepared by milling and mixing 2.0 wt. % of the additive, 6.0 wt. % of Polysorbate 80 and 6.0 wt. % of the rapeseed oil together, then adding water gradually and stirring (800 r/min) for 30 minutes. For the emulsions, the viscosity was measured by a Brookfield DV-I digital viscometer and the size distribution was analysed by a Malvern-ZS90 particle size and zeta potential analyser.

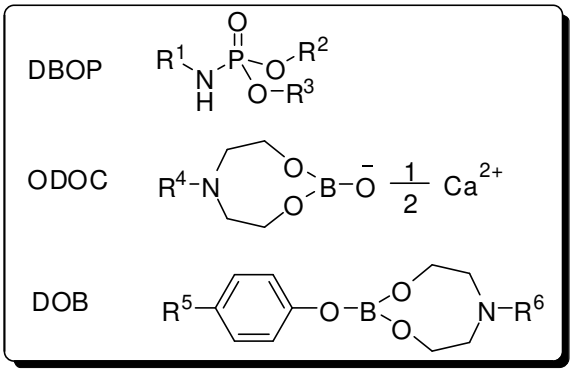

Fig. 1. The chemical structure of the additives applied in the tests

2.3. Test conditions

As shown in Table 2, the tests were performed by using a nanotribometer (ball on disk) which is provided by CSM-instruments. The detailed test conditions are listed in Table 2. Each test was repeated three times.

Table 2

Test conditions

Items	Nanotribometer
Diameter of ball	5 mm
Normal load	5 mN
Contact pressure	80-90 MPa
Velocity	35 mm/s, 10 mm/s
Sliding distance	100 m

2.4. Analysis of the worn surface and the wear scar

The samples used for the surface analyses were washed with acetone and dried before the detection. The morphology of the wear scar was characterized by the Micromap 560 interference microscope. X-ray Photoelectron Spectroscopy (XPS) analysis was conducted to determine the chemical state of the elements in the worn surface with a Quantera SXM (scanning XPS microprobe) from Physical Electronics at the Materials Characterisation Department at Nanolab, University of Twente. The Al Kα monochromatic radiation was used as the excitation source

with pass energy of 224.0 eV with a resolution of ±0.4 eV. The binding energy of C1s (284.8 eV) was used as the reference.

3. Results and discussions

3.1. The size distribution and viscosity of the emulsions

The oil droplet size distribution of the prepared emulsions is presented in Fig. 2 and the average particle diameter of DBOP, ODOC and DOB-based emulsions is 393 nm, 235 nm and 731 nm respectively, indicating that the average size of ODOC is smaller than that of DBOP and DOB. The viscosity of the additive-based emulsions is listed in Table 3.

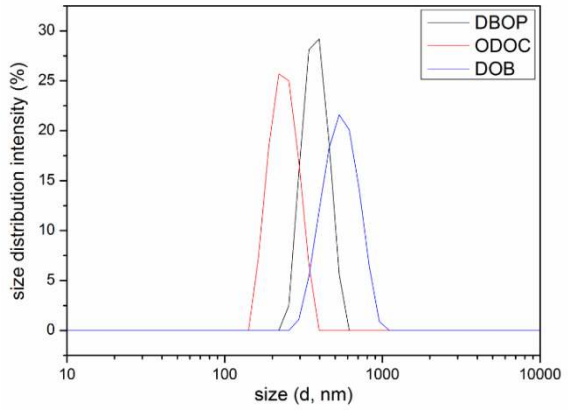

Fig. 2. The size distribution of DBOP, ODOC and DOB-based emulsions

Table 3

The viscosity of the additive-based emulsions

	DBOP	**ODOC**	**DOB**
Viscosity (10^{-3} Pa·s)	22.6	35.6	29.5

3.2. The influence of materials

The effects of the materials on the coefficient of friction (COF) are shown in Fig. 3, in which 2.0 wt. % DOB-based emulsion was used as a lubricant for different material combinations, i.e. A3 vs. A5, A5 vs. A5 and S21 vs. S21. The data is presented using the dimensionless lubrication number based on the viscosity η of the lubricant, the sliding velocity v, the average contact pressure P and the

composite roughness of the surfaces, R_a. The composite roughness R_a is defined as

$$R_a = \sqrt{R_{a1}^2 + R_{a2}^2} \quad (1)$$

In which R_{a1} and R_{a2} are the surface roughness based on the area of the surfaces 1 (ball) and 2 (ring). The lubrication regime can be estimated in the boundary lubrication regime [20] and the details are shown in supporting information.

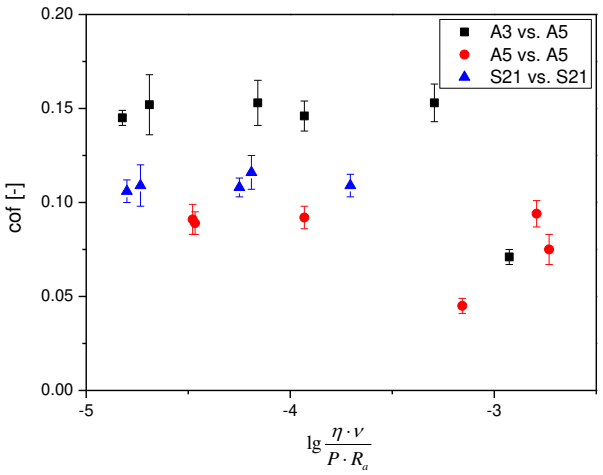

Fig. 3. The COF as a function of the materials (2.0 wt. % DOB-based emulsion)

For the base oil-in-water emulsion without 2.0 wt. % DOB, the COF of A5 vs. A5, S21 vs. S21 and A3 vs. A5 is 0.116, 0.122 and 0.167 respectively. For the results in the emulsion with 2.0 wt. % DOB, it can be seen from Fig.3 that for boundary lubrication conditions the COF of A5 vs. A5 changes from 0.089 to 0.092, and for S21 vs. S21, the COF varies between 0.106 and 0.116. When the material is changed to A3 vs. A5, the COF is in the range of 0.146 to 0.153. The reduction of friction can be due to the additives, which can form effective boundary films on the metal. The results also suggest that compared to standard ball bearing steel, the COF for boundary lubrication conditions is higher for the CoCrMo alloy. The COF for stainless steel (A3 vs. A5) is the highest. The different COF may be attributed to the different boundary layer. Generally, the boundary films are formed by physical adsorption, chemical adsorption and chemical reactions. It is

reported that the high content of Cr in CoCrMo alloy can form organometallics on top of the freshly exposed nascent surface [21]. In addition, the Cr-based carbides in CoCrMo alloy can easily react with the additives and form effective protection films, especially in an aqueous environment [22]. A5 mainly consists of iron, which can also easily react with the additives and form functional adsorption and reaction layers to reduce the friction. For A3, it contains less Fe than A5, and less Cr than S21, resulting in a higher friction coefficient.

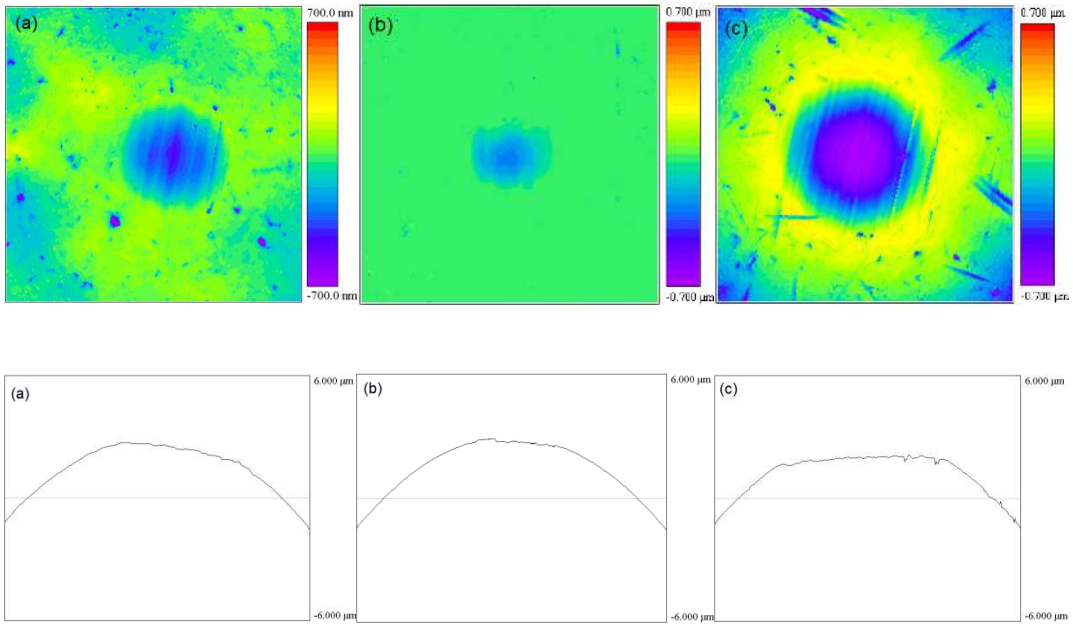

Fig. 4. The morphology and wear profile of the wear scars for different materials (2.0 wt. % DOB-based emulsion, sliding distance 2000m, 10X, the scales are all shown as height in µm, all of the morphology areas are 300µm×300 µm based on curvature mode, all of the wear profile length is 300 µm in the centre based on plane mode) (a) A3 vs. A5 (b) A5 vs. A5 (c) S21 vs. S21

After the tests, the wear rates were calculated based on the wear scar diameter (WSD) of the upper balls [23]. The wear rate for A3 vs. A5 in 2.0 wt. % DOB-based emulsion is at a level of 3 $\times 10^{-7}$ $mm^3 \cdot N^{-1} \cdot m^{-1}$. Under the same condition for A5 vs. A5 and S21 vs. S21, the wear rate is 8 $\times 10^{-8}$ $mm^3 \cdot N^{-1} \cdot m^{-1}$ and 8 $\times 10^{-7}$ $mm^3 \cdot N^{-1} \cdot m^{-1}$ respectively. The tendency is also reflected in the topographies shown in Fig. 4. As shown in the figure, there was a small wear scar on the A5 surface when the test was performed for 2000 m. The wear rate of A3 is slightly smaller than that of S21. The results indicate that compared to standard ball bearing steel, the wear rate of stainless steel, as well as CoCrMo

alloy, is higher under the same test conditions. On the one hand, this is in accordance with the differences in hardness: the wear rate increases with the reduction of hardness. A5 is much harder than A3 and S21, resulting in less wear. On the other hand, there is more carbide like CrC in A3 and S21 than that in A5, which may also cause corrosion [22].

3.3. The influence of additives

3.3.1. The performance of additives for A3 vs. A5

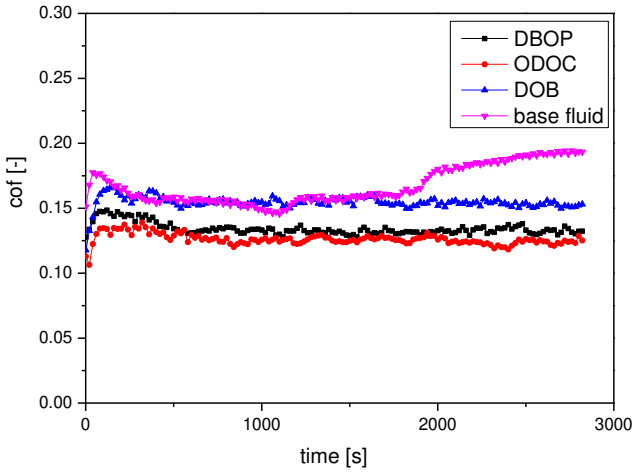

Fig. 5. The COF of 2.0 wt. % DBOP, ODOC and DOB-based emulsions for A3 vs. A5 with time

The COF of 2.0 wt. % DBOP, ODOC and DOB-based emulsions for A3 vs. A5 with time are shown in Fig. 5, and the average COF is 0.132, 0.124 and 0.153 respectively. The COF of base fluid without additives is 0.167 and is shown in the figure for comparison. It can be seen that the friction-reducing ability of the three additives is ranked as DOB < DBOP ~ ODOC under the test conditions. The profiles of the friction curve are similar for all three emulsions and the characteristics are interesting. After initially increasing within several runs of the tests, the curve shows a plateau for a period of around 500 seconds, followed by a slight decrease and the curve stabilizes again. This behaviour can possibly be

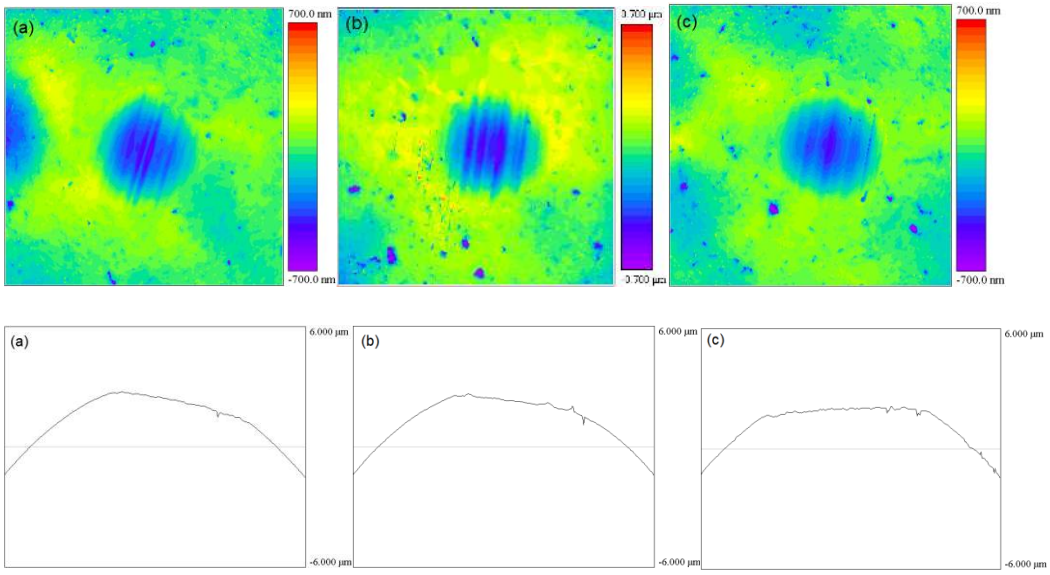

Fig. 6. The morphology and wear profile of the wear scars on A3 balls (sliding distance 2000m, 10X, the scales are all shown as height in µm, all of the morphology areas are 300µm×300 µm based on curvature mode, all of the wear profile length is 300 µm in the centre based on plane mode); (a) 2.0 wt. % DBOP, (b) 2.0 wt. % ODOC, (c) 2.0 wt. % DOB-based emulsion

explained from the structure of the O/W emulsion, i.e. a heterogeneous system consisting of oil droplets dispersed in water. The profile suggests that the water phase plays a dominant role after running-in, resulting in the higher COF. After the droplet is broken, the emulsifier and additives adsorb onto the metal surface because of the polarity orientation and then oil also provides protection for the rubbing pairs. Therefore, the COF becomes lower and stable as the role of the additives increases.

The wear rate of DBOP, ODOC and DOB-based emulsions for A3 vs. A5 is 3 $\times 10^{-7}$ $mm^3 \cdot N^{-1} \cdot m^{-1}$, 4×10^{-7} $mm^3 \cdot N^{-1} \cdot m^{-1}$ and 3 $\times 10^{-7}$ $mm^3 \cdot N^{-1} \cdot m^{-1}$ respectively. The similar anti-wear property can also be reflected from the morphology of the wear scars in Fig. 6. The different COF and wear rate can be attributed to the formation of different adsorption film and/or tribochemical reaction film by the additives on the rubbing metal surface.

3.3.2. The performance of additives for S21 vs. S21

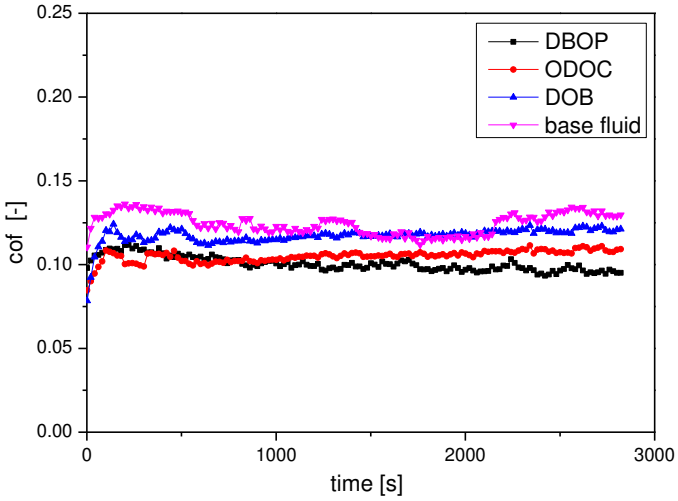

Fig. 7. The COF for 2.0 wt. % DBOP, ODOC and DOB-based emulsions in combination with S21 vs. S21 with time

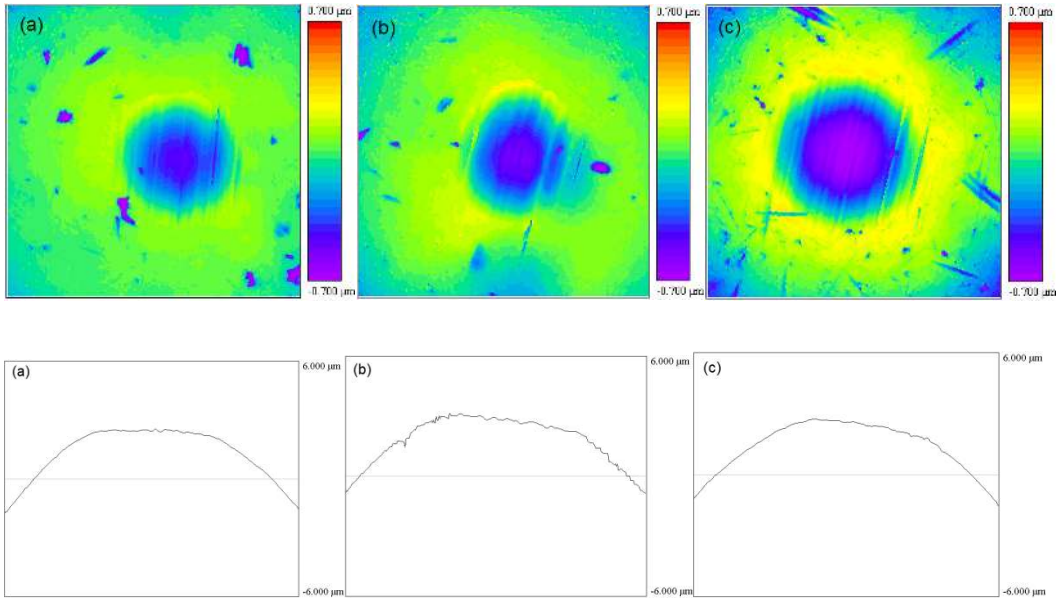

Fig. 8. The morphology and wear profile of the wear scars on S21 balls (sliding distance 2000m, 10X, the scales are all shown as height in µm, all of the morphology areas are 300µm×300 µm based on curvature mode, all of the wear profile length is 300 µm in the centre based on plane mode); (a) 2.0 wt. % DBOP, (b) 2.0 wt. % ODOC, (c) 2.0 wt. % DOB-based emulsion

The friction profiles of S21 vs. S21 lubricated by different additive-based emulsions are shown in Fig. 7. The COF of base fluid without additives is 0.122

and is shown in the figure as a reference. From Fig. 7, it can be seen that the friction reduction property of the three additives is ranked as DBOP ~ ODOC > DOB under the test condition. The average COF of the three emulsions is 0.100, 0.104 and 0.116 respectively. Similar to Fig. 5, the COF is higher at the beginning of the test and after around 600 seconds the curve becomes stable for DBOP. While for ODOC and DOB, the curves show a slight increase afterwards. The different tendency for S21 vs. S21 to that for A3 vs. A5 is probably due to the different material combinations and different reaction layers. The wear rate of DBOP, ODOC and DOB-based emulsions for S21 vs. S21 is 4×10^{-7} $mm^3 \cdot N^{-1} \cdot m^{-1}$, 4×10^{-7} $mm^3 \cdot N^{-1} \cdot m^{-1}$ and 8×10^{-7} $mm^3 \cdot N^{-1} \cdot m^{-1}$ respectively. The morphologies of the wear scars on S21 balls for different additives are shown in Fig. 8.

3.3.3. Discussion on the influence of the additives

For the influence of additives, the friction-reducing property of DBOP is more pronounced than that of DOB for both the A3 vs. A5 and the S21 vs. S21 material combinations. The difference is due to the different boundary layer. The film is highly dependent on the reaction activity, the active elements and the molecular structure of the additives. On the one hand, the content of the active elements of DBOP is about 6.71% P, 10.39% O and 3.03% N. DOB contains two long chains in the molecular structure and the content of the active elements is the lowest among the three additives with about 1.34% B, 8.64% O and 2.51% N. Hence it can be concluded that the reaction activity of DOB is the lowest among the three additives. On the other hand, it may be because of the type of the boundary films formed by the active elements. Normally phosphorous-containing additive can form phosphates e.g. $FePO_4$ and others, which give well-performing boundary lubrication film [24]. Boron-containing additives commonly form B_2O_3 and related films which are known to reduce friction during rubbing [25]. For boron and calcium-containing additives, besides B_2O_3, CaO or $CaCO_3$, films can be formed on the surface which can also be helpful for reducing friction [26]. Detailed information on the composition of the films formed on the rubbing surfaces is presented in Section 3.3.

From the friction profile of the COF curves with time shown in Fig. 5 and Fig. 7, it can be seen that the COF is more dependent on the emulsion, and especially on the additives. A common model for emulsion lubrication is the plate-out theory

[10]. When an oil droplet is exposed to a metal surface, the layer formed by the polar orientation of the emulsifier molecule induces droplets to adsorb onto the metal surface. Then the droplet spreads and a layer of oil can be plated on the surface and work as a protection layer. In this case, at the beginning of the test, water played the dominant role and all the additives showed a higher COF. After 500 to 600 seconds, the droplets broke and plated-out onto the surface. This process is schematically illustrated in Fig. 9. At the beginning, stage I can be attributed to the transition of friction behaviour from the running-in period to the steady-state sliding [27]. Then in stage II oil droplets are dispersed in water and adsorbed onto the metal surface. After the process of plate-out, the additives are adsorbed onto the metal surface and form the protection films, and this can be shown in stage III.

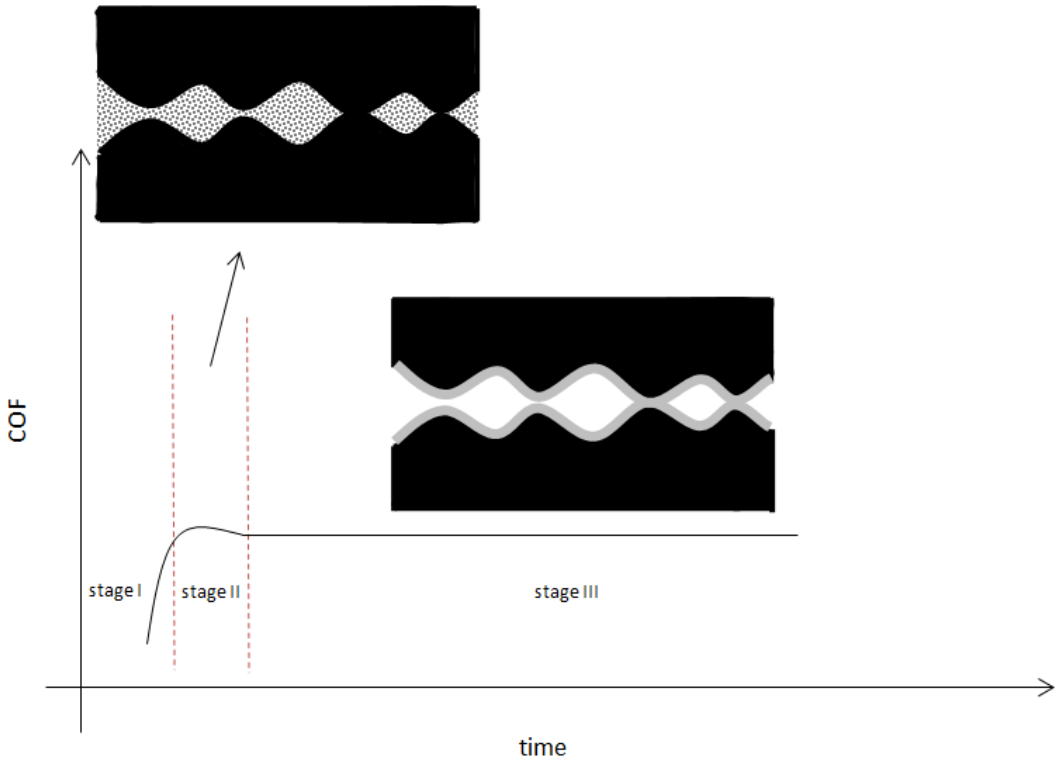

Fig. 9. Schematic friction curve and corresponding lubrication mechanism for the O/W emulsion

3.4. XPS analysis

XPS spectra of the elements in the worn surface were recorded to determine the chemical state of the elements and to examine possible film-forming mechanisms based on the known composition of the additives. Since the wear scars were too

small on the balls tested by using a nanotribometer for the XPS analysis, the same tests were conducted by using a pin-on-disk machine with a bigger specimen (an 80 mm diameter A3 pin). And the XPS measurements were performed on the A3 pin after the tribological tests under the same test conditions as those on the nanotribometer (same contact pressure, sliding velocity and sliding distance). The tribological data are shown in supporting information, which is similar to the results performed on the nanotribometer. The XPS spectra of Fe_{2p}, O_{1s}, N_{1s}, B_{1s}, Ca_{2p} and P_{2p} on the worn surfaces for A3 lubricated with 2.0 wt. % DBOP, ODOC and DOB-based emulsions are depicted in Fig. 10. For each of the binding energy curve of different elements it can be fitted, and the summarized results are shown in Table 4. The binding energies of some standard compounds containing the active elements are listed in Table 5 for comparison, which were obtained from the NIST XPS Database [28].

The Fe_{2p} peaks appear at around 711.70eV and 723.80eV, which can be ascribed to iron oxides (Fe_2O_3) and/or iron hydroxides (FeOOH), indicating that the lubricated surface is oxidized during the friction process. Interestingly, it can be seen from the spectra that the intensity of Fe_{2p} for DBOP is the highest, while for ODOC and DOB, the intensity is slightly weaker. The higher intensity for DBOP may lie in that phosphorous can easily react with iron. Generally phosphorous is proved to be an active element during the rubbing process [11]. The other interesting difference for DBOP is that there are peaks around 706.58eV and 719.68eV which can be attributed to the formation of renascent iron surface during rubbing.

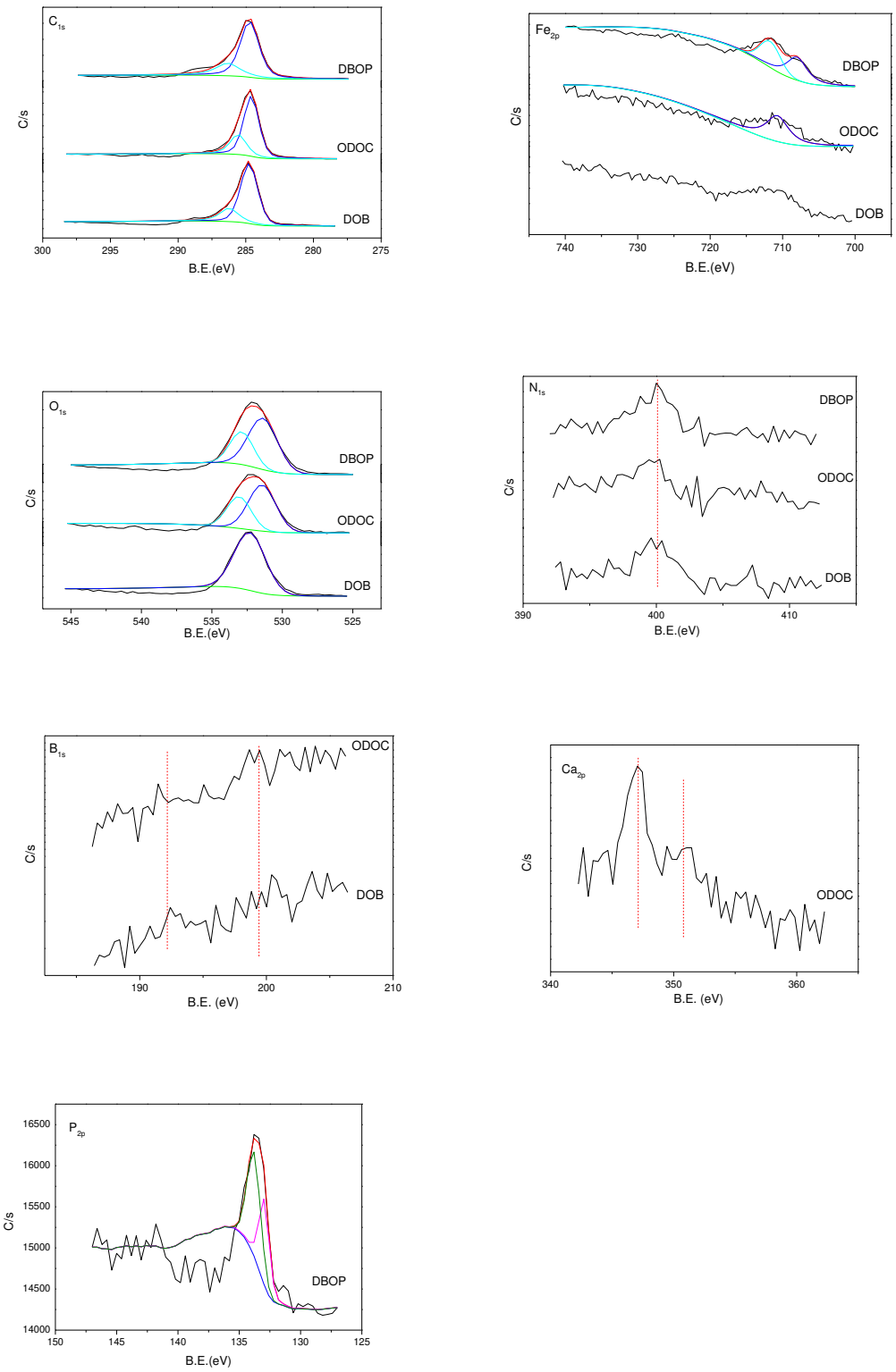

Fig. 10. XPS spectra of C_{1s}, Fe_{2p}, O_{1s}, N_{1s}, B_{1s}, Ca_{2p} and P_{2p} on the worn surfaces for A3 lubricated with 2.0 wt. % additives

Table 4

The fitted results of binding energy of the samples

	Binding energy (eV)						
Additive-based emulsion	Fe_{2p}	N_{1s}	Ca_{2p}	P_{2p}	B_{1s}	C_{1s}	O_{1s}
DBOP	706.58, 710.56, 719.68, 723.66	399.38		132.70, 133.54		284.76, 286.47	531.39, 533.70
ODOC	710.58, 723.68	399.59	347.14, 350.86		192.00	284.79, 286.57	531.89, 533.33
DOB	710.80, 723.90	399.89			192.10	284.85, 286.59	532.45

For other elements like nitrogen, there is a wide peak at around 399.60eV for all of the three additive lubricated surfaces, suggesting that the N element is still in the state of organic N-containing compounds. It may be the complex compounds of metal surface with the decomposed additives like organic amine, organic amide and other N-containing compounds [29]. The C_{1s} spectra confirm the existence of the organic compounds because of the sp2 peak (C–C), which is around 284.80 eV, and the C–O group which is around 286.50 eV [30]. The B_{1s} spectra show peak at around 192.10eV, corresponding to B_2O_3 and/or some borates. The binding energy of P_{2p} at 132.70eV and 133.54eV suggests the existence of $FePO_4$ formed on the worn surface. The wide Ca_{2p} peak at around 347.14eV and 350.86eV can be identified as $CaCO_3$ and CaO with the peak distance about 3.5eV.

Table 5

Binding energy of some standard compounds containing Fe, P, B, Ca, and N

Element	Compounds	Binding energy (eV)
Iron	Fe_2O_3	$Fe_{2p3/2}$(711.3); $Fe_{2p1/2}$(724.0); O_{1s}(529.8)
	Fe_3O_4	$Fe_{2p3/2}$(709.4); $Fe_{2p1/2}$(723.5); O_{1s}(529.7)
	FeO	Fe_{2p}(709.6); O_{1s}(530.1)
	FeOOH	$Fe_{2p3/2}$(711.5); $Fe_{2p1/2}$(724.3); O_{1s}(531.7)
	Fe(OH)O	Fe_{2p}(711-711.8); O_{1s}(531.2-531.8)
Phosphorous	$FePO_4$	Fe_{2p}(712.8); P_{2p}(133.7); O_{1s}(531.8)
Boron	Fe_xB_y	Fe_{2p}(706.9-707.4); B_{1s}(188.0)
	B_2O_3	B_{1s}(192.0); O_{1s}(532.5-533.8)
Calcium	CaO	Ca_{2p}(347.0); O_{1s}(531.3-531.5)
	$Ca(NO_3)_2$	Ca_{2p}(347.0); N_{1s}(407.6)
Nitrogen	N-containing organic	N_{1s}(399.7)
	NH_4NO_3	N_{1s}(403.1)

When taking a look at the XPS spectra for O_{1s}, all of the three additive lubricated systems exhibit an intensive wide peak in the range of 530-535eV. Firstly, it further confirms the existence of FeOOH and Fe_2O_3 on the A3 surfaces. For DBOP, it confirms the existence of $FePO_4$ with the characteristic peak at 531.39eV and 533.70eV. As for ODOC, CaO and $CaCO_3$ can exist because its characteristic peak is at 531.3-531.5eV. It is obvious that the peak for DOB is located in a higher

binding energy area compared to that of DBOP, which can be attributed to the formation of B_2O_3.

In summary, the surface analysis results demonstrate that under boundary lubrication conditions, the active additive molecules in the emulsion first adsorb on the metal surface after the oil droplet is broken, and then decompose and react with the metal surface during the rubbing process, forming stable lubricating films at the rubbing surfaces. The lubricating films are complex and consist of an adsorption layer and a reaction layer. The detailed compositions of the layers are listed in Table 6. The adsorption layer is formed mainly by the coordinate bonding of nitrogen-containing groups with the metal surface resulting from the decomposed products from the additives. The reaction layer originates from the tribochemical reaction of the active elements contained in the additives, which results in the formation of boron oxide, calcium oxide, phosphate and other oxidized compounds. The main difference of the films formed by these three additives lies in the reaction layer. The reaction layer for DBOP consists of iron oxides, iron hydroxides and phosphate, and the reaction layer for ODOC contains iron oxides, iron hydroxides, calcium oxide and carbonate. And the reaction layer for DOB is composed of iron oxides, iron hydroxides and boron oxide. Associating the results with the tribological performance in Section 3.2.1, it gives rise to the hypothesis that the good performance for ODOC and DBOP is associated with the films generated on the surface. For ODOC, mainly iron oxides, iron hydroxides and calcium oxide were generated which are demonstrated to be helpful for friction-reducing. For DBOP, besides iron oxides and iron hydroxides, the existence of $FePO_4$ could be responsible for the tribological performance which is consistent with results from the literature, see e.g. reference [11]. In addition, the freshly exposed metal surface has high surface energy and is known to form a protective layer by reacting with the additives. This may be the reason why DBOP shows better friction-reducing property in Fig. 5.

Table 6

Main composition of boundary films found at the surface of the wear scar

Additive	Adsorption film	Reaction film
DBOP	N-containing organic compounds	Iron oxides, iron hydroxides, phosphate
ODOC	N-containing organic compounds	Iron oxides, iron hydroxides, CaO, $CaCO_3$
DOB	N-containing organic compounds	Iron oxides, iron hydroxides, B_2O_3

3.5. The comparison of oil system with O/W system

The tribological performance of the additives in an oil-based system (2.0 wt. % additives in rapeseed oil as lubricants) for A3 vs. A5 was examined in previous work [31]. A summary of the COF and wear rate for the oil-based systems and for the O/W emulsion-based system is given in Table 7. The COF in the oil system is lower than that in the water system for DBOP and DOB. This can be attributed to the different viscosity and the oil content. On the one hand, it is reported that the coefficient of friction decreases with the increase of viscosity in a boundary lubrication regime [20]. In the oil system, the overall viscosity of the lubricant (around 90×10^{-3} Pa·s) is higher than that of the O/W emulsion (around 30×10^{-3} Pa·s). On the other hand, in an oil-based system, both the additives and the base oil can be adsorbed onto the metal surface to form a stable and compact protection layer. Interestingly, for ODOC, the friction reducing property in the oil system and O/W emulsion does not change so much. This can be related to the different structure of the additive-based emulsions. From the chemical compositions of the additives, ODOC is an ionic compound and Polysorbate 80 is a compound with hydroxyl groups. Therefore, the polarity of the additives and the emulsifier can be ranked as ODOC > Polysorbate 80 > DOB and DBOP. The polarity of the additives is different, and the structure of the oil droplet is

different. So within one oil droplet, there are different domains: for DOB and DBOP containing emulsions, DOB and DBOP are in the core of the oil droplet because of the similar polarity to oil, while for ODOC-based emulsion, ODOC is at the interface of the oil droplet and works as the co-emulsifier. Therefore, ODOC can be easier to adsorb onto the metal surface to form the protective layer, demonstrating similar friction-reducing performance to that of an ODOC oil system.

For the wear performance, the wear rates in an oil system and O/W emulsion are similar; this means that the oil and additives can also perform well and prevent wear when the oil droplet is broken. For the oil-based lubricants, the main difference on the films formed by the three additives was found in the reaction layer. The reaction layer for DBOP consisted of iron oxides, iron hydroxides and phosphate, and the reaction layer for DOB was composed of iron oxides, iron hydroxides and boron oxide. As for ODOC, besides iron oxides, iron hydroxides and boron oxide, calcium oxide and nitrate were generated at the surface. For the O/W emulsion system, the reaction layers for the additives are almost the same as those for the oil-based lubricating systems.

Table 7

Comparison of the COF and wear rate for oil lubricated and for O/W emulsions lubricated systems

	COF		Wear rate ($mm^3 \cdot N^{-1} \cdot m^{-1}$)	
Additive	in oil	in O/W emulsion	in oil	in O/W emulsion
DBOP	0.065	0.132	1×10^{-7}	3×10^{-7}
ODOC	0.114	0.124	4×10^{-7}	4×10^{-7}
DOB	0.065	0.153	5×10^{-7}	3×10^{-7}

4. Conclusion

Three O/W emulsions were used as lubricants for A3 and S21 materials. The following conclusions can be drawn:

1. For the materials used in this work, compared to A5, the COF and wear under boundary lubrication conditions are higher for S21 and A3.

2. The additives with different molecular structures and active elements form different emulsion structures and show different tribological behaviours. For ODOC-based emulsion, ODOC is at the interface of the oil and water, acting as a co-emulsifier due to the high polarity and ionic structure, while DOB and DBOP are closer to the core of the oil droplet in the emulsions. The results are also consistent with the smaller particle size of ODOC than that of DOB and DBOP. For A3 vs. A5 material combination, the three emulsions show similar anti-wear property, and the friction-reducing capabilities of DBOP and ODOC are slightly better than that of DOB. For S21 vs. S21 material combination, the friction-reducing property of the three emulsions is in the same order as that for A3 vs. A5, with the COFs of DBOP and ODOC slightly lower than that of DOB. And the anti-wear property of DBOP and ODOC is also slightly better than that of DOB.

3. From the XPS analysis it is concluded that under the boundary lubrication condition, the active additive molecule first adsorbs at the metal surface, decomposes and then reacts with the metal surface during the rubbing process. This process gives stable lubricating films formed at the rubbed surfaces. The main difference between the tribological performances of the films formed by the three additives used in this work originates from the reaction layer. For ODOC, besides iron oxide and iron hydroxide, calcium oxide was also generated, all of which are demonstrated to be helpful for friction-reducing. For DBOP, besides iron oxides and iron hydroxides, the existence of $FePO_4$ and the freshly exposed iron, which is proved to be reactive with the additives, could be related to the better performance.

4. From the friction profiles generated by different additive-based emulsions, the values of COF are all higher at the beginning of the test after running-in, and then

the curves tend to be stable. This suggests that the water phase may play the dominant role at the beginning, while after the droplet of the emulsion is broken, the additives will adsorb onto and react with the metal surface. The different boundary layer may lead to different friction behaviour.

5. The differences in friction and wear performance between the oil-based system and the O/W emulsion-based system with the same functional additives are related to the chemical structure of the reaction layer formed at the surface.

Acknowledgments

The authors are grateful to Marie Curie CIG (Grant no. PCIG10-GA-2011-303922), NSFC (National Natural Science Foundation of China)-NWO (The Netherlands Organisation for Scientific Research) Bilateral Programme Scientist Exchange (Grant no. 2013/05585/BOO) the Netherlands, and the NSFC of China (Grant No. 21272157) for the financial support.

References

[1] O. Isaksson, Rheology for water-based hydraulic fluids, Wear, 115 (1987) 3-17.

[2] S. Watanabe, T. Fujita, K. Suga, A. Inaba, New additives for water-based cutting fluids, Materials Chemistry and Physics, 8 (1983) 573-577.

[3] E.O. Bennett, Water-based cutting fluids and human health, Tribology International, 16 (1983) 133-136.

[4] J. Osten-Sacken, R. Pompe, R. Sköld, Thermoanalytical study of water-based aluminium rolling fluids combined with direct observation, Thermochimica Acta, 95 (1985) 431-434.

[5] K.E. Rich, An Investigation into the Biodegradability of Metalworking Lubricants with Regard to BOD/COD Parameter Data, in: T.N. Veziroğlu (Ed.) Studies in Environmental Science, Elsevier, 1984, pp. 487-498.

[6] L. Casabán Julián, A. Igual Muñoz, Influence of microstructure of HC CoCrMo biomedical alloys on the corrosion and wear behaviour in simulated body fluids, Tribology International, 44 (2011) 318-329.

[7] A. Tomala, A. Karpinska, W.S.M. Werner, A. Olver, H. Störi, Tribological properties of additives for water-based lubricants, Wear, 269 (2010) 804-810.

[8] J.J. Benner, M.R. Hoeprich, M.C. Frank, F. Sadeghi, Lubricating Properties of Water in Oil Emulsions, Journal of Tribology, 128 (2005) 296-311.

[9] K. Mohlin, K. Holmberg, Nonionic ortho ester surfactants as cleavable emulsifiers, Journal of Colloid and Interface Science, 299 (2006) 435-442.

[10] N. Fujita, Y. Kimura, Plate-out efficiency related to oil-in-water emulsions supply conditions on cold rolling strip, Proceedings of the Institution of Mechanical Engineers, Part J: Journal of Engineering Tribology, 227 (2013) 413-422.

[11] J. Yan, J. Bu, X. Bai, J. Li, T. Ren, Y. Zhao, The tribological study of novel phosphorus–nitrogen type phosphoramidate additives in rapeseed oil, Proceedings of the Institution of Mechanical Engineers, Part J: Journal of Engineering Tribology, 226 (2012) 377-388.

[12] D. Jin, L. Yue, Tribological properties study of spherical calcium carbonate composite as lubricant additive, Materials Letters, 62 (2008) 1565-1568.

[13] Z. Zheng, G. Shen, Y. Wan, L. Cao, X. Xu, Q. Yue, T. Sun, Synthesis, hydrolytic stability and tribological properties of novel borate esters containing nitrogen as lubricant additives, Wear, 222 (1998) 135-144.

[14] R. Skaer, P. Peters, J. Emmines, The localization of calcium and phosphorus in human platelets, Journal of Cell Science, 15 (1974) 679-692.

[15] H. Kosukegawa, V. Fridrici, P. Kapsa, Y. Sutou, K. Adachi, M. Ohta, Friction Properties of Medical Metallic Alloys on Soft Tissue–Mimicking Poly(Vinyl Alcohol) Hydrogel Biomodel, Tribology Letters, 51 (2013) 311-321.

[16] M. Niinomi, Fatigue characteristics of metallic biomaterials, International Journal of Fatigue, 29 (2007) 992-1000.

[17] M.K. Lei, X.M. Zhu, In vitro corrosion resistance of plasma source ion nitrided austenitic stainless steels, Biomaterials, 22 (2001) 641-647.

[18] T. Vorobyova, Adhesion interaction between electrolessly deposited copper film and polyimide, Journal of Adhesion Science and Technology, 11 (1997) 167-182.

[19] E. Hvattum, W.L. Yip, D. Grace, K. Dyrstad, Characterization of polysorbate 80 with liquid chromatography mass spectrometry and nuclear magnetic resonance spectroscopy: Specific determination of oxidation products of thermally oxidized polysorbate 80, Journal of Pharmaceutical and Biomedical Analysis, 62 (2012) 7-16.

[20] D. Dowson , Z. M. Jin, Metal-on-metal hip joint tribology, Proceedings of the Institution of Mechanical Engineers, Part H: Journal of Engineering in Medicine, 220 (2006) 107-118.

[21] S.M. Hsu, R.S. Gates, Effect of materials on tribochemical reactions between hydrocarbons and surfaces, Journal of Physics D-Applied Physics, 39 (2006) 3128-3137.

[22] A. Igual Muñoz, S. Mischler, Effect of the environment on wear ranking and corrosion of biomedical CoCrMo alloys, J Mater Sci: Mater Med, 22 (2011) 437-450.

[23] J. Qu, J.J. Truhan, An efficient method for accurately determining wear volumes of sliders with non-flat wear scars and compound curvatures, Wear, 261 (2006) 848-855.

[24] M.N. Najman, M. Kasrai, G.M. Bancroft, A. Miller, Study of the Chemistry of Films Generated from Phosphate Ester Additives on 52100 Steel Using X-ray Absorption Spectroscopy, Tribology Letters, 13 (2002) 209-218.

[25] J. Yan, X. Zeng, E. van der Heide, T. Ren, The tribological performance and tribochemical analysis of novel borate esters as lubricant additives in rapeseed oil, Tribology International, 71 (2014) 149-157.

[26] D. Liu, G. Zhao, X. Wang, Tribological Performance of Lubricating Greases Based on Calcium Carbonate Polymorphs Under the Boundary Lubrication Condition, Tribology Letters, 47 (2012) 183-194.

[27] M. Chen, K. Kato, K. Adachi, The Difference in Running-In Period and Friction Coefficient Between Self-Mated Si_3N_4 and SiC Under Water Lubrication, Tribology Letters, 11 (2001) 23-28.

[28] C. Wagner, A. Naumkin, A. Kraut-Vass, J. Allison, C. Powell, J. Rumble Jr, NIST X-ray Photoelectron Spectroscopy Database, Version 3.5 (National Institute of Standards and Technology, Gaithersburg, 2003).

[29] X. Zeng, H. Wu, H. Yi, T. Ren, Tribological behavior of three novel triazine derivatives as additives in rapeseed oil, Wear, 262 (2007) 718-726.

[30] O. Carton, D. Ben Salem, S. Bhatt, J. Pulpytel, F. Arefi-Khonsari, Plasma Polymerization of Acrylic Acid by Atmospheric Pressure Nitrogen Plasma Jet for Biomedical Applications, Plasma Processes and Polymers, 9 (2012) 984-993.

[31] J. Yan, X. Zeng, T. Ren, E. van der Heide. Boundary lubrication of stainless steel and CoCrMo alloy materials based on three ester-based additives, Tribology International, 73 (2014) 88-93.

Paper C

The synergy between graphene oxide and surface-active polymers in aqueous lubrication of CoCrMo alloys

Jincan Yan, Xiangqiong Zeng, Tianhui Ren, Emile van der Heide. Submitted to Scientific Reports, 06-2014.

The synergy between graphene oxide and surface-active polymers in aqueous lubrication of CoCrMo alloys

Jincan Yan, Xiangqiong Zeng, Tianhui Ren, Emile van der Heide

Abstract

The aqueous lubrication of CoCrMo alloys with graphene oxide and surface-active polymer coatings was studied in this work. Three different surface-active polymers - poly(acrylic acid) (PAA), poly(ethylene glycol) (PEG) and poly(ethylene oxide-lactide) (PEG-lactide) with or without graphene oxide (GO) - were coated on a CoCrMo alloy surface, and the samples were characterized by ATR, EDS and XPS. The tribological performance of the surface-active polymer coatings with or without GO was evaluated in water, phosphate buffered saline (PBS), bovine serum (BS) and oil-in-water emulsions. Synergetic effects have been found between GO and surface-active polymers. The tribological behaviour of PEG-lactide coating in oil-in-water emulsion was better than that of PEG coating, indicating the advantage of using hydrophilic and lipophilic group containing surface-active polymers for emulsion lubrication.

Keywords: Aqueous Lubrication, Surface-active Polymer, Graphene Oxide, Boundary Lubrication

1. Introduction

CoCrMo alloys are widely used as sliding or bearing surfaces in biomedical applications, for instance as artificial joint material, because of the biocompatibility, excellent mechanical properties and high corrosion resistance [1, 2]. Friction in these applications, however, could well reach levels a factor of one hundred higher than sliding under the same operational conditions in contact with human articular cartilage, resulting in wear and limited longevity of the joint replacement [3]. Research on solutions focuses mainly on exploring more wear resistant designs, materials and material combinations [4, 5]. High friction in artificial joints typically arises from poor boundary lubrication conditions [6]. Dedicated boundary layers with low interfacial shear strength and larger surface separation could possibly reduce friction and reduce the

associated risk on wear and wear particle generation, thereby increasing the durability of the implants.

One approach for generating low shear strength boundary layers could be bounding of surface-active hydrophilic polymer brushes. In an aqueous biological environment, the bounded surface-active hydrophilic polymer expands in the direction normal to the surface by adsorbing water and by hydrogen bonding with water forming a brush-like structure. On the approach of the interacting surface, the brush is compressed and a repulsive force arises so that the applied force is supported by the fluid, resulting in low interfacial shear strength on accommodating differences in sliding velocities of the interacting surfaces [7, 8]. Previous investigations were conducted on the hydration lubrication capability of various polymer brushes grafted on extremely smooth surfaces like mica and silicon wafer under contact pressure up to about 20MPa [9, 10]. The effectiveness of the polymer brushes on engineering surfaces with a certain roughness like on implant materials (CoCrMo alloy) at higher contact pressure (up to 100MPa) has not yet been investigated.

In this work, the macro-tribological performance of surface-active hydrophilic polymer bonded to CoCrMo with roughness was studied. The durability of the surface layer under severe operational conditions could be served by the combination of a solid lubricant and a surface-active polymer brush. Graphite, a solid lubricant with an anisotropic crystal structure consisting of strong covalent intralayer bonding and weaker interlayer dispersive interactions, was selected since it can easily be converted to graphene oxide, a two-dimensional lattice of partially broken sp^2-bonded carbon networks with hydroxyl and epoxide groups on the basal planes and carboxylic acid groups at the edges, enabling it to be produced onto various large area substrates with strong adhesion as well as to be functionalized with hydrophilic polymer brushes [11, 12]. Moreover, carbon materials have been used in the treatment of soft and hard tissue injuries, and graphene and its derivatives have attracted much attention in numerous applications in biotechnology, indicating the biocompatibility of graphene oxide [13-16].

Since biomedical applications consist of a variety of physiological fluids, several aqueous media were investigated. Water, as a reference, was selected as it was

used before to examine the wear and corrosion of CoCrMo alloy [17]. Phosphate buffered saline (PBS) is a water-based salt solution containing sodium phosphate, potassium chloride and potassium phosphate. It is widely used in biomedical research because the osmolarity and ion concentrations of the solutions match those of the human body [18, 19]. Bovine serum (BS) is a representative body lubricant, and it is widely used to simulate the synovial fluid in human joints [20, 21]. In addition, emulsion lubrication is evaluated based on similarities in aqueous lubrication for metal forming operations. Its potential in the biomedical field, especially in combination with surface-active polymer brushes, has not previously been the subject of research.

In this work, several surface-active polymers with and without an intermediate GO layer were prepared on CoCrMo surfaces with roughness, and their tribological performances under simulated test conditions were studied.

2. Experimental

2.1 Materials

The CoCrMo alloy (Stellite 21, coded S21) was used as substrate in this work and obtained from Kennametal and complied with the standard ASTM F–75. It contains 27.0 wt. % chromium, 5.5 wt. % molybdenum, 2.5 wt. % nickel and 0.3 wt. % carbon, balanced by cobalt. The carbides in Stellite 21 are intergranular and interdendritic, according to the information of the supplier. The alloy was used after polishing and without any other treatment. The hardness of the materials was tested on a DLH–200 Shimadzu Micro Hardness Tester with the hardness of 375 ± 3 Vickers. The roughness of the specimen was characterized by the Micromap 560 interference microscope.

3-Aminopropyltrimethoxysilane (APTMS) was obtained from Aldrich. Poly(acrylic acid) (PAA) with Mn of 5.5 kg/mol was obtained from Acros Organics. Amino-terminated poly(ethylene glycol) (PEG, Mn = 5.0 kg/mol) and amino-terminated poly(ethylene oxide-lactide) (PEG-lactide, PEG Mn = 10.0 kg/mol, lactide Mn = 1.4 kg/mol) were obtained from Polymer Source Inc. Graphite was 30 μm in diameter powder and obtained from Shanghai Chemicals. $NaNO_3$ and $KMnO_4$ were purchased from Shanghai Chemicals, China.

HCl, H_2SO_4 and H_2O_2 were purchased from Merck Chemicals. All chemicals were used as received.

2.2 Preparation of the coatings

2.2.1 Preparation of graphene oxide (GO)

A typical Hummers method [22] was used to prepare graphene oxide by using graphite powder as the starting material. In the experiment, graphite (2 g, 30 μm) and concentrated sulphuric acid (50 mL) were added in a 250 mL flask with stirring. Subsequently, 5 g $NaNO_3$ was added and after 1hr of stirring it was cooled to 0 ^oC using an ice–water bath. Then 7.3 g $KMnO_4$ was added in small portions during 2hr. When the addition was completed, the reaction mixture was warmed to 35 ^oC. After 2hr of stirring, the reaction was quenched by adding 200 mL of ice water and 7 mL of H_2O_2 (30%) consumed the excess $KMnO_4$ and MnO_2. The resultant graphite oxide was filtered off and washed with aqueous HCl (3%). The graphite oxide was further washed with water (5 × 100 mL) and dried at 40 ^oC for 24hr in the vacuum oven. Graphite oxide (0.075 g) in 150 mL of H_2O was sonicated (200 W) at room temperature for 1hr, in order to exfoliate the graphite oxide into GO sheets. Then a suspension of 0.5 mg/mL GO in H_2O was obtained.

2.2.2 Preparation of coatings

The preparation of the coatings as well as the symbols are shown in Fig. 1. The S21 substrate coated with PAA and PEG (coded S21-PAA-PEG) has been selected as an example to explain the coating procedure. The S21 substrate (10 × 10 × 3 mm) was washed and sonicated with acetone for 30min. After drying, it was dipped into piranha solution (H_2O_2: H_2SO_4 = 1:3 (vol %)) for 2hr. To enhance the hydroxyl groups on the surface of S21 plate, the oxidized S21 plate (S21-OH) was immersed in boiling H_2O_2 solution for 1hr. Then the plate was washed with ultrapure water and flushed with N_2. After cooling down, APTMS was grafted by a chemical vapour deposition (CVD) process as follows. The plate was put in a vacuum vessel together with 1mL APTMS and the vacuum was kept lower than 10^{-7} Pa overnight. Then the sample S21-APTMS was received. PAA was coated onto S21-APTMS by a spin coating process. 0.1mL 5.0 wt. % of PAA in water was applied on the centre of the specimen. The substrate then rotated at 1000 rpm for 60 seconds. Then the specimen was put into a vacuum oven at 100 ^oC for 2hr.

After cooling down, the sample was washed with ultrapure water and flushed with N_2 and coded as S21-PAA. PEG (5.0 wt. % in water) was coated by using the same spin coating procedure as that for PAA and then treated in the vacuum oven at 120 ^oC for 2hr. After the washing and drying process, the sample (S21-PAA-PEG) was kept in a vacuum desiccator. By replacing PEG with PEG–lactide, the S21–PAA–PEG–lactide sample was prepared. Similar to the procedure described above, after the coating of APTMS, 0.1mL 0.5 mg/mL GO in H_2O was spin coated on the sample. The sample was treated in a vacuum oven at 100 ^oC for 2hr and coded S21-GO. PAA, PEG and PEG-lactide were coated in the same way as above and the samples are coded S21-GO-PAA, S21-GO-PAA-PEG and S21-GO-PAA-PEG-lactide, respectively.

2.3 Characterization of the samples

The samples were characterized by infrared spectroscopy (IR spectroscopy), scanning electron microscopy/energy dispersive X-ray spectroscopy (SEM–EDS) and X-ray photoelectron spectroscopy (XPS) [15]. For the coated samples, attenuated total reflectance Fourier transform infrared (ATR–FTIR) spectra were recorded with spectrum 100 FT–IR Spectrometer, Perkin Elmer. The spectrum was collected for 64 scans with a resolution of 4 cm^{-1}, and the background was collected in the absence of the samples. For comparison, FTIR spectra of the powder standard compounds were recorded with an ALPHA FT–IR Spectrometer, Bruker.

X–ray photoelectron spectroscopy (XPS, Physical Electronics PHI–5702) was performed using amonochromated Al irradiation. The chamber pressure was $\sim 3\times10^{-8}$ Torr under testing conditions. Peak deconvolution and quantification of elements were accomplished using Origin 7.0.

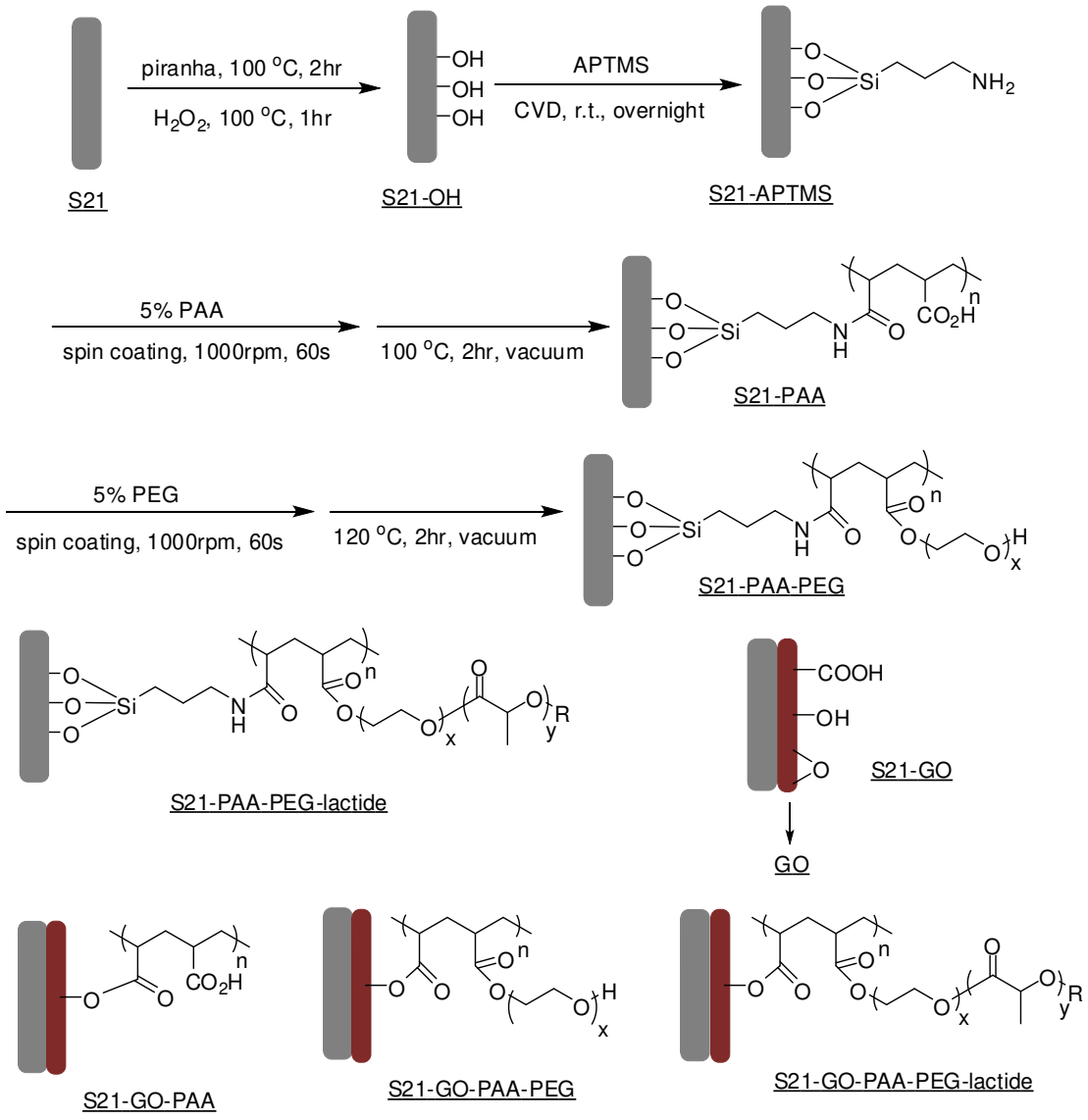

PAA: Poly(acrylic acid), Mn = 5.5 kg/mol
PEG: Amino-terminated poly(ethylene glycol), Mn = 5.0 kg/mol
PEG-lactide: poly(ethylene oxide-lactide)(PEG-lactide, PEG Mn = 10.0 kg/mol, lactide Mn = 1.4 kg/mol)
GO: graphene oxide

Fig. 1 The preparation and symbols of the coatings

2.4 The aqueous media

The aqueous media used in the experiments as well as the abbreviations are listed in Table 1.

Deionized water was used as one of the media as well as for the preparation of other aqueous media. The O/W emulsions were prepared by milling and mixing

2.0 wt. % of the additive, 6.0 wt. % of Polysorbate 80 and 6.0 wt. % of the rapeseed oil together, then adding water gradually and stirring (800 r/min) for 30 minutes. The additive, dibutyl octadecylphosphoramidate (DBOP), was prepared according to [23] and the structure is depicted in Fig. 2. Polyoxyethylene (20) sorbitan monooleate (Polysorbate 80) is a nonionic surfactant derived from polyethoxylated sorbitan and oleic acid [24]. It was purchased from Sigma-Aldrich and used as emulsifier without further treatment. The rapeseed oil, provided by Grease Factory of Lanzhou, China, was used with no further treatment. The main chemical constituents of fatty acids in the rapeseed oil are as follows: 7.46 wt. % of saturated fatty acids, 64.06 wt. % of monounsaturated fatty acid and 28.48 wt. % of total polyunsaturated fatty acid.

Table 1 The aqueous media used in the tests

Abbreviation	**The aqueous media**
water	Deionized water
PBS	Phosphate buffered saline
BS	Bovine serum
O/W 0%	Oil-in-water emulsion without additive
O/W 2%	Oil-in-water emulsion with 2.0 wt. % additive

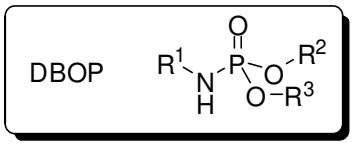

$R^1 = C_{18}H_{37}$, $R^2 = R^3 = C_4H_9$

Fig. 2 The chemical structure of the additive applied in the tests

2.5 Tribological tests

The tribological tests were performed by a nanotribometer (ball on disk) which is provided by CSM-instruments. The roughness of the specimen was characterized by the Micromap 560 interference microscope. The average roughness Ra_1 of the CoCrMo balls and Ra_2 of the CoCrMo disks are based on surface measurements, not on line scans. The balls are 5 mm in diameter with a

roughness of about 70±20 nm. To investigate the influence of the surface roughness on the tribological performance of the surface-active polymer coatings, the disks were polished with surface roughness of 150±50 nm. The polished disks were then coated with the surface-active polymers as illustrated in Fig. 1. The normal force is 5 mN, therefore the mean contact pressure is 90 MPa as calculated by Hertz equation. With the sliding velocity of 35 mm/s, the lubrication regime can be estimated to be in the boundary lubrication regime[5]. The detailed test conditions are summarized in Table 2.

Table 2 Test conditions used in this work

Items	**Nanotribometer**
Diameter of ball	5 mm
Normal force	5 mN
Contact pressure	90 MPa
Velocity	35 mm/s
Sliding distance	100 m
Surface roughness (ball)	70±20 nm
Surface roughness (disk)	150±50 nm

3. Results and discussion

3.1 Characterization results of the samples

3.1.1 FTIR analysis of the samples

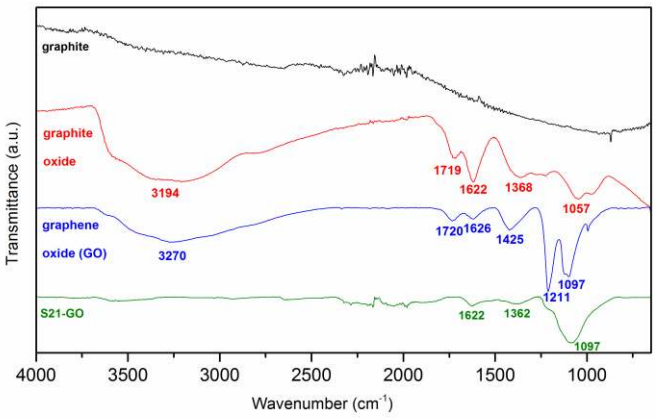

Fig. 3 IR spectra of graphite, graphite oxide, graphene oxide and S21-GO

The IR spectra of graphite, graphite oxide, graphene oxide and S21-GO are shown in Fig. 3. From Fig. 3, no distinct peak can be found from the spectrum of graphite. Graphite oxide exhibits representative peaks at 3194, 1719, 1622, 1368 and 1057 cm^{-1} corresponding to O–H stretch, C=O stretch, aromatic C=C, C–O stretch, respectively. The FTIR spectrum of the GO sample accorded well with the previous works [25, 26]. The peaks at 3270, 1720, 1626, 1425, 1211 and 1097 cm^{-1} correspond to O–H stretch, C=O stretch, aromatic C=C, and COO- bending, epoxy C-O and C–O stretch, respectively. From the spectrum of S21 -GO, the peaks at 1622, 1362 and 1097 cm^{-1} can be assigned to aromatic C=C, O–H bending and C–O stretch, respectively.

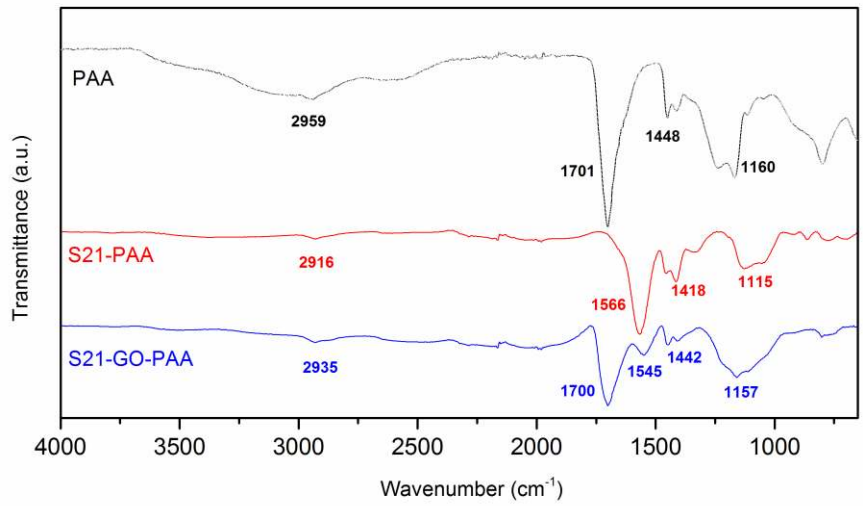

Fig. 4 IR spectra of PAA, S21-PAA and S21-GO-PAA

As shown in Fig. 4, two peaks located at 2959 and 1448 cm^{-1} were observed in the pure PAA sample which can be assigned to the stretching and bending modes of CH_2. The signals at 1701 and 1160 cm^{-1} can be ascribed to the stretching modes of C=O and C–O in COOH group, respectively [15, 27]. For the spectrum of S21–PAA, the signals at 1700 cm^{-1} can also be ascribed to the stretching modes of C=O and two peaks located at 2916 and 1418 cm^{-1} can be assigned to the

stretching and bending modes of CH_2. The signals at 1566 and 1115 cm^{-1} can be the stretch vibration of C–N and C–O groups. From the spectrum of S21–GO–PAA, it can be seen that the peaks located at 2935 and 1442 cm^{-1} can be the stretching and bending modes of CH_2. The signals at 1700 and 1157 cm^{-1} can be the stretch vibration of C=O and C–O groups. The signal at 1545 cm^{-1} can be the stretch vibration of C–N groups.

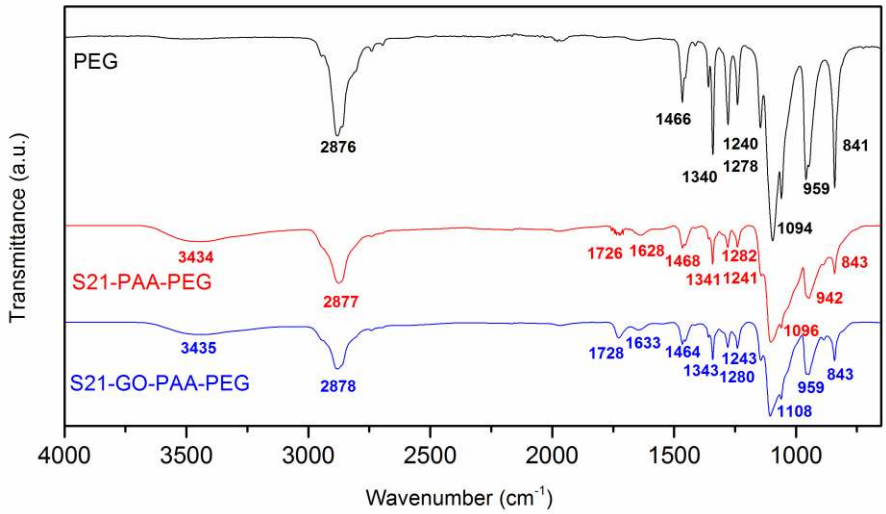

Fig. 5 IR spectra of PEG, S21-PAA-PEG and S21-GO-PAA-PEG

Fig. 5 shows the IR spectra of PEG and PEG coated surfaces. From the spectrum of PEG, the peaks at 841 and 959 cm^{-1} in PEG can be assigned to C–H bending vibration. The peak at 1094 cm^{-1} corresponds to the C–O–C stretch vibration in PEG. The peaks at 1240, 1278 and 1340 cm^{-1} in PEG correspond to C–C stretching vibrations. The peak at 1466 cm^{-1} can be attributed to the scissoring and bending vibration of C–H group. The peak at 2876 cm^{-1} in PEG represents C–H stretch vibrations. For the spectra of S21–PAA–PEG and S21–GO–PAA–PEG, the aforementioned characteristic peaks can also be found. The broad band structure appearing at 3434 cm^{-1} in S21–PAA–PEG and 3435 cm^{-1} in S21–GO–PAA–PEG indicates the presence of O–H bonds (stretch vibration of O–H group) [28]. In addition, the peaks at 1726 cm^{-1} in S21–PAA–PEG and 1728 cm^{-1} in S21–GO–

PAA–PEG are ascribed to the stretch vibration of ester C=O group due to the esterification functionalities between the PAA and PEG [29]. The peaks at 1628 cm^{-1} in S21–PAA–PEG and 1633 cm^{-1} in S21–GO–PAA–PEG are ascribed to the stretch vibration of amide C=O group due to the reaction between the PAA and PEG terminal amino groups [30]. Therefore, the formation of ester and amide was confirmed by this evidence.

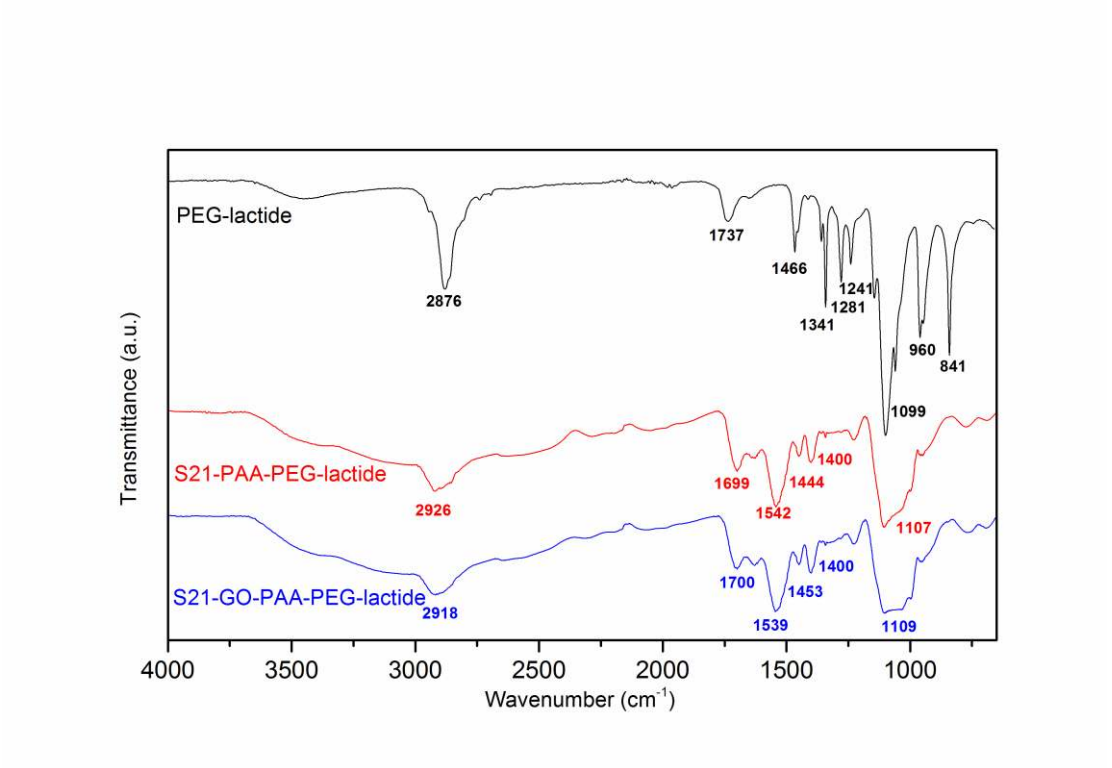

Fig. 6 IR spectra of PEG-lactide, S21-PAA-PEG-lactide and S21-GO-PAA-PEG-lactide

Fig. 6 shows the IR spectra of PEG–lactide and coated PEG–lactide. From the spectrum of PEG–lactide, the peaks at 841 and 960 cm-1 can be assigned to C–H bending vibration. The peak at 1099 cm-1 corresponds to the C–O–C stretch vibration in PEG. The peaks at 1240, 1278 and 1340 cm-1 in PEG correspond to C–C stretching vibrations. The peak at 1466 cm-1 can be attributed to the scissoring and bending vibration of C–H group. The peak at 2876 cm-1 in PEG represents C–H stretch vibrations. From the spectrum of S21–PAA–PEG–lactide, the peak at 1099 can be attributed to the stretch vibration of C–O–C group; 2926 stretch vibration of C–H group; 1400 scissoring and bending vibration of C–H group. From the spectrum of S21–GO–PAA–PEG–lactide, the peak at 1109 can be

attributed to the stretch vibration of C–O–C group; 2918 stretch vibration of C–H group; 1453 scissoring and bending vibration of C–H group.

3.1.2 SEM–EDS analysis of the coatings

From SEM-EDS results in Table 3, the content of carbon and oxygen of all the coating samples is higher than the original Stellite 21. Meanwhile, the content of Co, Cr and Mo reduced gradually as the coating became thicker and thicker. Therefore, the surface of the coated samples is different from the original Stellite 21 and there are some layers on top of the metal surface. The increasing content of C and O suggests the formation of polymer brushes. For S21-GO, almost no oxygen can be found on the top, this may be because the oxygen content on graphene oxide is low and the EDS detection depth is deep.

Table 3 The element composition of the samples

Element (wt. %)	**Co**	**Cr**	**Mo**	**C**	**O**
S21	63.48	26.62	6.11	1.25	
S21–PAA	61.27	25.67	5.05	3.37	0.52
S21–PAA–PEG	50.15	24.11	5.63	9.90	7.07
S21–PAA–PEG–lactide	51.33	24.35	5.71	11.30	7.06
S21–GO	60.35	27.49	5.25	4.28	
S21–GO–PAA	59.62	25.64	4.88	4.38	0.67
S21–GO–PAA–PEG	46.96	23.20	5.08	10.43	11.62
S21–GO–PAA–PEG–lactide	45.96	24.10	4.32	15.43	8.91

3.1.3 XPS analysis of the coatings

The C_{1s} XPS analyses of the coated surfaces are shown in Fig. 7 and the fit binding energy of C_{1s}, O_{1s}, Si_{2p} and N_{1s} spectra are listed in Table 4. For S21-PAA in Fig. 6a there are three kinds of carbon atoms that correspondingly exist in different functional groups: the non-oxygenated carbon atoms in the ring (around 284.0 eV), the carbon atoms in carbon–oxygen bonds (285.0 eV), and the carboxylate

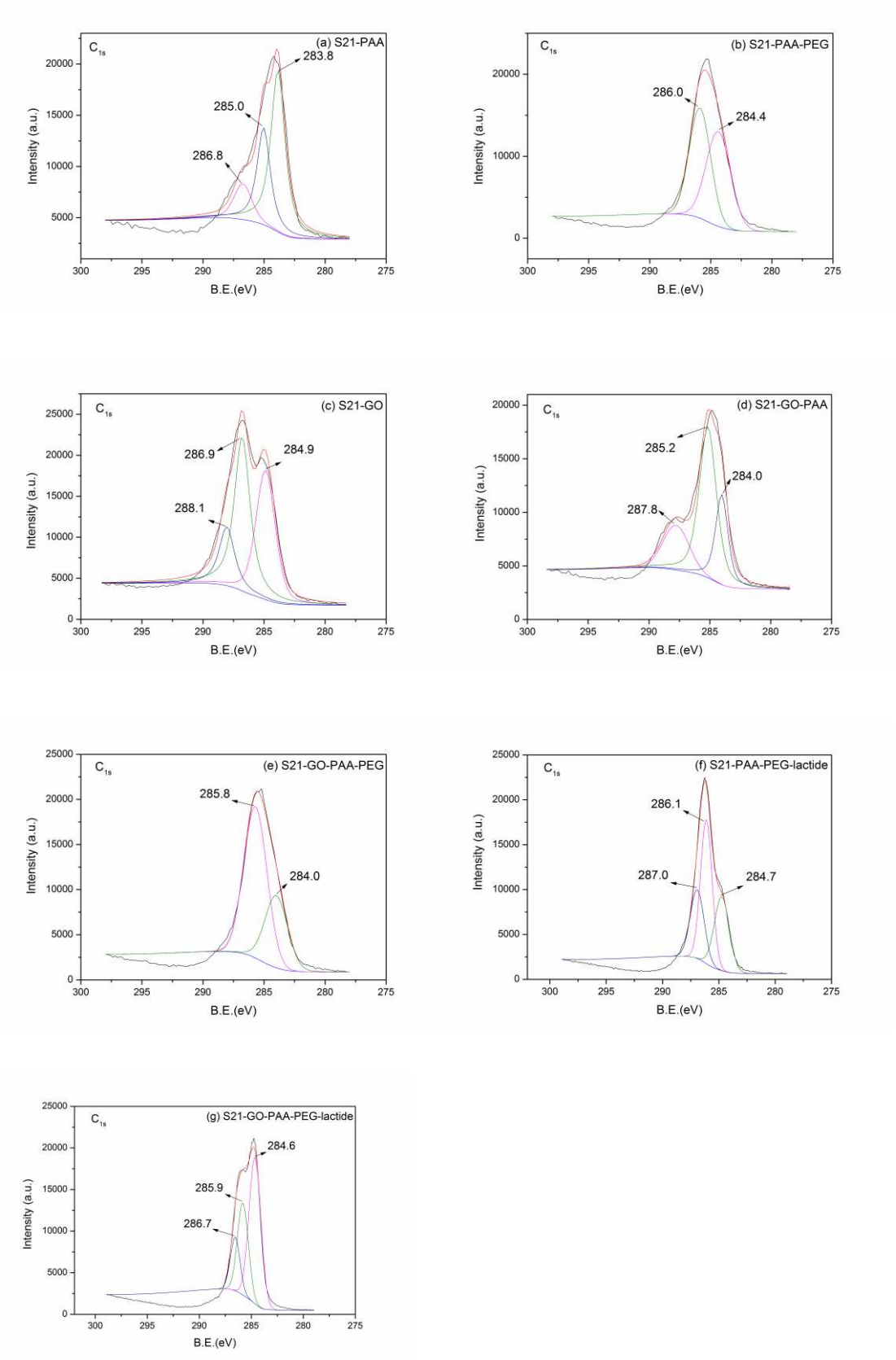

Fig. 7 C_{1s} XPS analysis of the coated surfaces

carbon (287.0 eV) [31]. Almost the same spectra can be found for S21-GO-PAA from Fig.6d. For S21-GO in Fig. 6c, the sp2 peak (C–C) of the C1s spectrum is centred on around 284.9 eV. The strong component at 286.9 eV is attributed to the epoxide group (C–O–C), and the components around 288.1 eV correspond to carbonyl (C=O) and carboxyl (O=C–OH) groups, respectively [32-35]. For S21-PAA-PEG and S21-GO-PAA-PEG, the spectra show mainly two components which are the functional groups of C–C (around 284.0 eV) and C–O–C (around 286.0 eV), and almost no O=C–OH groups can be found [36, 37] due to the detection depth of XPS, which is around 3-10nm, which may indicate that the thickness of the superficial PEG layer is higher than 3-10nm so that the middle PAA layer cannot be detected. For S21-PAA-PEG-lactide and S21-GO-PAA-PEG-lactide, the binding energies are 284.6 eV for C_{C-C}, 286.0 eV for C_{C-O}, 287.0 for $C_{C=O}$, respectively.

The O_{1s} XPS analyses of the coated surfaces are shown in Fig. 8. For S21-PAA in Fig. 7a and S21-GO-PAA in Fig. 7d, there are two kinds of oxygen that correspondingly exist in different functional groups: O-C (around 531.4 eV) and O–C=O (around 533.0 eV) [38]. For S21-GO, the O1s spectra (Fig. 7c) contains three components: O–C at 531.7 eV, O=C at 532.5 eV, and O–C=O at 533.7 eV [39]. For S21-PAA-PEG and S21-GO-PAA-PEG, the peaks at around 531.8 eV mean the O-C groups [40]. For S21-PAA-PEG-lactide and S21-GO-PAA-PEG-lactide, the binding energies are around 531.6 eV and 533.4 eV for O-C and O=C groups, respectively.

Table 4 The fit binding energy of C_{1s}, O_{1s}, Si_{2p} and N_{1s} spectra for on the coated surface

	Binding energy (eV)	
	C_{1s}	O_{1s}
S21-PAA	283.8, 285.0, 286.8	532.1, 534.2
S21-PAA-PEG	284.4, 286.0	530.8, 533.2, 535.4
S21-GO	284.9, 286.9, 288.1	532.7, 535.8
S21-GO-PAA	284.0, 285.2, 287.8	531.2, 532.3, 533.9
S21-GO-PAA-PEG	284.0, 285.8	533.0, 534.6
S21-PAA-PEG-lactide	284.7, 286.1, 287.0	532.6, 534.0
S21-GO-PAA-PEG-lactide	284.6, 285.9, 286.7	532.6, 534.7

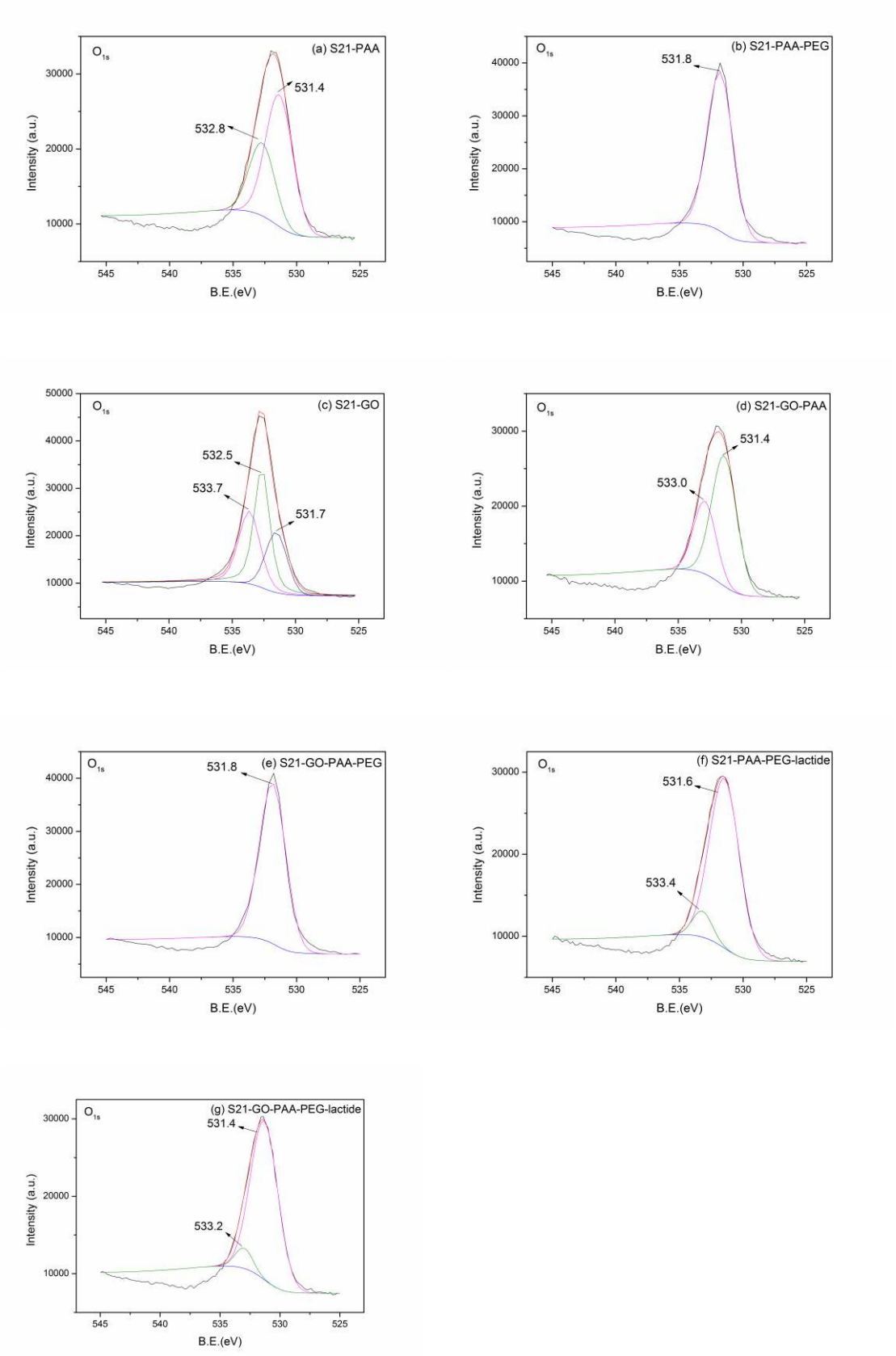

Fig. 8 O_{1s} XPS analysis of the coated surfaces

3.2 The tribological performance of the hydrophilic coatings in different aqueous media

3.2.1 The tribological behaviour of the hydrophilic coatings in water

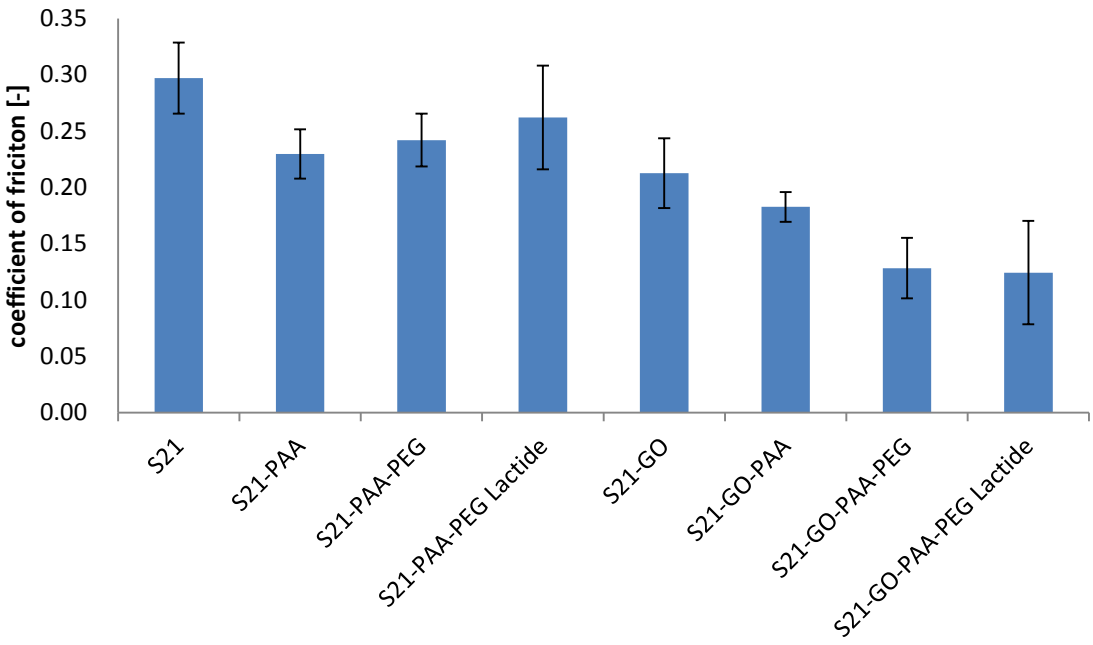

Fig. 9 The coefficient of friction in water as a function of the applied coatings

Fig. 9 shows the coefficient of friction (COF) of different coatings in water. It can be seen from the figure that S21 reveals a high COF of 0.30 and that S21 with coatings always shows a lower COF in water. The COF for S21-PAA, S21-PAA-PEG and S21-PAA-PEG-lactide in water is 0.23, 0.24 and 0.26 respectively. When there is a GO layer in between, the COF for S21-GO and S21-GO-PAA is 0.21 and 0.18. For the S21-GO-PAA-PEG and S21-GO-PAA-PEG-lactide, the COF is largely reduced to 0.13 and 0.12. Therefore, it can be summarized that the CoCrMo alloy coated with both GO and surface-active polymer layers shows better friction reducing capability than only with a GO layer or only with a surface-active polymer layer, indicating the synergy effect of a GO layer and surface-active polymer layer for the boundary lubrication of CoCrMo alloy in water condition.

When the coatings are used in a water environment, the hydrophilic coatings can bind water in their structure and result in a lubricating water layer formed by

the chains [7]. When there is no GO layer, the friction coefficient of the coatings is in the order of S21-PAA<S21-PAA-PEG<S21-PAA-PEG-lactide. PEG ended brushes can form hydrogen bonds in water and form a hydrated layer [41, 42]. For PAA ended coatings, the hydrated –COOH group ended brushes may transfer to –COO- groups in water and water tends to exist in H_3O^+, i.e., the brushes change to charged polymers [10]. Charges affect the translational and rotational degrees of freedom of close-by water molecules causing hydration layers around ions. When positive and negative charges are sufficiently close together, cooperative interaction of the water molecules with the anion and cation can be induced, resulting in non-additive effects and potentially stronger hydration around the polymers, which cause a higher osmotic pressure and then lower friction [43-45]. This is probably the reason why the friction coefficient of S21-PAA is lower than that of S21-PAA-PEG. PEG-lactide contains a long alkyl chain which is lipophilic and may affect the compactness of the extended polymer structures in an aqueous system, resulting in a higher friction coefficient of S21-PAA-PEG-lactide. GO layer has a strong influence on the friction behaviour of the coated materials. The order of the friction coefficient changes to S21-GO-PAA-PEG≈S21-GO-PAA-PEG-lactide<S21-GO-PAA. Due to the incorporation of the GO layer, the grafting density of the polymers may decrease [46]. In this situation, the GO layer and the thickness of the polymers may play the dominant role in the friction behaviour instead of the end groups.

3.2. 2 The interactions between PEG coatings and different aqueous media

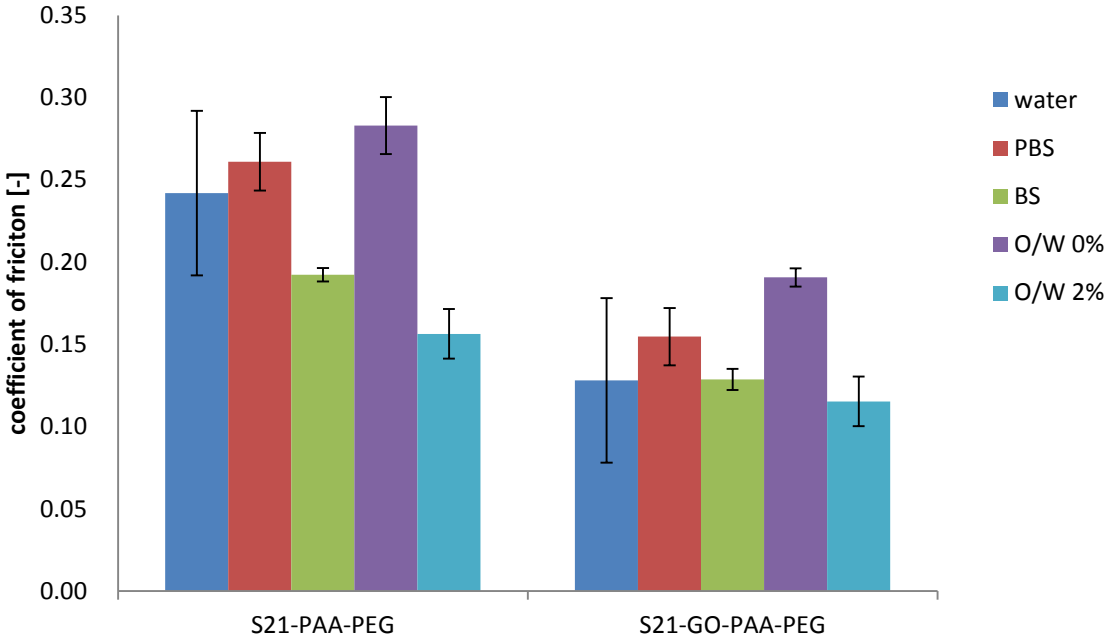

Fig. 10 The coefficient of friction of S21-PAA-PEG and S21-GO-PAA-PEG in different aqueous media

The coefficient of friction of S21-PAA-PEG and S21-GO-PAA-PEG in different aqueous media is shown in Fig. 10. The friction coefficient of the coatings with GO layer is lower than that without GO layer in all the test aqueous media, indicating the effectiveness of incorporating the GO layer.

For the coating of S21-PAA-PEG, it can be seen that it performs better in BS and 2.0 wt. % emulsion than that in water, PBS and 0 wt. % emulsion. For S21-GO-PAA-PEG, the COF is ranked as 0 wt. % emulsion>PBS≥BS≥water>2.0 wt. % emulsion. The data clearly suggest that the aqueous media play a significant role on the friction performance. It can be seen that the coatings perform better in water than in PBS, and this may be because PBS contains ions which affect the formation of the extended polymer structures in an aqueous system. In PBS the concentration of salt is around 0.15 mol/L, and the high concentration is not preferable for the interaction of hydrophilic chains with water. When tested under emulsion without additive (O/W 0%), the friction coefficient is the highest among all the media. During the test, the emulsion droplet will be broken and the release of the base oil from the droplet will destroy the structure of the hydrophilic polymer because the base oil can be

regarded as a bad solvent for the formation of hydrophilic polymer brushes. The performance of the hydrophilic polymers in BS and emulsion with additive (O/W 2%) is in both cases better than the performance in water. Besides the contribution of the polymer brushes, the formation of boundary layers from the other components in BS and emulsion with additive may also play a role. It is reported that the proteins in BS can adsorb at the CrCoMo surface to form thin, discontinuous deposited films to protect the metal [47]. The additive used in the emulsion can form effective boundary layers on the rubbing surface by adsorption and tribo-chemical reaction [48].

3.2. 3 The interactions between PEG lactide coatings and emulsions

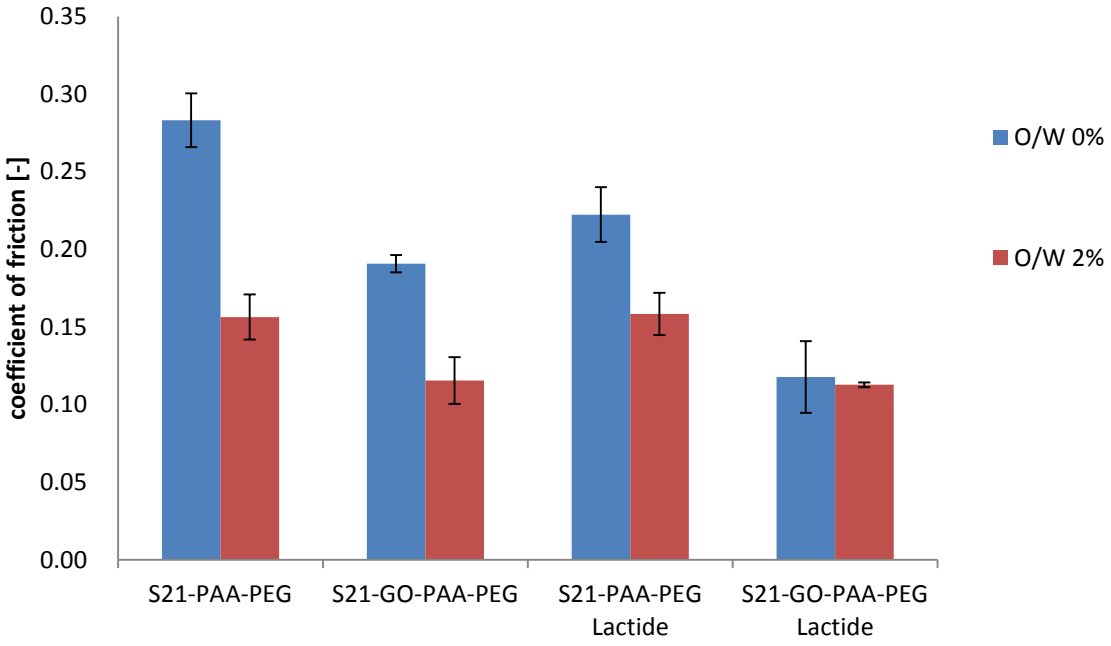

Fig. 11 The coefficient of friction of S21-PAA-PEG-lactide and S21-GO-PAA-PEG-lactide in emulsions

Since PEG-lactide contains both long alkyl chain (lipophilic) and PEG (hydrophilic), it is assumed that when used in O/W emulsion, the lipophilic part may interact with the oil component of the emulsion and the hydrophilic part will interact with water. Therefore, the tribological performance of the PEG-lactide containing coatings in emulsion was investigated. Fig. 11 shows the

coefficient of friction of S21-PAA-PEG-lactide and S21-GO-PAA-PEG-lactide in emulsions. The performance of S21-PAA-PEG and S21-GO-PAA-PEG is also shown for comparison. From the figure, it can be found again that the coatings with GO perform better than those without GO. For the same coating, the COF in the emulsion with 2.0 wt. % additive (O/W 2%) is lower than that without additive (O/W 0%). Moreover, the COF of the coating with lactide is almost the same as that without lactide. It suggests that when using emulsion with additive, the additive effect is predominant due to the formation of protective boundary layer from the additive. When using emulsion without additive, the coating with lactide always performs better than that without lactide. According to the friction profile as shown in Fig. 12, the COF of the coatings in water increases with time, while in 0% emulsion the COF increases before 600 seconds and after that the COF drops and then increases gradually with time.

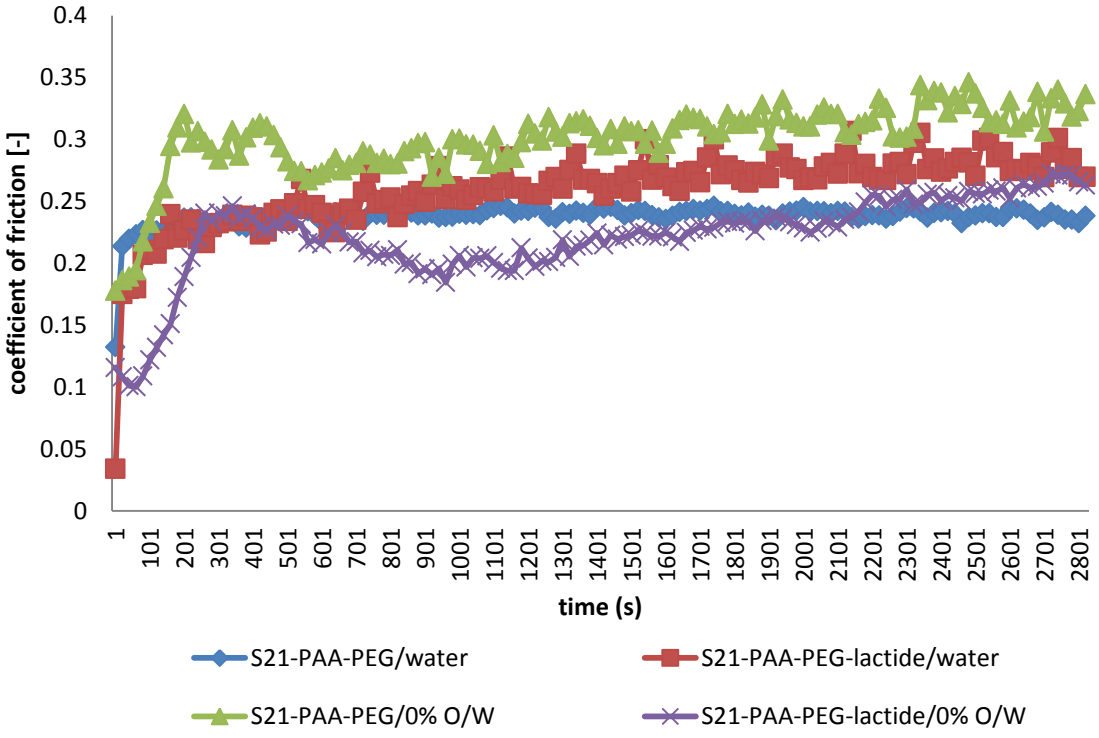

Fig. 12 The variations of COF with time for different coatings in different lubricants

By comparing the friction profile, the interaction between PEG-lactide coating and water is quite different to that between PEG-lactide coating and emulsion. In water, the COF increases with water because of the increasing worn asperities. While in the emulsion, the emulsion droplet first adsorbed onto the metal surface due to the polarity of the emulsifier at the droplet interface. With continuing sliding, the emulsion droplet started to break, and the oil component in the emulsion came out. Under the test conditions, the oil component adsorbed and reacted with the metal surface, generating protection film. Due to this plate-out behaviour of emulsion [49], the friction profile shows three stage phenomena[48]. At the beginning of the test, after the first stage of running-in, water plays the dominant role and a higher COF can be found in stage two. After 500 to 600 seconds, the droplets broke and plated-out onto the surface in stage three. After the oil droplet broke, the oil component of the emulsion interacted with the metal surface to form boundary lubrication films, resulting in lower friction. The tribological performance of PEG-lactide coating in emulsion is better than that of PEG coating, which can be attributed to the interaction between the hydrophilic group with water phase at stage two, and the interaction between lipophilic group with oil phase at stage three. The tribological interaction between PEG-lactide coating and emulsions is schematically shown in Fig. 13. At stage two, the surface is exposed to a water environment, the lipophilic chains in PEG-lactide collapse, while the hydrophilic chains extend due to the formation of hydrogen bonds with water. At stage three, the surface is covered by the oil component, the hydrophilic chains in PEG-lactide collapse, but the lipophilic chains extend because of the interaction between the lipophilic chain and the oil component.

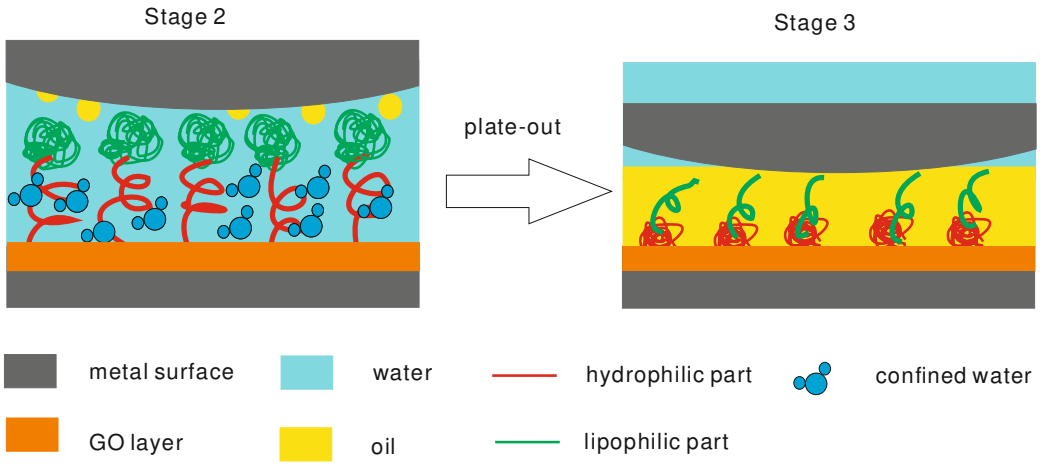

Fig. 13 The tribological interaction between PEG-lactide coating and emulsions

4. Conclusions

1. Three different kinds of surface-active polymers with or without GO were coated on CoCrMo alloy surface, and the samples were characterized by ATR, EDS and XPS.

2. The tribological performance of the surface-active polymer coatings with or without GO was evaluated in different aqueous media. Synergetic effects have been observed between GO and surface-active polymers.

3. The tribological behaviour of PEG-lactide coating in emulsion was better than that of PEG coating, indicating the advantage of using hydrophilic and lipophilic group containing surface-active polymers for emulsion lubrication.

References

[1] Granchi D, Ciapetti G, Stea S, Savarino L, Filippini F, Sudanese A, et al. Cytokine release in mononuclear cells of patients with Co–Cr hip prosthesis. Biomaterials. 1999;20:1079-86.

[2] Mischler S, Muñoz AI. Wear of CoCrMo alloys used in metal-on-metal hip joints: A tribocorrosion appraisal. Wear. 2013;297:1081-94.

[3] Gonzalez-Mora V, Hoffmann M, Stroosnijder R, Gil F. Wear tests in a hip joint simulator of different CoCrMo counterfaces on UHMWPE. Materials Science and Engineering: C. 2009;29:153-8.
[4] Dowson D, Hardaker C, Flett M, Isaac GH. A hip joint simulator study of the performance of metal-on-metal joints: Part II: design. The Journal of Arthroplasty. 2004;19:124-30.
[5] Dowson D. Tribological principles in metal-on-metal hip joint design. Proceedings of the Institution of Mechanical Engineers, Part H: Journal of Engineering in Medicine. 2006;220:161-71.
[6] RGale L. Biotribological assessment for artificial synovial joints: the role of boundary lubrication: School of Engineering Systems, Institute of Health and Biomedical Innovation (IHBI), Queensland University of Technology; 2007.
[7] Van Der Heide E, Zeng X, Masen M. Skin tribology: Science friction? Friction. 2013;1:130-42.
[8] Van Der Heide E, Lossie C, Van Bommel K, Reinders S, Lenting H. Experimental investigation of a polymer coating in sliding contact with skin-equivalent silicone rubber in an aqueous environment. Tribology Transactions. 2010;53:842-7.
[9] Ikeuchi K. Origin and future of hydration lubrication. Proceedings of the Institution of Mechanical Engineers, Part J: Journal of Engineering Tribology. 2007;221:301-5.
[10] Gaisinskaya A, Ma L, Silbert G, Sorkin R, Tairy O, Goldberg R, et al. Hydration lubrication: exploring a new paradigm. Faraday Discussions. 2012;156:217-33.
[11] Leven I, Krepel D, Shemesh O, Hod O. Robust superlubricity in graphene/h-BN heterojunctions. The Journal of Physical Chemistry Letters. 2012;4:115-20.
[12] Bustos-Ramírez K, Martínez-Hernández AL, Martínez-Barrera G, Icaza Md, Castaño VM, Velasco-Santos C. Covalently bonded chitosan on graphene oxide via redox reaction. Materials. 2013;6:911-26.
[13] Blazewicz M. Carbon materials in the treatment of soft and hard tissue injuries. European Cells and Materials. 2001;2:21-9.
[14] Chung C, Kim Y-K, Shin D, Ryoo S-R, Hong BH, Min D-H. Biomedical applications of graphene and graphene oxide. Accounts of Chemical Research. 2013;46:2211-24.
[15] Ou J, Wang J, Liu S, Mu B, Ren J, Wang H, et al. Tribology Study of Reduced Graphene Oxide Sheets on Silicon Substrate Synthesized via Covalent Assembly. Langmuir. 2010;26:15830-6.

[16] Wang Y, Pu J, Xia L, Ding J, Yuan N, Zhu Y, et al. Fabrication and Tribological Study of Graphene Oxide/Multiply-Alkylated Cyclopentanes Multilayer Lubrication Films on Si Substrates. Tribology Letters. 2014;53:207-14.
[17] Lewis AC, Kilburn MR, Papageorgiou I, Allen GC, Case CP. Effect of synovial fluid, phosphate-buffered saline solution, and water on the dissolution and corrosion properties of CoCrMo alloys as used in orthopedic implants. Journal of Biomedical Materials Research Part A. 2005;73A:456-67.
[18] Mishina H, Kojima M. Changes in human serum albumin on arthroplasty frictional surfaces. Wear. 2008;265:655-63.
[19] Santos CB, Haubold L, Holeczek H, Becker M, Metzner M. Wear–Corrosion Resistance of DLC/CoCrMo System for Medical Implants with Different Surface Finishing. Tribology Letters. 2010;37:251-9.
[20] Yan Y, Neville A, Dowson D. Understanding the role of corrosion in the degradation of metal-on-metal implants. Proceedings of the Institution of Mechanical Engineers, Part H: Journal of Engineering in Medicine. 2006;220:173-80.
[21] Yan Y, Neville A, Dowson D. Biotribocorrosion—an appraisal of the time dependence of wear and corrosion interactions: I. The role of corrosion. J Phys D: Appl Phys. 2006;39:3200.
[22] Marcano DC, Kosynkin DV, Berlin JM, Sinitskii A, Sun ZZ, Slesarev A, et al. Improved Synthesis of Graphene Oxide. Acs Nano. 2010;4:4806-14.
[23] Yan J, Bu J, Bai X, Li J, Ren T, Zhao Y. The tribological study of novel phosphorous–nitrogen type phosphoramidate additives in rapeseed oil. Proceedings of the Institution of Mechanical Engineers, Part J: Journal of Engineering Tribology. 2012;226:377-88.
[24] Hvattum E, Yip WL, Grace D, Dyrstad K. Characterization of polysorbate 80 with liquid chromatography mass spectrometry and nuclear magnetic resonance spectroscopy: Specific determination of oxidation products of thermally oxidized polysorbate 80. J Pharm Biomed Anal. 2012;62:7-16.
[25] Oh J, Lee J-H, Koo JC, Choi HR, Lee Y, Kim T, et al. Graphene oxide porous paper from amine-functionalized poly(glycidyl methacrylate)/graphene oxide core-shell microspheres. Journal of Materials Chemistry. 2010;20:9200-4.
[26] Yang T, Liu L-H, Liu J-W, Chen M-L, Wang J-H. Cyanobacterium metallothionein decorated graphene oxide nanosheets for highly selective adsorption of ultra-trace cadmium. Journal of Materials Chemistry. 2012;22:21909-16.

[27] Bywalez R, Karacuban H, Nienhaus H, Schulz C, Wiggers H. Stabilization of mid-sized silicon nanoparticles by functionalization with acrylic acid. Nanoscale Research Letters. 2012;7:76.

[28] Sakthi Kumar D, Fujioka M, Asano K, Shoji A, Jayakrishnan A, Yoshida Y. Surface modification of poly(ethylene terephthalate) by plasma polymerization of poly(ethylene glycol). J Mater Sci: Mater Med. 2007;18:1831-5.

[29] Kim H-M, Kim H-R, Kim B. Soybean Oil-Based Photo-Crosslinked Polymer Networks. J Polym Environ. 2010;18:291-7.

[30] Byler DM, Wilson R, Randall C, Sokoloski T. Second Derivative Infrared Spectroscopy as a Non-Destructive Tool to Assess the Purity and Structural Integrity of Proteins. Pharm Res. 1995;12:446-50.

[31] Carton O, Ben Salem D, Bhatt S, Pulpytel J, Arefi-Khonsari F. Plasma Polymerization of Acrylic Acid by Atmospheric Pressure Nitrogen Plasma Jet for Biomedical Applications. Plasma Processes and Polymers. 2012;9:984-93.

[32] Yang S-Y, Chang K-H, Tien H-W, Lee Y-F, Li S-M, Wang Y-S, et al. Design and tailoring of a hierarchical graphene-carbon nanotube architecture for supercapacitors. Journal of Materials Chemistry. 2011;21:2374-80.

[33] Feng R, Guan G, Zhou W, Li C, Zhang D, Xiao Y. In situ synthesis of poly(ethylene terephthalate)/graphene composites using a catalyst supported on graphite oxide. Journal of Materials Chemistry. 2011;21:3931-9.

[34] Some S, Kim Y, Hwang E, Yoo H, Lee H. Binol salt as a completely removable graphene surfactant. Chemical Communications. 2012;48:7732-4.

[35] Wang D-W, Du A, Taran E, Lu GQ, Gentle IR. A water-dielectric capacitor using hydrated graphene oxide film. Journal of Materials Chemistry. 2012;22:21085-91.

[36] Schlapak R, Caruana D, Armitage D, Howorka S. Semipermeable poly(ethylene glycol) films: the relationship between permeability and molecular structure of polymer chains. Soft Matter. 2009;5:4104-12.

[37] Cai T, Yang WJ, Zhang Z, Zhu X, Neoh K-G, Kang E-T. Preparation of stimuli-responsive hydrogel networks with threaded β-cyclodextrin end-capped chains via combination of controlled radical polymerization and click chemistry. Soft Matter. 2012;8:5612-20.

[38] Giglio E, Cometa S, Cioffi N, Torsi L, Sabbatini L. Analytical investigations of poly(acrylic acid) coatings electrodeposited on titanium-based implants: a versatile approach to biocompatibility enhancement. Anal Bioanal Chem. 2007;389:2055-63.

[39] Zhao Y, Zhou Y, Xiong B, Wang J, Chen X, O'Hayre R, et al. Facile single-step preparation of Pt/N-graphene catalysts with improved methanol electrooxidation activity. J Solid State Electrochem. 2013;17:1089-98.
[40] Zhang XG, Teng DY, Wu ZM, Wang X, Wang Z, Yu DM, et al. PEG-grafted chitosan nanoparticles as an injectable carrier for sustained protein release. J Mater Sci: Mater Med. 2008;19:3525-33.
[41] Sheth SR, Efremova N, Leckband DE. Interactions of Poly(ethylene oxide) Brushes with Chemically Selective Surfaces. The Journal of Physical Chemistry B. 2000;104:7652-62.
[42] Efremova NV, Huang Y, Peppas NA, Leckband DE. Direct Measurement of Interactions between Tethered Poly(ethylene glycol) Chains and Adsorbed Mucin Layers. Langmuir. 2002;18:836-45.
[43] Chen M, Briscoe WH, Armes SP, Klein J. Lubrication at physiological pressures by polyzwitterionic brushes. Science. 2009;323:1698-701.
[44] Tobias DJ, Hemminger JC. Chemistry. Getting specific about specific ion effects. Science (New York, NY). 2008;319:1197.
[45] Tielrooij K, Garcia-Araez N, Bonn M, Bakker H. Cooperativity in ion hydration. Science. 2010;328:1006-9.
[46] Brittain WJ, Minko S. A structural definition of polymer brushes. Journal of Polymer Science Part A: Polymer Chemistry. 2007;45:3505-12.
[47] Fan J, Myant C, Underwood R, Cann P. Synovial fluid lubrication of artificial joints: protein film formation and composition. Faraday Discuss. 2012;156:69-85.
[48] Yan J, Zeng X, Ren T, Heide Evd. Boundary lubrication of stainless steel and CoCrMo alloy based on phosphorus and boron compounds in oil-in-water emulsion. Applied Surface Science, 2014;315:415-24.
[49] Steven RS. Lubrication Mechanisms for Oil-In-Water Emulsions. LubEn. 1995;52:168-75.

Paper D

The tribological performance and tribochemical analysis of novel borate esters as lubricant additives in rapeseed oil

Jincan Yan, Xiangqiong Zeng , Emile van der Heide, Tianhui Ren. Tribological International, 2014, 71, 149–157

The tribological performance and tribochemical analysis of novel borate esters as lubricant additives in rapeseed oil

Jincan Yan, Xiangqiong Zeng , Emile van der Heide, Tianhui Ren

Abstract

Two novel borate esters, tris (4-dodecylphenyl) borate and 2-(2-(4-dodecylphenoxy)-1, 3, 6, 2-dioxazaborocan-6-yl) ethanol were synthesized and applied as anti-wear and extreme pressure additives in rapeseed oil. The borate esters possess high anti-wear and extreme pressure properties. XANES and XPS were used to analyse the composition and structure of boundary films at the worn surfaces. It is shown that the additives form a protective film at the rubbed surfaces based on B_2O_3 and/or BN. B-N synergetic effect was found in the results which suggests that tribofilms composed of BN are to be preferred over tribofilms that consists of B_2O_3.

Keywords borate ester, tribological performance, tribochemistry, B-N synergetic effect

1. Introduction

Anti-wear (AW) and extreme pressure (EP) additives are added to gear oils and hydraulic oils to decrease wear during use and to ensure that seizure is prevented over the full range of operational conditions [1, 2]. Zinc dialkyldithiophosphates (ZDDPs or ZnDTPs) are well known and widely used as AW additives in engine lubricants and hydraulic oils [3–6]. However, the concern for zinc as an environmental contaminant and for phosphorus as poisons for automotive catalysts as well as the bad smell from sulfur leads to the exploration of new, effective and “green” additives for both automotive and industrial applications [7, 8].

In recent years, boron-containing lubricant additives have attracted more and more attention. Borate salts were introduced to the lubrication system, but their application is limited because they cannot easily be dispersed in oil [9–11]. Organic borate esters are recognized as “green” additives and have received extensive attention because of the expected AW and EP performance, low toxicity,

and pleasant odor [12]. However, borate esters are susceptible to hydrolysis resulting in insolubility or precipitation in oil [13–17]. The hydrolysis process is common because the electron-deficient boron element can be easily combined to water in the air. Some of the studies were focused on the introduction of nitrogen to the additive molecules, partly because of the enhanced AW performance [18] and partly because of the lone pair electrons in nitrogen which can stabilize the electron-deficient boron element [19, 20].

As for the base stock, mineral oil is widely used in lubricants, yet current and future regulations with respect to limiting emissions to the environment and controlling contamination and pollution increases the need for biodegradable lubricants. Rapeseed oils can meet the requirement as potential source of environmentally friendly lubricants, due to a combination of biodegradability and excellent lubrication performance [21].

As the tribochemical reactions during the friction process cannot be detected in situ yet, for a steel-steel combination, surface analysis after rubbing is typically selected and regarded as an effective method to explore the mechanism [22–24]. X-ray absorption near edge structure spectroscopy (XANES) is recognized as a non-destructive method for the surface and can be used to investigate the chemical nature of boundary films generated in tribological contacts [25, 26]. X-Ray photoelectron spectroscopy (XPS) and scanning electron microscope (SEM) are used to analyze the character of the worn surface [27]. Studies on XANES analysis of boundary films generated in tribo-contacts lubricated with borate esters indicate the feasibility of this method to reveal the presence of B_2O_3, BPO_4 and BN [28–30].

In this work, two novel borate esters were designed, prepared and used as antiwear agents in rapeseed oil. The tribological performance of the additives was evaluated using a four-ball machine. XANES, XPS and SEM were used to analyse the composition and structure of boundary films at the worn surfaces.

2. Experimental details

2.1 Preparation of the additives

The chemicals and solvents were purchased from commercial suppliers from Shanghai Chemical Company, Shanghai, China and were used without

purification. A commercial rapeseed oil (referred to rapeseed oil), provided by Grease Factory of China, Lanzhou, China was used as the lubricating oil without any further treatment.

For the design of the additives, aromatic groups and nitrogen were introduced to the borate esters, see Fig. 1, with the aim to improve the oil-solubility and hydrolytic stability of lubricants based on rapeseed oil, while maintaining the tribological performance at high contact pressures. The oxygen, nitrogen as well as the aromatic groups can be helpful for stabilizing the molecules and the long chain which is symbolised by R groups in the image was designed to increase the oil-solubility, and then form stable film on the metal surface.

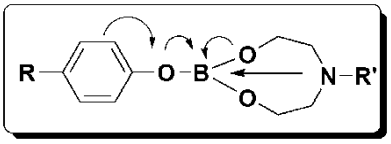

Fig. 1. Design of novel borate esters

Specifically in this work, tris (4-dodecylphenyl) borate (coded TDB) and 2-(2-(4-dodecylphenoxy)-1, 3, 6, 2-dioxazaborocan-6-yl) ethanol (coded DDB) were synthesized according to [18]. The synthetic route as well as the prepared borate esters is depicted in Fig. 2 and the procedure is described as follow. In a 500 mL of round bottomed flask, 26.3 g (0.1 mol) of octadecan-1-amine and 2.2 g (0.035 mol) of boric acid were added to some solvent and some catalyst was added to the above mixture with the temperature of 110^{o}C. As the reaction proceeded, more and more water were generated and removed. Then the above solution were reflux for 2 hrs till the reaction terminated. The solution was filtered, evaporated and treated with routine protocol and at last produced 25.3 g (yield 95.3%) of TDB. DDB can be prepared by the reaction of TDB and 2,2'-(tridecylazanediyl)diethanol with similar procedure, and 92.5% of DDB yielded. All of the compounds were characterized by Infra-Red spectroscopy, NMR and elemental analysis. The results of the elemental analysis are shown in Table 1, which are in good agreement with the calculated data and within the limits and experimental error.

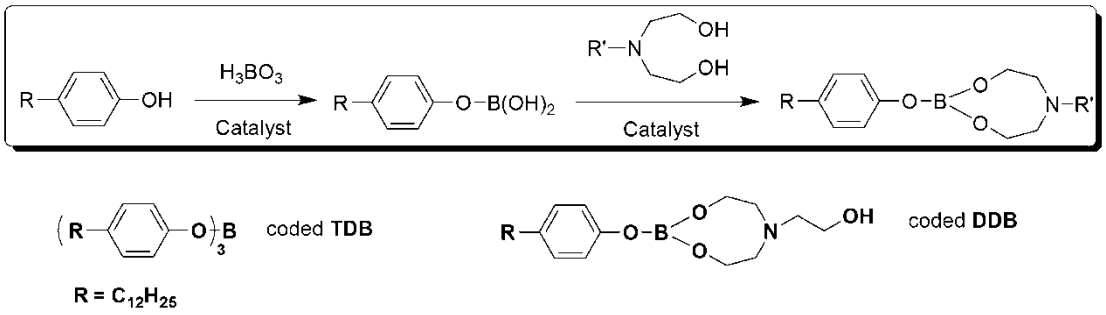

Fig. 2. The preparation, structure and code of novel borate esters

Table 1

The elemental analysis of the synthesized compounds

Items	C (wt. %)	H (wt. %)	B (wt. %)	N (wt. %)
TDB	81.96 (81.57) [a]	11.88 (11.03) [a]	1.25 (1.36) [a]	-
DDB	69.25 (68.73) [a]	10.20 (10.09) [a]	1.62 (2.58) [a]	2.05 (3.34) [a]

[a] Calculated value (balanced by oxygen)

2.2 Evaluation of oil-solubility and hydrolytic stability

The oil solubility and hydrolytic stability of the borate esters were evaluated by the standard method presented in [18] and was tested as follows. Oil-solubility: The additives were mixed with rapeseed oil at a fixed concentration and the solution was stirred at 50 ˚C until the additives were completely dissolved. Then the solution was sealed and allowed to stand for several days. If there is not any solid precipitating in the solution, it is regarded as soluble in base stock. Hydrolytic stability (accelerated hydrolysis method by wet heating treatment): 150 g oil sample (0.5 wt. % additive in base stock) was added into a 200 ml beaker and then placed in a hot and humid oven (temperature at 50±2 ˚C, relative humidity more than 95%). The sample was monitored every hour; the time was recorded. If precipitation was observed in the sample or the sample was no longer transparent, it means that the additives have been hydrolyzed.

2.3 Tribological test

The friction-reducing and anti-wear capacities of the additives were evaluated on a MRS-1J four ball machine. An optical microscope was used to measure the wear scar diameters (WSD) and the friction coefficients were automatically calculated

from the friction signal and recorded. Chinese national standard GB3142-82 similar to ASTM D-2783 is adopted for the tests. As such, a velocity of 1450 rpm was applied for 30 min at room temperature. The balls used for the experiments have a diameter of 12.7 mm which are made of AISI 52100 bearing steel. The balls are hardened to 59–61 HRC.

2.4 The analysis of the worn surfaces

The samples used for XANES and XPS analysis were washed ultrasonically with petroleum ether and dried before the detection. XANES analysis was performed at the Beijing Synchrotron Radiation Facility (BSRF), situated at the 2.2G eV storage ring, Beijing Electron Positron Collider (BEPC), Beijing, China. Boron K-edge spectra were collected separately on the double-crystal monochromator (DCM) covering an energy of 185–200 eV. The photo-adsorption spectra were collected with total electron yield (TEY) modes of detection, to provide chemical information on the bulk of the reaction film. XPS analysis was conducted with a PHI-5702 multifunctional X-ray electron spectrometer at the Lanzhou Institute of Chemical Physics, Lanzhou, China. The Mg Kα radiation was used as the excitation source with pass energy of 29.4 eV with a resolution of ±0.3 eV. The binding energy of C_{1s} (284.6 eV) was used as the reference. The morphology of the wear scar were characterized by the VK 9700 Keyence laser scanning microscope.

3. Experimental results and discussions

3.1 Oil-solubility and hydrolytic stability

The results of oil-solubility and hydrolytic stability of the lubricants (0.5 wt. % additives in rapeseed oil) and the detailed data are listed in Table 2. It can be seen from the results that the synthetic additives can be dissolved very well in rapeseed oil. The oil-solubilities of the synthetic additives are much better than that of the commercially available trimethyl borate (coded TB). Only 0.5 wt. % TB can be dissolved in rapeseed oil, while 6.0 wt. % DDB can be dissolved in rapeseed oil, and for TDB, even 8.0 wt. % of it can be dissolved. As we know, there are polar groups like carboxyl groups in rapeseed oil [31]. Meanwhile, there are also polar groups like aromatic and hydroxyl groups in TDB and DDB, respectively. According to similarity principle, the similar substance is more

likely to be dissolved by each other. Therefore, since TDB and DDB may both have similar polarity as the fatty acids in rapeseed oil, they can be dissolved well in rapeseed oil leading to the high oil-solubility. And the fact that the solubility of TDB is better than that of DDB suggests that the polarity of TDB is more similar to the fatty acids of the rapeseed oil than that of DDB.

For the hydrolytic stability, when the accelerated hydrolysis experiment was performed, the TB solution became turbid within half an hour. While TDB and DDB both show much better performance compared with TB, especially for TDB. The hydrolysis of borate esters is mainly due to the existence of unoccupied p-orbit in electron-deficient boron which tends to combine water. Oxygen-containing, nitrogen-containing groups and the aromatic groups are electron-rich because of the lone pair electrons in oxygen and nitrogen and the π-bond in the aromatic ring. Therefore, with the introduction of these electron-rich groups to the borate esters, the electron-deficient B element in the molecules can be stabilized. Generally, the electron-donating performance of π-bond in the aromatic ring is stronger than the lone pair electrons in oxygen-containing and nitrogen-containing groups. There are more aromatic rings in the molecule of TDB than that of DDB. Therefore, the hydrolytic stability of TDB is better than that of DDB.

Table 2

The oil solubility and hydrolytic stability of the additives

Additives	Oil-solubility (wt. %)	Hydrolytic stability (hr)
TB	0.5	0.5
TDB	8.0	83
DDB	6.0	67

3.2 The EP properties

The EP properties of the additives in the rapeseed oil were evaluated by the maximum non-seizure load (P_B value). The P_B values of the base oil (rapeseed oil), 2.0 wt. % TDB and 2.0 wt. % DDB in base stock are shown in Fig. 3. The results show that the P_B value of TDB is slightly higher than that of the base stock, indicating that TDB cannot serve as EP agent. Meanwhile, the P_B value of DDB is higher than that of the base oil, showing that the additive has high EP

performance. The results suggest that the additive with B and N elements in molecular structure possesses better load-carrying capacity than the corresponding additive that only contains B. TDB only contains active B element, therefore, the tribofilm could only be composed of B-containing compounds. While the tribofilms formed by DDB could consist of both B-containing and N-containing compounds, which performs much better than that of TDB, indicating the synergetic effect of B and N elements in borate additives [19]. In addition, it is worth mentioning that the duration of the EP measurement is only ten seconds, the faster the adsorption film formed, the faster the tribofilm will be formed, and then the better EP property can be generated. It can be seen from the molecular structures and solubility data of TDB and DDB that the polarity of DDB is higher than that of TDB, so DDB can be adsorbed faster and more easily onto the polar metal surface due to the polar hydroxyl groups. Therefore, DDB can form stronger adsorption film, leading to the higher EP performance of DDB than that of TDB.

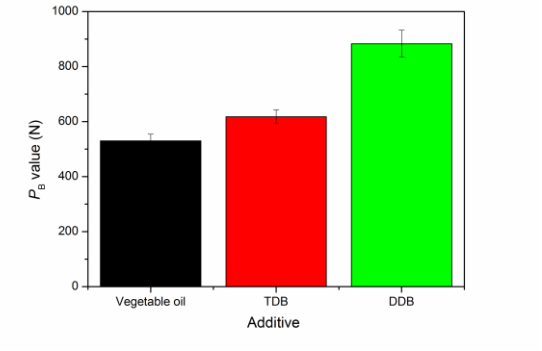

Fig. 3. P_B values of the additives (2.0 wt. % additive in rapeseed oil, four-ball machine, rotation velocity of 1760 rpm for 10 s)

3.3 AW properties of the borate additives

The variation of wear scar diameter (WSD) with the concentration of the additives in rapeseed oil at 294N is shown in Fig. 4. It can be seen that DDB can improve the anti-wear property of base oil and the performance of DDB is better at the same concentration than that of TDB. The synergetic effect of B and N elements in borate additives can also be found in AW properties. Associating with the element analysis, there are 1.62 wt. % of B and 2.05 wt. % of N in DDB, while the content of B in TDB is only 1.25 wt. %. Therefore, the good performance of

DDB may be ascribed to the high content of B and N elements, which indicates that the tribological behavior of the additives is highly dependent on the adsorbed amount of active B and N during the rubbing process. When 2.0 wt. % DDB was added, the WSD reduced by 42.5%, while for TDB, the highest reduction is 16.5%. The difference is also supposed to be related to their active element content and molecular structure which affect the adsorption ability and the reaction activity. Moreover, for DDB it can be seen that when the concentration of DDB is lower than 2.0 wt. %, the WSD decreases with the increasing of additive concentration. While when the additive concentration is higher than 2.0 wt. %, the WSD increases with increasing concentration of DDB. And for TDB, the optimum concentration is 0.5 wt. %. This indicates that the AW ability of the synthetic additives is dependent on their concentration in the base stock, and there is an optimum concentration. On the one hand, at the first duration of the test, when the additive concentration in the base stock is below the optimum concentration, more and more polar additives adsorbed gradually onto the rubbing metallic surfaces to form the films. As we know, the unsaturated fatty acids in rapeseed oil may have similar polarity as the synthesized additives, and they can also be adsorbed onto the metal surface. Therefore, when the concentration is more than the optimum concentration, the adsorption of the additives tend to be saturated, and the fatty acids in rapeseed oil can also be adsorbed. And there is equilibrium of the competitive adsorption between the additive and the fatty acids. The equilibrium resulted in the flat curve of TDB after the concentration of 0.5 wt. %. For DDB, when the concentration is higher than 2.0 wt. %, the adsorption of DDB is saturated, the rapeseed oil will competitively adsorb onto the metallic surface, resulting in a boundary lubricating film of relatively poor AW ability. On the other hand, the difference may also suggest that different films are formed by the active elements in the additive molecules which can be reflected from the XPS results later. From the figure, the optimum concentration of TDB is much lower than DDB, this may be due to the polarity of TDB is lower than DDB. When TDB was added in the rapeseed oil, the saturated adsorption concentration is lower, therefore, less molecules of TDB can be adsorbed onto the polar metal surface. On the contrary, more DDB can be adsorbed onto the surface of metal, and then the higher optimum concentration of DDB than TDB can be explained.

In addition, the curves in Fig. 5 depict the AW properties of 2.0 wt. % additives in

rapeseed oil at different applied loads. The increasing of normal load results in the increase of WSD. This may be because that with the increasing of normal load, the film thickness formed between the contact area decreases, resulting in the increasing of direct contact of asperities, and then WSD increases [32]. Compared with the WSD of rapeseed oil, the WSD of DDB reduced significantly, which demonstrates that DDB can improve the AW performance of base fluid for the 98–490 N load range. Moreover, at different applied loads, DDB shows better AW property than that of TDB. On the one hand, the polarity of DDB is higher than that of TDB, so the stronger adsorption is produced by DDB during the rubbing process. On the other hand, DDB and TDB can form different tribofilm because of different content of B and N. And the performance of DDB is much better than that of TDB, indicating the synergetic effect of B and N. This will be further discussed during the analysis of the tribofilms. In addition, the performance of TDB is almost the same as that of the base stock at the load range 98N, which means the boundary film formed by TDB is similar to that of the base oil. This may be related to the similarity in polarity of TDB to that of rapeseed oil, as described before. When TDB was used, seizure happened at the load 490 N and for DDB the WSD increases rapidly when the load increases after 294N. Therefore, these additives are more suitable for lower loads. The wear increases with the increase of load maybe because of the increased surface roughing and wear debris.

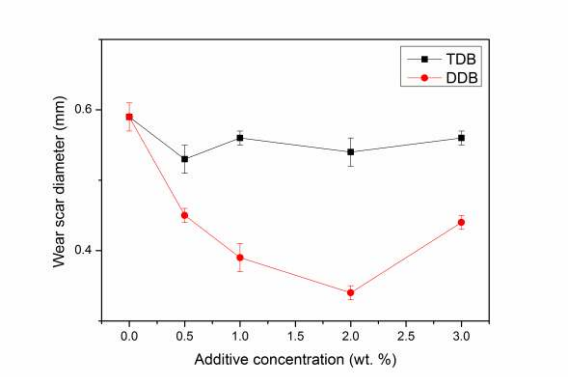

Fig. 4. Effect of the concentration of additives on wear scar diameter (four-ball machine, 294 N, rotation velocity of 1450 rpm for 30 min)

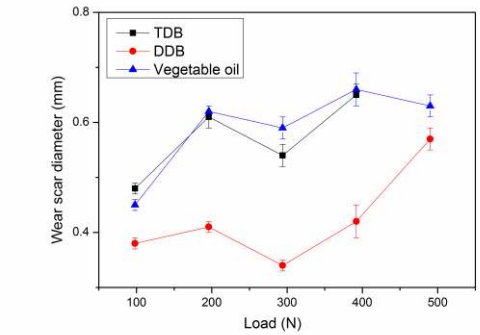

Fig. 5. Effect of the applied load on wear scar diameter (four-ball machine, additive concentration of 2.0 wt. %, velocity of 1450 rpm for 30 min)

3.4 Friction-reducing properties of the borate additives

The coefficient of friction (COF) of synthesized compounds with different concentrations under the load of 294 N is shown in Fig. 6. For the performance of TDB, as can be seen from the curve, the COF decreases when the concentration increases at the concentration range from 0.5 wt. % to 1.0 wt. %. The decreases in COF can be attributed to the formation of adsorption film and/or reaction film by the additive on the rubbing metal surface. When the additive is added to the base oil, the molecules interact with the freshly exposed worn surface to form a protective adsorption film and/or reaction film. The shearing strength of the films is less than that of the metal, and accordingly the COF decreases [33]. But when the addition continued, the curve became flat, which means that the adsorption tend to be an equilibrium, or in other words, when the addition is more than 1.0 wt. %, an excess addition of TDB cannot form the proper film on the metal surface any more. From the curve of DDB, we can see that the COF also decreases with the increasing of DDB from 0.5 wt. % to 2.0 wt. %, but when the concentration is higher than 2.0 wt. %, the COF starts increasing. The optimum concentration may be also due to the proper adsorbed film formed onto the surface and then the formation of proper tribofilm during the rubbing process. At the same time, the COF of DDB is lower than that of TDB, revealing that different film are formed by the active elements in the additive molecules.

The COF of 2.0 wt. % synthesized compounds in rapeseed oil with different applied load is shown in Fig. 7. For comparison, the performance of the base oil was also evaluated at the same condition. It can be seen that the base stock

doped with DDB shows good and stable friction-reducing properties in applied load 98–490 N, but for TDB, seizure happened when the load is increased to 490 N. Generally, during the friction process, the higher load would result in larger friction heat, which may be responsible for the formation of a chemical adsorption and reaction film and lead to lower shear strength between friction pairs.

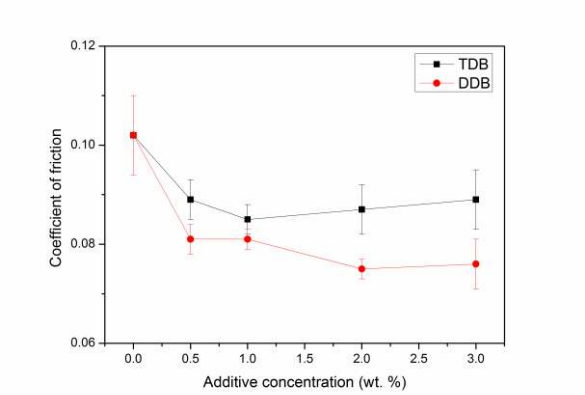

Fig. 6. Effect of the concentration of additives on coefficient of friction (four-ball machine, 294 N, rotation velocity of 1450 rpm for 30 min)

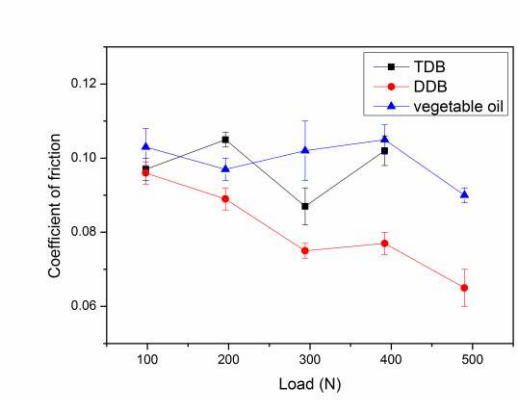

Fig. 7. Effect of the applied load on coefficient of friction (four-ball machine, additive concentration of 2.0 wt. %, rotation velocity of 1450 rpm for 30 min)

3.4 Surface analysis

3.4.1 XPS analysis of the worn surface

In this work, XPS spectra of the elements in the worn surface were recorded to determine the chemical state of the elements and examine possible film forming mechanisms based on the known composition of the additives in base oil. The

binding energy of some standard compounds containing Fe, O, B and N was listed in Table 3 for comparison, which could be obtained in NIST XPS Database [34].

Table 3

Binding energy of some standard compounds containing Fe, O, B, and N

	Compounds	**Binding Energy (eV)**		**Compounds**	**Binding Energy (eV)**
Oxide of ferrum	Fe_2O_3	Fe_{2p}(713.1); O_{1s}(529.8)	Boride	Fe_xB_y	Fe_{2p}(707.0); B_{1s}(188.0)
	Fe_3O_4	Fe_{2p}(709.4); O_{1s}(529.7)		B_2O_3	B_{1s}(192.0); O_{1s}(532.6)
	FeO	Fe_{2p}(709.6); O_{1s}(530.1)		BN	B_{1s}(190.8); N_{1s}(397.9)

The XPS spectra of 2.0 wt. % TDB in rapeseed oil are shown in Fig. 8. The curve fitting is performed with the software XPS PEAK and origin 7.5 respectively. It can be seen that for the binding energies of Fe_{2p} and O_{1s}, the XPS signals are intense, but the signals are very weak for the binding energies of B_{1s}. This is mainly because the contents of Fe and O are much higher than those of B. The binding energies of Fe_{2p} are located at 709.5eV, 710.6eV, and 713.5eV respectively. For the four values of binding energy, iron oxides are identified after contrasted with the standard spectra of the elements. As for oxygen, the binding energies of O_{1s} are founded to be at 529.8eV, 531.1eV, and 532.4eV, which can be attributed to iron oxides and B_2O_3. No peak of Fe_xB_y or B_2O_3 was found from the binding energy of B_{1s}.

The detailed XPS spectra information of the DDB is shown in Fig. 9. Similar to that of TDB, the binding energies of Fe_{2p} of DDB are located at 707.3eV, 709.0eV, 710.8eV, and 713.8eV which suggest the existence of Fe_xB_y and other iron oxides. As for oxygen, the binding energies are also the same as those of TDB. The binding energies of B_{1s} located at 190.9eV and N_{1s} at 398.1eV are corresponded to BN, which suggests that the borate ester was degraded and reacted with nitrogen on the rubbing pairs during the friction process. No peak of Fe_xB_y or B_2O_3, but they can be found in the binding energy of Fe_{2p} and O_{1s}.

From the XPS spectrum of TDB and DDB, it can be concluded that the difference

of the reaction films mainly lies in the formation of BN. Associating with the tribological test results, the better performance of DDB than that of TDB reveals that BN plays a crucial role in reducing wear and friction, suggesting the importance of B-N synergetic effect.

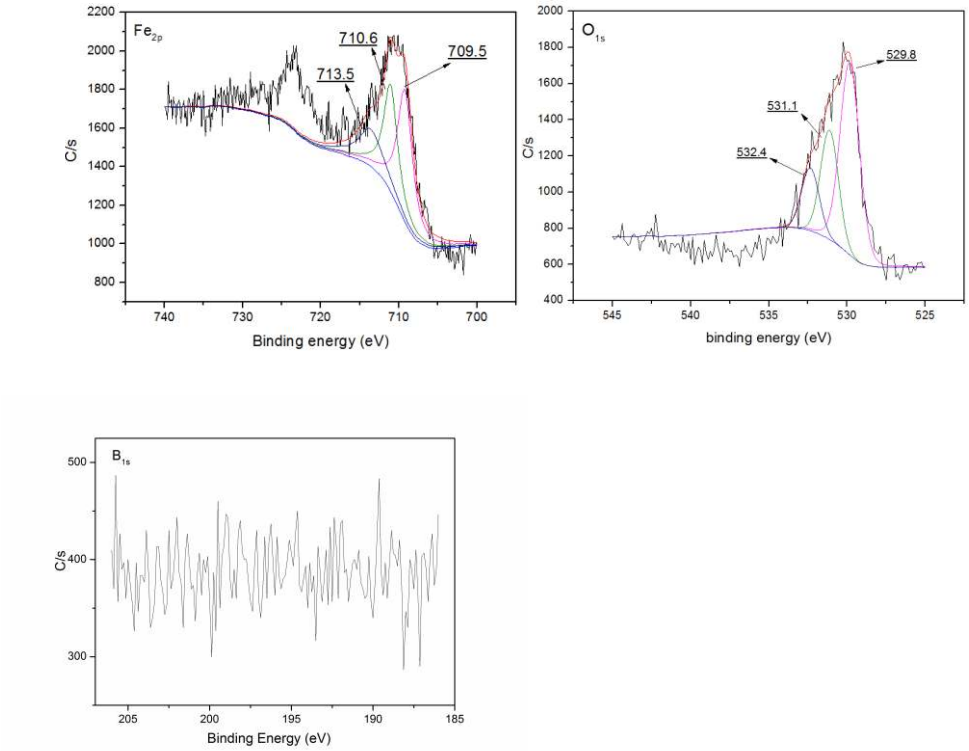

Fig. 8. XPS spectra of 2.0 wt. % TDB in rapeseed oil (294N for 30min)

3.4.2 XANES analysis of the worn surface

More investigation on the formation of BN was conducted by using XANES since boron K-edge and nitrogen K-edge XANES spectra can give detailed information about the chemical state of B and N in the film or on the surface. The B K-edge XANES (TEY) of tribofilms generated from different additives in rapeseed oil are shown in Fig. 10. The peak positions of each spectrum and model compounds are listed in Table 4 [28-30]. Peak b is the characteristic position of B_2O_3, and peaks a, c, d and e correspond to BN. Therefore, it is further confirmed that the tribofilm generated by 2.0 wt. % TDB mainly contains B_2O_3, and for DDB, the films are mainly composed of BN. The formation of B_2O_3 by TDB prevents the direct contact between the metal surfaces, and the melting point and shear strength of B_2O_3 are lower than that of metal surface, resulting in the friction reducing and wear resistance properties of TDB under relatively low normal load. When under

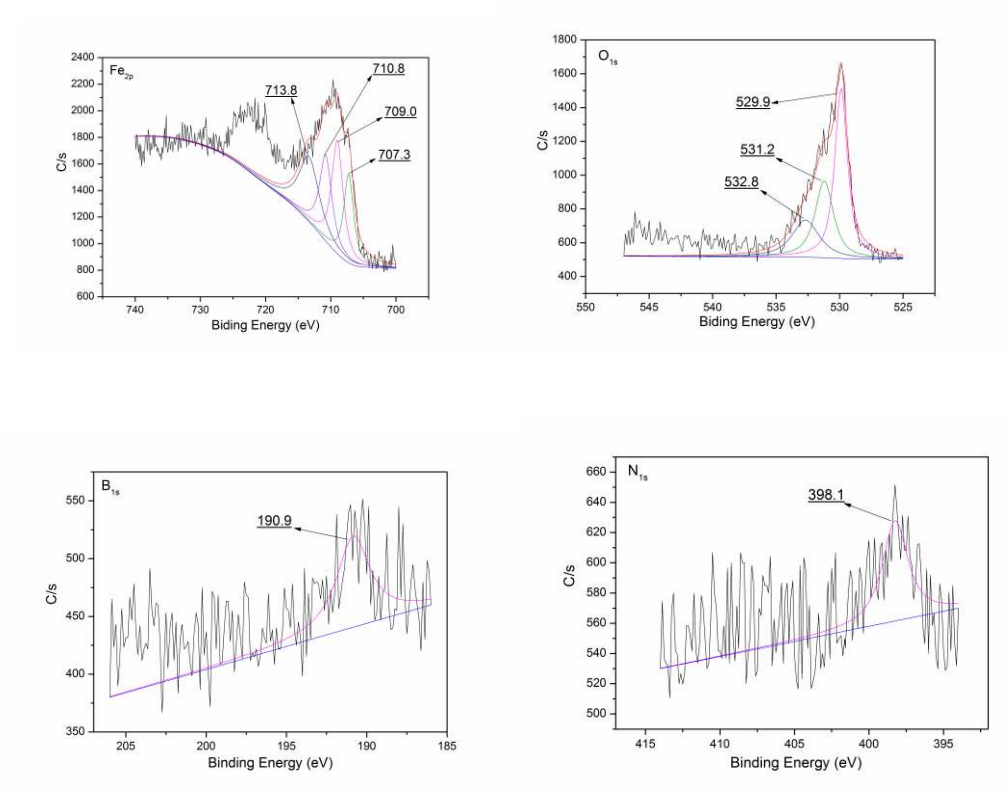

Fig. 9. XPS spectra of 2.0 wt. % DDB in rapeseed oil (294N for 30min)

high normal load, the B_2O_3 can be easily removed from the surface due to weak adhesion to the metal surface, and the reactivity of TDB is not high enough to form new B_2O_3 film immediately, thus the tribological performance becomes worse. For DDB, it can be adsorbed onto the metal surface and then the absorbed B and N can react with the metal surface under high load and triboheat to generate tribofilms. Generally, when BN is formed, the initial form is amorphous BN powder, which can be converted to hexagonal BN (h-BN) by heating with nitrogen-containing compounds. Cubic BN (c-BN) is made by annealing h-BN powder at even higher temperatures under high pressure. As indicated in [30], the h-BN spectrum is with a sharp peak at 192.4 eV and two weak and broad peaks at 198.7 eV and 204.6 eV. Spectrum of c-BN gives a broad intense peak at 198.4eV, and two weak peaks at 195.0 eV (sharp) and 205.1 eV (broad). Compared with the spectra of DDB, it can be concluded that the tribofilm is mainly formed by h-BN and there can be little c-BN due to the mismatch in peak intensities. This suggests that under the test condition, the energy generated during the rubbing process is enough to form h-BN, while not high enough to form c-BN due to the protection of the surface from the tribofilms, which further

indicates the high efficiency of the tribofilm formed. Associating these results with tribological data, the conclusion can be drawn that the tribofilms which contains BN will get better AW performance than B_2O_3. This may be due to the reason that BN has a layered structure similar to that of graphite, which can provide a solid interfacial film of low shear strength [35], leading to the good lubricating performance.

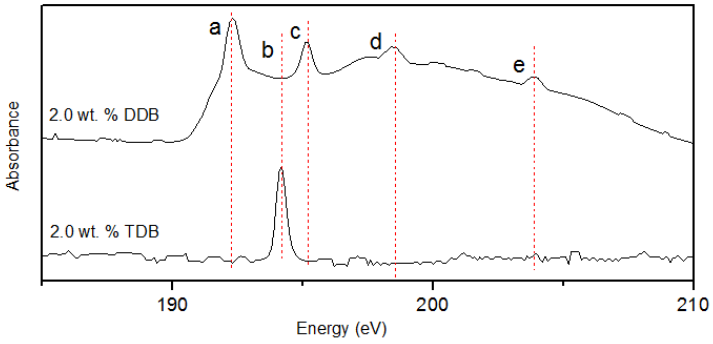

Fig. 10. B K-edge XANES spectra of the tribofilms

Table 4

Peak positions of the B K-edge (TEY) spectra of tribofilms generated from additives

	B K-edge (eV)				
peak	a	b	c	d	e
Sample					
2.0 wt. % TDB		194.1			
2.0 wt. % DDB	192.3		195.1	198.3	204.6
Compounds					
h-BN	192.4			198.7	204.6
c-BN			195.0	198.4	205.1
B_2O_3		194.0			

The peak positions of the N K-edge XANES (TEY) spectra of tribofilms generated from DDB in rapeseed oil are listed in Table 5. By comparison with the model compounds, the peaks at around 402.0 eV and 407.0 eV can also be attributed to h-BN which is in good agreement with the results of B spectra.

Table 5

Peak positions of the N K-edge (TEY) spectra of tribofilms generated from additives

	N K-edge (eV)	
Sample		
2.0 wt. % DDB	402.4	407.1
Compounds		
h-BN	402.2	407.3

3.4.3 Analysis of the worn surface

Fig. 11 shows the 3D morphologies collected by confocal microscopy of the worn surfaces. It can be seen from the images (×100) that the worn surface of 2.0 wt. % TDB (b) and 2.0 wt. % DDB (c) in rapeseed oil are much smoother than that of rapeseed oil (a). The worn surface of 2.0 wt. % DDB (c) is uniform and smooth and indicates the existence of good surface protective film, which is in agreement with the good tribological behavior of DDB. Also the cracks and furrows on the surface of DDB are smoother than that of the rapeseed oil and 2.0 wt. % TDB (b) in rapeseed oil. This suggests that the boundary lubricating films of the DDB could effectively prevent the rubbing surface from direct contact, while the films of rapeseed oil and TDB might have poor strength and can be easily destroyed by pressure and mechanical force.

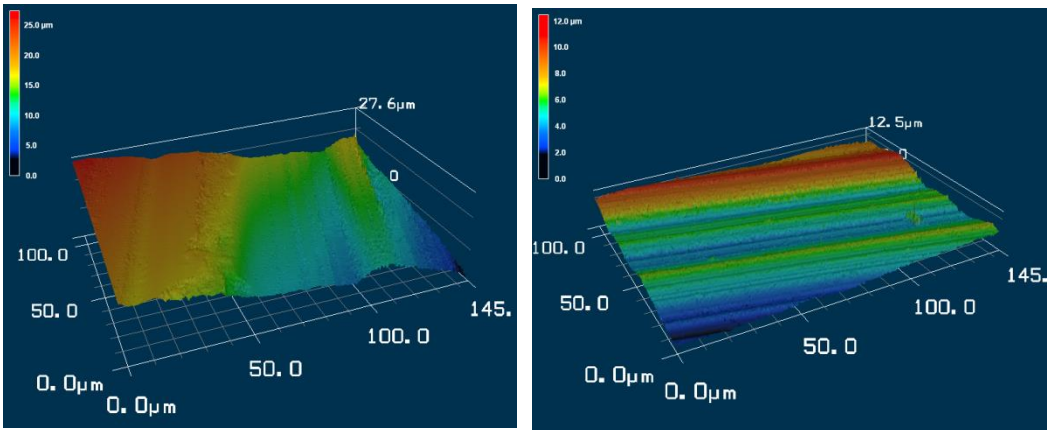

a) Rapeseed oil

b) 2.0 wt. % TDB in rapeseed oil

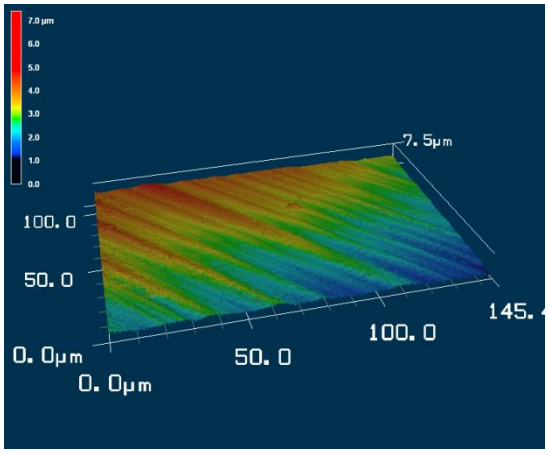

c) 2.0 wt. % DDB in rapeseed oil

Fig. 11. The 3D morphology (×100) of the worn surfaces (four-ball tester, load 294 N, velocity 1450rpm, duration 30 min)

4. Conclusions

1. Two novel borate esters with aromatic group and nitrogen were readily synthesized and served as additives in rapeseed oil. The additives show good oil solubility and hydrolytic stability. The fact that the solubility of TDB is better than that of DDB suggests that the polarity of TDB is more similar to that of the rapeseed oil than that of DDB. The hydrolytic stability of TDB is better than that of DDB mainly because of that the electron-donating performance of π-bond in the aromatic ring which can be found more in TDB is stronger than the lone pair electrons in oxygen-containing and nitrogen-containing groups.

2. Both additives can improve the EP, AW and friction-reducing properties of the

rapeseed oil, and the performance of DDB is better than that of TDB. Firstly, from the molecular structures and solubility data, it is found that the polarity of DDB is higher than that of TDB, so DDB can form stronger adsorption film than that of TDB. Secondly, the reaction activity of DDB is higher than that of TDB due to both the high polarity and high content of active elements, which can establish a better balance between the build-up and removal of tribofilms. Thirdly, DDB contains both B and N elements, while TDB only contains B. Therefore, the tribofilms formed are difference. The better tribological behavior of DDB than that of TDB indicates the synergetic effect of B and N.

3. The XPS analysis of TDB and DDB suggests that different reaction films were generated on the rubbing surface, and the better performance of DDB mainly lies in the formation of BN. Associating with the tribological test results, it reveals that BN plays a crucial role in reducing wear and friction, suggesting the importance of B-N synergetic effect. XANES analyses also indicate that the tribofilms which contains BN formed by DDB are more helpful for AW properties than B_2O_3 formed by TDB. This may be due to the reason that BN has a layered structure similar to that of graphite, which can provide a solid interfacial film of low shear strength, leading to the good lubricating performance.

Acknowledgments

The authors are grateful to the National Natural Science Foundation of China (Grant No. 21272157) and Marie Curie CIG (grant no. PCIG10-GA-2011-303922) for the financial support. We gratefully thank Dr. Jigang Zhou in Canadian Light Source Inc, Saskatoon, SK, Canada for the XANES analysis.

References

[1] Bovington CH. Friction, wear and the role of additives in controlling them. In: Roy M, Mortier RM, Fox MF, Orszulik ST, editors. Chemistry and technology of lubricants, Heidelberg: Springer; 2010, p. 77–105.

[2] Farng LO. Ashless antiwear and extreme-pressure additives. In: Rudnick LR, editors. Chemistry and Applications, Boca Raton: CRC; 2010, p. 214–36.

[3] Barnes AM, Bartle KD, Thibon VRA. A review of zinc dialkyldithiophosphates (ZDDPS): characterisation and role in the lubricating oil. Tribol Int 2001;34(6):389–95.

[4] Sheasby JS, Jennings MC, Cassells KD. The effect of sample spin on boundary lubrication by several oil blends based upon zinc dialkyldithiophosphates. Wear 1999;231(2):256–64

[5] Spikes H. The history and mechanisms of ZDDP. Tribol Lett 2004;17(3):469–89.

[6] Nicholls MA, Do T, Norton PR, Kasrai M, Bancroft GM. Review of the lubrication of metallic surfaces by zinc dialkyl-dithiophosphates. Tribol Int 2005;38(1):15–39.

[7] Spikes H. Low- and zero-sulphated ash, phosphorus and sulphur anti-wear additives for engine oils. Lubri Sci 2008;20(2):103–36.

[8] Betton CI. Lubricants and their environmental impact. In: Roy M, Mortier RM, Fox MF, Orszulik ST, editors. Chemistry and technology of lubricants, Heidelberg: Springer; 2010, p. 435–57.

[9] Bakunin VN, Suslov AY, Kuzmina GN, Parenago OP. Synthesis and application of inorganic nanoparticles as lubricant components - a review. J Nano Res 2004;6(2-3):273–84.

[10] Dong JX, Hu ZS. A study of the anti-wear and friction-reducing properties of the lubricant additive, nanometer zinc borate. Tribol Int 1998;31(5):219–23.

[11] Hao LF, Li JS, Xu XH, Ren TH. Preparation, characterization, and tribological evaluation of triethanolamine monooleate-modified lanthanum borate nanoparticles. Proc IMechE Part J: J Engineering Tribology 2010;224(J11):1163–71.

[12] Shah FU, Glavatskih S, Antzutkin ON. Boron in Tribology: From Borates to Ionic Liquids. Tribol Lett 2013;51 (3):281–301.

[13] Wang YG, Li JS, Ren, TH. Tribological study of a novel borate ester containing dialkylthiophosphate group as multifunctional additive. Ind Lubr Tribol 2009;61(1):33–9.

[14] Wang YG, Li JS, Ren TH. Using a novel disulphide compound containing boron as a potential substitute for sulphurized olefins in lubricants. Proc IMechE Part J: J Engineering Tribology 2007;221(J5):553–9.

[15] Li JS, Xu XH, Wang YG, Ren TH. Tribological studies on a novel borate ester containing benzothiazol-2-yl and disulfide groups as multifunctional additive. Tribol Int 2010;43(5-6):1048–53.

[16] Wang YG, Li JS, Ren TH. Tribological study of a novel borate ester containing S, P with high hydrolytic stability as a multifunctional lubricating additive. Tribol Trans 2008;51(2):160–5.

[17] Wang YG, Li JS, Ren TH. A potential approach to replace sulfurized olefins with borate ester containing xanthate group in lubricating oil. Chin Sci Bull 2008;53(7):992–7.

[18] Zheng Z, Shen GQ, Wan Y, Cao LL, Xu XD, Yue QX, Sun TJ. Synthesis, hydrolytic stability and tribological properties of novel borate esters containing nitrogen as lubricant additives. Wear 1998;222(2):135–44.

[19] Yao JB. Antiwear function and mechanism of borate containing nitrogen. Tribol Int 1997;30(6):387–9.

[20] Shen GQ, Zheng Z, Wan Y, Xu XD, Cao LL. Synergistic lubricating effects of borate ester with heterocyclic compound. Wear 2000;246(1-2):55–8.

[21] Crawford J, Psaila A, Orszulik ST. Miscellaneous additives and rapeseed oils. In: Roy M, Mortier RM, Fox MF, Orszulik ST, editors. Chemistry and technology of lubricants, Heidelberg: Springer; 2010, p. 189–211.

[22] Kasrai M, Lennard WN, Brunner RW, Bancroft GM, Bardwell JA, Tan KH. Sampling depth of total electron and fluorescence measurements in Si L- and K-edge absorption spectroscopy. Appl Surf Sci 1996;99(4):303–12.

[23] Najman MN, Kasrai M, Bancroft GM. X-ray absorption spectroscopy and atomic force microscopy of films generated from organosulfur extreme-pressure (EP) oil additives. Tribol Lett 2003;14(4):225–35.

[24] Najman MN, Kasrai M, Bancroft GM. Chemistry of antiwear films from ashless thiophosphate oil additives. Tribol Lett 2004;17(2):217–29.

[25] Najman MN, Kasrai M, Bancroft GM. Investigating binary oil additive systems containing P and S using X-ray absorption near-edge structure spectroscopy. Wear 2004;257(1–2):32–40.

[26] Zhang Z, Najman M, Kasrai M, Bancroft GM, Yamaguchi ES. Study of interaction of EP and AW additives with dispersants using XANES. Tribol Lett 2005;18(1):43–51.

[27] Luo JB, Meng YG, Shao TM, Zhao Q. Advanced Tribology. Heidelberg: Springer; 2010.

[28] Kasrai M, Fleet ME, Muthupari S, Li D, Bancroft GM. Surface modification study of borate materials from B K-edge X-ray absorption spectroscopy. Phys Chem Miner 1998;25(4):268–72

[29] Varlot K, Kasrai M, Bancroft GM, Yamaguchi ES, Ryason PR, Igarashi J. X-ray absorption study of antiwear films generated from ZDDP and borate micelles. Wear 2001;249(12):1029–35.

[30] Zhang Z, Yamaguchi ES, Kasrai M, Bancroft GM. Interaction of ZDDP with borated dispersant using XANES and XPS. Tribol Trans 2004;47(4):527–36.

[31] Salih N, Salimon J, Yousif E, Abdullah BM. Biolubricant basestocks from chemically modified plant oils: ricinoleic acid based-tetraesters. Chemistry Central Journal 2013;7:128.

[32] Ji HB, Nicholls MA, Norton PR, Kasrai M, Capehart TW, Perry TA, Cheng YT. Zinc-dialkyl-dithiophosphate antiwear films: dependence on contact pressure and sliding speed. Wear 2005;258(5-6):789–99.

[33] Aoki S, Suzuki A, Masuko, M. Comparison of sliding speed dependency of friction between steel surfaces lubricated with several ZnDTPs with different hydrocarbon moieties. Proc IMechE Part J: J Engineering Tribology 2006;220(J4):343–51.

[34] NIST X-ray Photoelectron Spectroscopy Database, Version 4.1 (National Institute of Standards and Technology, Gaithersburg, 2012); http://srdata.nist.gov/xps/.

[35] Ji C. Levitas VI, Zhu HY, Chaudhuri J, Marathe A, Ma YZ. Shear-induced phase transition of nanocrystalline hexagonal boron nitride to wurtzitic structure at room temperature and lower pressure. Proc Natl Acad Sci USA 2012;109(47):19108–12.